NUMERICAL SIMULATION OF BIOLOGICAL CLOGGING IN BIOFILTERS

By

SAHAR SOLEIMANI

A thesis presented to the Faculty of Graduate Studies and Research

in partial fulfillment of the requirements for the degree of

Master of Applied Science*

Department of Civil and Environmental Engineering

Carleton University

Ottawa, Ontario, Canada

August 2007

* The Master of Applied Science in Environmental Engineering is a joint program with the University of Ottawa administered by the Ottawa-Carleton Institute for Environmental Engineering (OCIENE)

Your file Votre référence
ISBN: 978-0-494-33668-7
Our file Notre référence
ISBN: 978-0-494-33668-7

ABSTRACT

A two-dimensional unsaturated flow and transport model, which includes microbial growth and decay, has been developed to simulate biological clogging in unsaturated soils, namely biofilters. The bacterial growth and rate of solute reduction due to biodegradation is estimated using the Monod equation. The equations are coupled together and the effect of bioclogging is considered in the proposed conceptual models that relate the relative permeability term to the microbial growth. The model was used to evaluate the impact of different waste distribution approaches (continuous vs. pulse) on filter clogging and to study the effect of the kinetic parameters of the Monod equation on biomat formation. The model was also used to simulate the progressive clogging of a septic bed as a biomat initially forms at the up-gradient end of the distribution pipe, displacing wastewater infiltration and biomat formation further down-gradient over time.

ACKNOWLEDGEMENTS

I would like to express my sincere gratitude to my supervisor Dr. Paul J. Van Geel for giving me permission to commence this research in the first instance, and for his help, and suggestions all the time in completing this research. I really appreciate his detailed review, constructive criticism and excellent advice during the preparation of this thesis.

I am deeply indebted to my other supervisor Dr. O. Burkan Isgor who kept an eye on the progress of my work and always was available when I needed his advises. I should also thank him for his encouragement, valuable advice and friendly help.

I also want to thank my both supervisors, Dr. P. Van Geel and Dr. B. Isgor, again for the financial support that they provided to continue this research.

Especially, I feel a deep sense of gratitude for my mother and father who formed part of my vision and taught me the good things that are really matters in life. They have lost a lot due to my research abroad. My special gratitude is due to my sisters, and my brother for their loving support. The happy memories of my family always provided a persistent inspiration for the completion of this research.

This acknowledgement would not finish without thanking my uncle and his family specially my aunt who helped me a lot to adopt with new life in Canada.

I also want to thank my colleague, Mohammed Mostafa, who was a great help whenever I needed him and for the data that he provided me.

I would like to give my special thanks to my fiancé, Pouria Ghods, whose love enabled me to complete this work. Without his encouragement and understanding, it would have been impossible for me to finish this work.

TABLE OF CONTENTS

LIST OF TABLES

LIST OF FIGURES

LIST OF SYMBOLS

A	Cross sectional area [L^2]
A_s	Surface area of spread zone [L^2]
b	Biomass decay [T^{-1}]
C	Organic matter or substrate concentration [ML^{-3}]
$c_0(x,y)$	A known concentration distribution in the entire domain [ML^{-3}]
$c_i(x,y)$	A known concentration along the boundary [ML^{-3}]
D	Diffusion coefficient in Fick's law [L^2T^{-1}]
D_x	Dispersion coefficients in the transverse direction [L^2T^{-1}]
D_y	Dispersion coefficients in the longitudinal directions[L^2T^{-1}]
D^*	Effective diffusion coefficient in porous media [L^2T^{-1}]
E_x	Material properties in x direction
E_y	Material properties in y direction
F_D	Rate of diffusion in Fick's law [$ML^{-2}T^{-1}$]
$f_i(x,y)$	A function representing the dispersive flux normal to the boundary
$g_i(x,y)$	A function representing the total flux (dispersive and advective) normal to the boundary
h	Total head (piezometric head or hydraulic head) [L]
h_w	Water pressure head [L]
h_i	Prescribed head for node i on that boundary [L]
IR_t	Infiltration rate at time t [LT^{-1}]
j	Iteration number
k	First order decay rate [T^{-1}]
$K(\theta)$	Unsaturated hydraulic conductivity [LT^{-1}]
K_b	Hydraulic conductivity of the biomat zone [LT^{-1}]
K_r	Relative permeability
K_{sat}	Saturated hydraulic conductivity [LT^{-1}]
K_s	Half-velocity constant [ML^{-3}]

L	Length of the column [L]
M_T	Biomass (microorganism) concentration [ML^{-3}]
$M_T^{t_1}$	Microbial concentration at time equalling t_1 [ML^{-3}]
M_{db}	Mass of dead bacteria [M]
P	Water pressure [$MT^{-2}L^{-1}$]
P_c	Capillary pressure [L]
P_b	Bubbling pressure [$MT^{-2}L^{-1}$]
Q	Flow rate [L^3T^{-1}]
Q_b	Flux through the biomat [L^3T^{-1}]
Q_S	Flux in the subsurface soils [L^3T^{-1}]
q	Specific discharge (Darcy velocity) [LT^{-1}]
q_0	Initial specific discharge [LT^{-1}]
$\vec{q}_m$	Mass vector of solute crossing the plane per unit time [$ML^{-2}T^{-1}$]
$\vec{q}$	Darcy velocity vector [LT^{-1}]
q_x	Component of Darcy velocity in x direction [LT^{-1}]
q_y	Component of Darcy velocity in y direction [LT^{-1}]
$q_{In,x}$	Mass flux entering the element in x direction [L^3T^{-1}]
$q_{In,y}$	Mass flux entering the element in y direction [L^3T^{-1}]
$q_{Out,x}$	Mass flux exiting the element in x direction [L^3T^{-1}]
$q_{Out,y}$	Mass flux exiting the element in y direction [L^3T^{-1}]
q_m	Maximum specific substrate utilization rate [T^{-1}]
R_s	Sink term [$ML^{-3}T^{-1}$]
R_b	Resistance of biomat
r_i	Radius of capillary tube i [L]
S_{em}	Effective microbial saturation
S_{am}	Actual microbial saturation
$\bar{\bar{S}}_w$	Apparent water saturation
S_{ea}	Effective trapped air saturation

S_{et}	Effective total saturation
S_w	Water saturation
S_e	Effective saturation
S_r	Irreducible saturation
S_{el}	Effective saturation at the steady state condition
t^*	Travel time [T]
t_b	Thickness of biofilm [L]
$tBOD$	Cumulative density loadings of total BOD [ML^{-2}]
TSS	Cumulative density loadings of suspended solids [ML^{-2}]
Y	Synthesis yield coefficient
V_x	Seepage velocity in x direction [LT^{-1}]
V_y	Seepage velocity in y direction [LT^{-1}]
$\|V\|$	Magnitude of velocity [LT^{-1}]
V_m	Microbial volume [L^3]
ν_x, ν_y, G, R, c, f	Coefficients in the general transient quasi-harmonic equation
V	Seepage velocity [LT^{-1}]
z	Elevation head [L]
Z_b	Thickness of biomat [L]
σ	Surface tension [$ML^{-1}T^{-2}$]
θ_r	Irreducible water content
λ	Pore-size distribution index
Δx	Size of element in x direction [L]
Δy	Size of element in y direction [L]
Δz	Size of element in z direction [L]
α_L	Dispersivity in the longitudinal direction [L]
α_T	Dispersivity in transverse direction [L]
θ	Volumetric water content
φ	Soil porosity
θ_s	Actual saturated moisture of biozone
θ_{sm}	Porosity of parent soil with zero plaque

$\theta_{i,j}^{t}$	Volumetric water content of element (i,j) at time equalling t
Φ	Field variable of interest
$\rho_{\text{dry density}}$	Density of microorganisms [ML^{-3}]
γ	Specific weight of water [$MT^{-2}L^{-2}$]
ϕ	Factor defining the contribution of iterations
α, n, m	Van Genuchten fitting parameters
μ_m	Maximum specific growth rate of biomass [T^{-1}]
ρ_p	Average density of plaque [ML^{-3}]

CHAPTER 1 -INTRODUCTION

1.1 BIOFILTERS

Biofilters are widely used for onsite treatment of water and wastewater. A biofilter consists of a group of bacteria cultivated in a soil media (porous media) which operates aerobically under unsaturated soil conditions. The bacteria break down organic material in the wastewater and thus improve water quality.

The most common type of biofilter is the septic bed, which treats and/or discharges sewage within the site where the sewage originates (Kaplan 1987). The septic systems are common in areas that do not have access to public sewer network systems. For example, the existence of over one million septic systems was reported in Ontario (Septic Smart!, 1999), and the growing demand for rural development has seen an increase in use of septic systems. A septic system typically includes the septic tank and one type of leaching bed or soil absorption system (Biofilter) (Figure 1-1). Septic tanks generally have two water tight chambers buried underground and are constructed of concrete, steel, fibreglass or polyethylene (Figure 1-2). The purpose of the septic tank is to remove suspended solids and oil/grease in the wastewater stream, and begin the anaerobic digestion process of contaminants. Solids in the sewage settle at the bottom of the tank, whereas floatable materials (oils, greases, and some fecal constituents) float to the top of the tank. The floatable materials go through some microbial decomposition and form a buoyant layer of scum (Figure 1-2). The sewage with smaller amount of solids and floatable materials (grey water) enters the second compartment of the tank. Then, it is

released through a distribution box and perforated pipe to the septic bed area where infiltration to the subsurface is promoted.

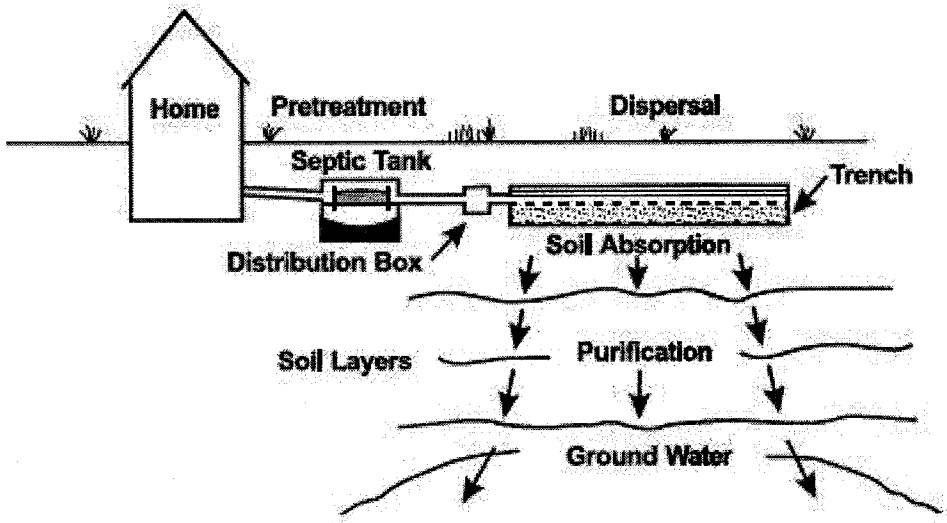

Figure 1-1: Lateral view of conventional wastewater infiltration system (USEPA, 2002)

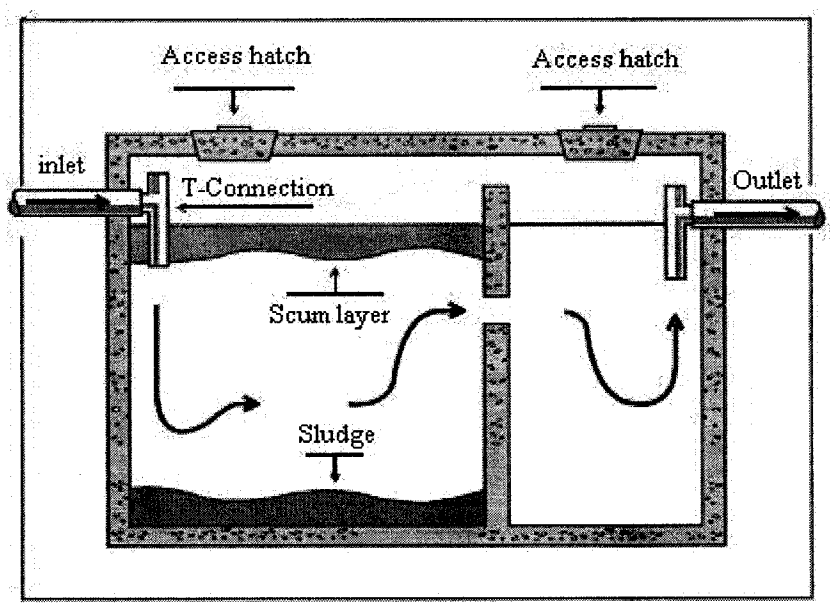

Figure 1-2: Typical septic tank compartments (Ministry of Municipal Affairs and Housing Website)

The septic bed is typically a network of perforated distribution pipes laid in gravel trenches, which distribute the septic tank effluent over the filter media before it reaches the native soil. The septic bed mostly operates aerobically above the water table (unsaturated zone).

1.2 BIOFILTER CLOGGING

The flow through the biofilter can be impacted by both the particulate materials that plug the soil pores, and by the growth and decay of microorganisms which can create a biomat which decrease infiltration. A clogged biofilter may cause the sewage to pond on the filter and wastewater exposure on the ground surface poses a health concern.

Clogging due to biological growth (biological clogging) has been found to be a very common cause of biofilter failure. This thesis, therefore, will focus on clogging that results from microbial growth. Different approaches for waste distribution on filter materials have been suggested in order to change the spatial and temporal distribution of biomass and hence, improve the system treatment efficiency and postpone filter failure. Continuous loading of effluent into the filter at a low flow rate results in the formation of a thin layer of biomat at the filter surface. Pulse loading (high flow over a short period of time) causes the influent wastewater stream to infiltrate into the filter bed to a greater depth causing the biomass to form over greater depth, which in turn reduces the chances for the development of a thin biomat.

Understanding and properly simulating bacterial growth and its impact on the relative permeability of unsaturated soils will aid in improving the design of biofilters. The simulation of biomass formation requires the selection of values for parameters whose relationship to soil clogging is poorly understood. The evaluation of the impact of

the growth and decay kinetic parameters in Monod equation is important in understanding the process of biomat formation.

1.3 OBJECTIVE

The objective of the current study is to implement and verify a numerical model to simulate the biological clogging of biofilters and the effect of continuous loading versus pulse loading on the clogging process. As well, the impacts of different parameters in the estimation of the biomat growth have been investigated. The particular objectives and contribution of this thesis are to:

- Develop a numerical model for the advection-dispersion contaminant transport equation that incorporates:
  - A sink term to account for the reduction of organic material due to bacterial consumption or biodegradation.
  - The Monod equation to estimate microbial growth and decay.
- Develop a two-dimensional unsaturated flow model, which considers the effect of bioclogging based on three different conceptual models, proposed by Mostafa and Van Geel (2007), which relate the microbial growth to the relative permeability term.
- Investigate the influence of the kinetic parameters of the Monod equation on the development of biomass within unsaturated soil media.
- Illustrate how the clogging is impacted by changing the waste loading configuration (continuous vs. pulse loading).

- Illustrate how clogging in a septic bed progresses as the biomat initially forms at the up-gradient end of the distribution pipe, displacing wastewater infiltration and biomat formation further down-gradient over time.
- Predict the concentration variations of substrate and microbial saturation along a soil profile over time, as well as the biofilter longevity based on the biomass growth.

1.4 THESIS OUTLINE

Chapter One provides an overview of the objectives of this research study. Chapter Two provides background information on the clogging mechanisms occurring within biofilters, the effect of biomass formation on hydraulic conductivity reduction, an overview of different clogging models, and the relationship between bacteria growth and substrate utilization.

Chapter Three describes the development of the flow model based on the mass balance approach. The verification of the flow model against the previous experimental and numerical studies is also provided in this chapter.

In Chapter Four, the transport equation development and development of the model for the complete biological growth scenario is described. This chapter also includes description of the method by which the system is defined and the method of coupling the flow, transport and Monod equations. In addition, the model is compared to an analytical solution and published numerical simulations to verify the transport equation itself and the complete developed model.

Chapter Five outlines the application of the model and illustrates the results of different case studies that evaluate the impact of the Monod kinetic parameters on

clogging. A two-dimensional illustration of the progressive clogging of septic beds is also provided.

The final chapter, Chapter Six, presents the conclusions of this work and recommendations for further extension of this work toward the ultimate goal of prediction and prevention of biofilter clogging.

CHAPTER 2 -BACKGROUND

2.1 INTRODUCTION

Infiltration through soil is an effective and simple technique for wastewater treatment. The treatment is performed by the growth of microorganisms which attach themselves to the soil particles in the form of a biofilm. When the soil is provided with the continuous organic source, the biomass grows and potentially leads to clogging of the pore structure. This clogged soil layer is often called a biomat. The failure of biofilters begins with bioclogging due to the excessive biomat formation in the upper layer of soil where the organic load is introduced.

The effective control of clogging, and its impact on the hydraulic conductivity reduction of unsaturated porous media resulting in the infiltration rate reduction, is an important field of study. Hydraulic performance of biofilters is complicated because it is highly influenced by the biomat zone development on the soil infiltrative surface of biofilters (Bouma 1975, Seki et al. 1998, Siegrist and Boyle 1987). As biofilters work under unsaturated conditions, their treatment is considered as aerobic treatment and it is necessary to understand the process of clogging in the unsaturated zone. In the literature, most of the research evaluates the clogging of porous media under saturated conditions (Siegrist and Boyle 1987, Taylor and Jaffé 1990, Okubo and Matsumoto 1983). Only a few papers describe the biological modeling of porous media under unsaturated flow conditions (e.g. Weintraub et al. 2002, Beach and McCray 2003, Mostafa and Van Geel 2007).

2.2 MECHANISM OF CLOGGING IN SOIL FILTRATION

Soil clogging is a well known mechanism that reduces the hydraulic conductivity and infiltration. A review of the literature was carried out in order to identify the mechanisms and factors affecting clogging. The application of wastewater may be such that the increased growth of microorganisms may form a biomat layer which impedes infiltration (biological clogging). By-product of microbial growth is another factor which reduces the hydraulic conductivity of the soil by reducing the number of saturated pores. These by-products can be either the produced gases from the microbial activities or solid products such as slime or polysaccharides. Not only biological activity but also other physical and chemical factors such as decomposition of organic and inorganic materials at the soil grain surface in the pore space, deposition of suspended solids and chemical precipitation, reduce the hydraulic conductivity (Platzer and Mauch 1997, Otis 1985).

A significant reduction of infiltration rate due to biological clogging has been described in the literature as a process with three or four phases (Alison 1947, Jones and Taylor 1965, Okubo and Matsumoto 1979). Allison (1947) applied tab water to the surface of saturated soil and produced an S-shape infiltration rate versus time curve with three distinct phases, similar to Figure2-1(a). Allison (1947) attributed the initial decrease to swelling and dispersion of soil particles followed by a sudden increase for the next stage attributed to removal of entrapped air. The final portion had a slow decrease in infiltration rate. This slow reduction was partly due to a slow physical deterioration of aggregates and movement of soil aggregates because of bacterial growth (i.e. the microbial growth displaces the loose aggregate particles), and mainly due to biological clogging resulting from microbial growth.

Intermittent and continuous application of septic tank effluent to a sand column by Jones and Taylor (1965) also resulted in different three-phase infiltration rate reduction but with a different shape as it is shown in Figure2-1(b). Jones and Taylor (1965) observed that the reduction in infiltration rate occurs quite rapidly in continuous loading rather than intermittent loading. In both continuous and intermittent loading of effluent, the stage of rapid decline of infiltration rate is attributed to the anaerobic condition resulting from microbial activity. Okubo and Matsumoto (1979) investigated the effect of biological clogging on hydraulic conductivity reduction of medium sand columns and defined four stages of clogging from their experiments with application of synthetic wastewater (Figure2-1(c)). In the first stage, the infiltration rate decreased rapidly due to aerobic microbial growth. In the second stage, the infiltration rate remained constant or sometimes increased. The second stage is the transitional period from an aerobic condition to an anaerobic condition. The third stage also showed rapid decline because of clogging due to anaerobic degradation in the surface layer. Finally, the forth stage consists of a very slow decline at a low level which was due to the formation of a clogged layer on the top of soil surface.

The differences in these three relationships for the infiltration rate over time can be due to the difference in the water quality, soil properties and condition, or method of application. However, all three curves show a very significant decrease in infiltration rate

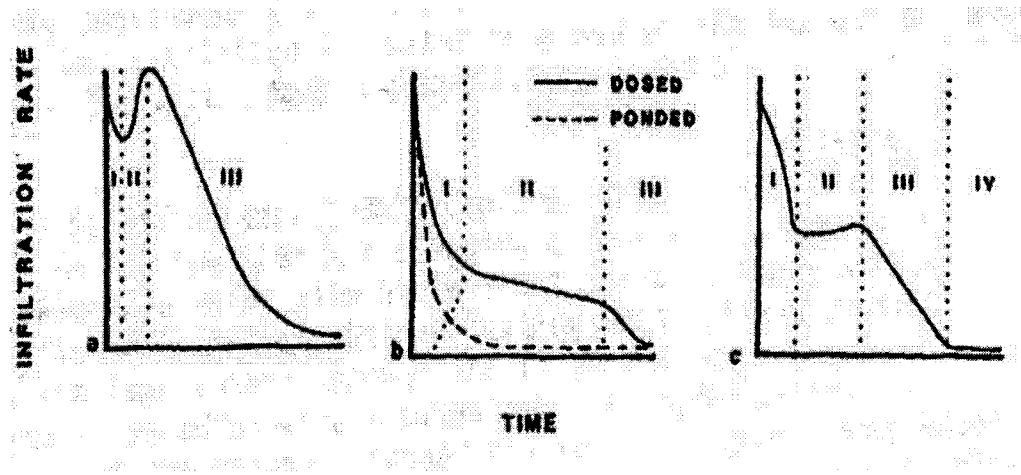

Figure 2-1: Hydraulic conductivity reduction due to biological clogging through soils: Alison (1947); b) Jones and Taylor (1965); c) Okubo and Matsumoto (1979) (Taken from Otis 1985)

to a low limit. The phase of rapid decline in infiltration rate suggests that a significant chemical or biological change occurs within the soil (Otis 1985).

2.3 THE BIOCLOGGING PROCESS AND BIOMAT FORMATION

The reduction in effective hydraulic conductivity is affected by physical, chemical and biological factors. Biological factors such as production of gases due to biological activity, microbial destruction of soil structure and accumulation of metabolic products in pore spaces, are the major concerns in the hydraulic conductivity reduction. The degradation of organic matter generates biomass which accumulates in the pore space of soil and alters the microstuctural configuration of pores. The effective hydraulic conductivity of the soils is affected by a change in the pore geometry and microstructure.

McCalla (1944, 1950) performed a series of studies to show that biological activity of microorganisms is the cause of water percolation reduction. He concluded that microbial growth reduces water percolation either by the by-products produced by the microorganisms such as gases, and slimes or by decomposing or changing the structural

stability of soil grains. In one study, McCalla (1950) concluded that the addition of materials with high organic content would increase the number of microorganisms and biological activity, as a result reduces the number and size of pores. Alison (1947) concluded that soil aggregate breakdown is not only due to physical causes but also it is because of microbial sealing. Alison (1947) also concluded that the clogging is entirely due to microbial activities, since in their experiments on the soil column, there was no evidence of infiltration rate reduction in the soil column fed by the sterile water.

Otis (1985) stated that biological clogging in onsite wastewater treatment systems primarily occurs at the infiltration surface. He reviewed the study of Thomas et al. (1966) which confirmed that 87 percent of total flow impedance occurs at the top 1 cm of the sand filter. Pell and Nyberg (1989b) confirmed the results of Thomas and concluded that organic material and availability of oxygen are the dominant agents of clogging, as they are greatest in the top zone. Their study on a sand filter fed by wastewater revealed that the microbial decomposition of organic matter occurs mainly in the upper 1.5 cm of the surface layer where 84% of phosphorous and organic matters have disappeared.

To isolate the mechanism responsible for the clogging, Mitchel and Nevo (1964) conducted experiments on saturated sand columns fed by synthetic wastewater containing high levels of organic matters. They tried to investigate the effect of accumulation of clogging materials such as polysaccharides on the clogging process. The products of microbial growth such as polysaccharides enhance soil aggregation by binding soil particles together (Otis 1985). Mitchel and Nevo (1964) concluded that the accumulation of polysaccharides in a clogged layer of sand is associated with an increase in the number

of bacteria. A high correlation was found between clogging, as measured by infiltration rate, and the accumulative concentration of polysaccharides.

2.3.1 Control of Clogging

Excessive clogging can reduce infiltration and lead to biofilter failure. Whereas, limited biomass growth can reduce the treatment efficiency of the filter if the retention time is insufficient. As the excessive clogging causes biofilter failure and presents health concerns due to surface seeps, most control efforts have been directed toward reducing the development of a biomat (Otis 1985).

Factors affecting the biomat formation include hydraulic and organic loading rates (Mitchell and Nevo 1964), the dosing regime (Siegrist and Boyle 1987), the aeration status of infiltration surfaces (Siegrist and Boyle 1987), and the biogeochemical properties of the filter medium (Bouma 1975). Biomat formation is also affected by the temperature of the wastewater being applied to the soil (Jone and Taylor 1965, Kristiansen 1981b). Kristiansen (1981b) studied the effect of temperature on the clogging process by measuring the concentration of fecal coliforms in sand columns and the effluent organic concentration. Kristiansen (1981b) concluded that the organic matter concentration of effluent at lower temperatures were considerably higher than at the higher temperature due to lower amount of biomass formation.

Many methods to control clogging in biofilters have been proposed (Otis 1985, Bouma at al. 1974, Converse 1974, Jones and Taylor 1965, McGauhey and Winneberger 1964). The most commonly employed methods include: changing the hydraulic loading on different soil materials (high loading vs. low loading), resting and dosing, and pre-treatment of wastewater to reduce organic matters.

Storing the wastewater for intermittent dosing to the infiltration system as an alternative to gravity distribution has been shown to reduce clogging by many researchers (Bouma at al. 1974, McGauhey and Winneberger 1964, Jones and Taylor 1965, Converse 1974). Larger, less frequent doses were found to be more desirable in terms of reduction in clogging than smaller more frequent doses (Otis 1985). The dosing regime provides better distribution of the wastewater effluent over the infiltration surface and causes the influent wastewater stream to infiltrate into the filter bed to a greater depth. This will cause the biomass to form over a greater depth, which in turn reduces the chances for a thin biomat to form leading to filter failure. Using lysimeters installed in an infiltration trench, McGauhey and Winneberger (1964) found that resting and draining of a filter periodically, maintains the highest possible infiltration rate, thus minimizing the occurrence of failure. Converse (1974) evaluated the effective flow distribution patterns over the entire septic bed area for both gravity and pump flows considering various hole spacing and hole location for the distribution pipe. He found that pumping and dosing the liquid into the bed improved the uniform distribution of effluent over the entire bed area and as a result increases the lifetime of the septic bed.

Siegrist and Boyle (1987) conducted an experiment on a wastewater infiltration system with different loading rates and different influent compositions to predict the effect of hydraulic loading and organic loading on the clogging development. Their results proved that clogging development in the filter media accelerates at a higher hydraulic loading rate with a given influent or with more concentrated influents at a given hydraulic loading rate.

Improving the quality of wastewater before applying it to the filters is commonly suggested as a means to control clogging (Laak 1967). Laak (1967) suggested that as the clogging depends on the BOD (Biological Oxygen Demand) and the total suspended solids load, pre-treatment can be an effective way of controlling the clogging layer by controlling the organics and solids load.

2.3.2 Biological Clogging Models

Although factors generating clogging are known, predicting biomat development and hydraulic conductivity decline is difficult and requires a greater knowledge of growth rate modeling and its effect on hydraulic capacity. Several models have been introduced to simulate the observed interactions between the biomat zone and the hydraulic properties of porous media. Theses models can be divided into two groups for saturated and unsaturated conditions. Usually the models for saturated conditions are based on the assumption of a homogeneous biofilm covering the surface of the filter grains and the models for unsaturated conditions are based on formation of a fixed thickness layer of clogging zone at the filter surface.

2.1.1.1 Bioclogging Models for Saturated Conditions

Siegrist and Boyle (1987) proposed a model for predicting infiltration rate to quantify biomat development as a function of the organic loading. However, the applicability of this model is limited to their specific set of experimental design conditions. Siegrist and Boyle's (1987) model is described as:

$$IR_t = 241 \times \frac{\{\exp[2.63 - 5.7(tBOD) + 41.08(TSS) - 0.048(tBOD \times TSS)]\}}{\{1 + \exp[2.63 - 5.70(tBOD) + 41.08(TSS) - 0.048(tBOD \times TSS]\}} \qquad (2\text{-}1)$$

where IR_t is the infiltration rate at time t in cm/day; and *tBOD* and *TSS* are the cumulative density loadings of total *BOD* (*cBOD* and *nBOD*) and suspended solids in kg/m^2. This model suggests that the effluent rate would approach zero with continuous effluent loading. Although Eq.2-1 considers cumulative density loadings of organic and inorganic fractions of waste, it does not consider the dynamically bioactive nature of the biomat zone (Beal et al. 2005).

Okubo and Matsumoto (1979, 1983) did a series of experiments on sand, under saturated conditions, in different temperature and organic loading conditions to propose a model for biological clogging. Their model is based on Hagen-Poisseuille's law and considers a bundle of capillary tubes with diameter d_0 which become narrow uniformly by the development of biological clogging. They showed that the change of accumulative discharge can be evaluated by the following equation, which has almost the same form as the Monod equation (Okubo and Matsumoto 1979, Okubo and Matsumoto 1983):

$$Q = \frac{k_1 q_0 t}{k_2 + t} \tag{2-2}$$

where Q is the accumulative discharge, q_0 is the initial specific discharge, and t is time (day). In this equation, k_1 and k_2 are the parameters which define the effect of organic matter concentration, suspended solid concentration and temperature.

Taylor and Jaffé (1990) proposed a model for substrate and biomass transport in saturated soil, which accounts for the growth and decay of biomass suspended in the water phase, and attached to the solid matrix as a biofilm. The transfer of biomass between the water phase and attached biofilm phase due to fluid mechanical shear is also considered. The porosity, permeability and dispersivity of the porous media are changed due to the growth of biofilm altering the microscopic geometry of the pore space (Taylor

et al. 1990). The biofilm approach is used, which assumes that biomass occurs in a continuous film completely covering the solid grains of the medium. This model represents a significant advancement in substrate and biomass transport modeling which considers the clogging of porous media; however, this model is not applicable for biofilters since the model assumes saturated conditions in porous media.

2.1.1.2 Bioclogging Models for Unsaturated Conditions

To evaluate the effect of clogging under unsaturated conditions on hydraulic conductivity, Bouma (1975) related the hydraulic conductivity of the biomat zone (K_b) to both the resistance of biomat (R_b) and the thickness of biomat (Z_b). Bouma (1975) assumed a steady-state infiltration soil profile such that the flux through the biomat, Q_b, is equal to the flux in the subsurface soils (Q_S) as follow:

$$Q_S = Q_b \Leftrightarrow K(\psi)\left(\frac{dH}{dZ}\right)_{Soil} = K_b\left(\frac{dH}{dZ}\right)_{biomat} = K_b\left(\frac{H_0 + \psi + Z_b}{Z_b}\right) \tag{2-3}$$

The hydraulic head gradient of the soil below the biomat, $\left(\frac{dH}{dZ}\right)_{Soil}$, will be approximately unity at the steady-state infiltration so that:

$$\frac{K(\psi)}{H_0 + \psi + Z_b} = \frac{K_b}{Z_b} \equiv \frac{1}{R_b} \tag{2-4}$$

where $K(\psi)$, the unsaturated hydraulic conductivity of underlying soil, is a function of soil moisture potential (ψ) and H_0 is the positive hydraulic head on top of the barrier due to the ponded liquid (Figure2-2).

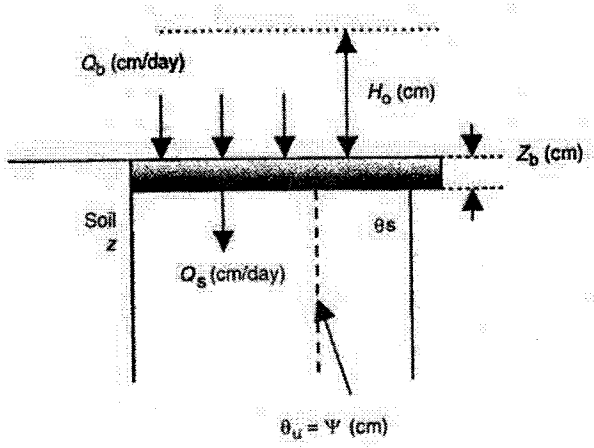

Figure 2-2: Definition diagram of Eq.2-4. θ_s, θ_u, z and ψ are the saturated volumetric water content and volumetric water content, soil depth and soil moisture potential of underlying soil, respectively (edited from Beal et al. 2005).

Bouma (1975) calculated R_b from in-situ measurement of the soil moisture potentials and hydraulic conductivity of filter media and reported different ranges for four different soil types used for septic beds (e.g. sand, sandy loam, silt loam, and clay). The variation in values of biomat resistance for different soils is attributed to differences in porosity, structural stability and biomass distribution in the pore space. From the field observation, he also assumed that biomat thickness is 2 centimetres. The weakness in Bouma's model of hydraulic conductivity is that it does not account for the biomat growth due to the organic loading and it considers a constant thickness of biomat with a constant biomat resistance through the lifetime of the filter.

Beach and McCray (2003) used HYDRUS-2D to predict a relationship between the biomat zone hydraulic properties and the steady-state (long-term) infiltration rates within the unsaturated zone. In their model, they assumed that the clogging zone, which has a fixed thickness between 2-3 centimetres, restricted the infiltration and created an impedance to flow. They considered different hydraulic properties (e.g. saturated hydraulic conductivity, Van Genuchten parameters, etc.) for the clogging zone to account

for the degree of clogging under concern. The weakness of Beach and McCray's (2003) model is that they need an accurate knowledge of clogging zone hydraulic properties, and their model does not consider the clogging development due to the growth of bacteria.

Weintraub et al. (2002) developed a model which includes microorganism growth and decay as a function of organic matter in the 2cm depth of the biomat zone (biozone). Two mass balance equations for the live bacteria and dead bacteria (Plaque, M_{db}) have been solved simultaneously to obtain the biomass of dead bacteria and residue. They assumed that the porosity (saturated moisture) of the biozone decreases with the build up of dead bacteria and solid residue as follows.

$$\theta_s = \theta_{sm} - (M_{db})/(\rho_p Z_b A_s) \tag{2-5}$$

where θ_s is actual saturated moisture of biozone, θ_{sm} is porosity of parent soil with zero plaque ρ_p is average density of plaque, and A_s is the surface area of spread zone. Reduction in the saturated moisture content reduces the infiltration rate which leads to the hydraulic failure of onsite wastewater systems.

The strength of this model is the simulation of bacterial growth as a function of organic matter and incorporation of porosity reduction and increase in water content by the accumulation of dead bacteria and solid residue. However, the link between soil matrix potential (ψ) and unsaturated hydraulic conductivity of the filter media below the biomat is not obvious (Beal et al. 2005).

2.4 ROLE OF THE UNSATURATED ZONE AND BIOMAT FORMATION

High removal rate of influent pollutants (e.g. pathogens, nutrients, organics and suspended solids) has been correlated with a well developed biomat zone under aerobic conditions (Kristiansen 1981a, Pell and Nyberg 1989 a and b, Beach and McCray 2003, Jones and Taylor 1965).

Kristiansen (1981a) in their study of the effectiveness of sand-filter trenches on the purification of septic tank effluent stated that the oxygen content in the sand atmosphere is influenced by the degree of clogging. Therefore, the possibility for nitrification is better with an increase in clogging as the clogging mat impedes the flow into the sand and only a portion of the pores will be water–filled which provides aerobic conditions. In their experiments on the fate of nitrogen in filters, Kristiansen (1981a) found that the highest amount of nitrification was either between 7.5cm and 27cm below the crust where it has the highest clogging intensity or near the bottom air vent due to the presence of aerobic conditions.

Pell and Nyberg (1989a, 1989b) measured nutrient and organic matter removal rates both in a newly operating sand filter under aerobic conditions and in columns under anaerobic conditions. They observed 83 % P removal in approximately 75 cm of the unsaturated sand filter and total N removal in less than 15 cm of the sand filter. They also concluded that the columns were less efficient at reduction of COD comparing with the sand filter because of the anaerobic conditions that were developed in the columns. In the aerobic conditions, the aerobic and denitrifying bacteria grow faster and their population

remain in the steady state conditions, so that the higher efficiency in organic matter reduction was observed (Pell and Nyberg 1989a).

Jones and Taylor (1965) conducted a laboratory investigation to evaluate the effect of septic effluent application in sand media under primarily aerobic or primarily anaerobic conditions. They also evaluated variable effluent loading rates under conditions of intermittent ponding. They observed that a zone of low conductivity developed at or just below the interface, slowly under aerobic conditions but quiet rapidly under anaerobic conditions. The result of the biochemical changes in the effluent showed that the percentage reduction in organic and inorganic materials was of the same order of magnitude for both intermittent and continuous ponding. However, the more aerobic soil environment should bring about greater decomposition of organic matter.

A key difference between pulse loading (dosing and resting) of wastewater and conventional continuous gravity loading in the sand filter is the inability of the gravity-fed system to evenly distribute effluent across the full length of the filter (Beal et al. 2005). Intermittent dosing can also eliminate saturated conditions to prevent a suitable condition for the growth of anaerobic bacteria and improve the treatment efficiency (Beal et al. 2005).

Beal et al. (2004) used HYDRUS-2D to model two-dimensional flow in unsaturated soil and evaluated the impact of biomat resistance (R_b) on long-term flow rates for various soils. They utilized Eq.2-2 to measure the hydraulic conductivity of biomat zone and used the Van Genuchten equation with the pore-size distribution model of Mualem for predicting the unsaturated soil hydraulic conductivity function, $K(\psi)$. The result from Beal et al. (2004) were similar to Beach and McCray (2003), in which a 2-3

order of magnitude reduction in saturated hydraulic conductivity results in an order of magnitude reduction in steady state flow rate.

2.5 BACTERIAL INTERACTIONS IN SOILS

Biological treatment of wastewater in biofilters is brought about by growth of microorganisms on the surface of solid particles in soil. An understanding of factors affecting the rate of microbial growth and substrate utilization is very useful in estimating treatment efficiency and modeling the biomass formation on the surface of soil grains. Baveye and Valocchi (1989) evaluated three conceptual models that were developed by previous researchers for the bacterial growth and biomass formation in saturated conditions. Model I, which is categorized as the Strictly Macroscopic Model, considers that the bacteria are attached to and growing on the solid particles in groups or isolated. Model II, which was developed by Molz et. al (1986), is named as the Microcolony Model, and assumes the growth of microorganisms in microcolonies attached to the solid particles. Each of theses microcolonies has the form of a cylindrical plate with a predefined radius and thickness, and it is assumed that the increase in the number of microcolonies represents the growth of biomass. Model III, Biofilm Model, assumes that the surface of the solid particles is continuously covered by biofilm. The representation of these three models is presented in Figure 2-3. Baveye and Valocchi (1989) concluded that if one of the models can be successfully fit to the experimental data, the other two could also be fitted to the same experimental data.

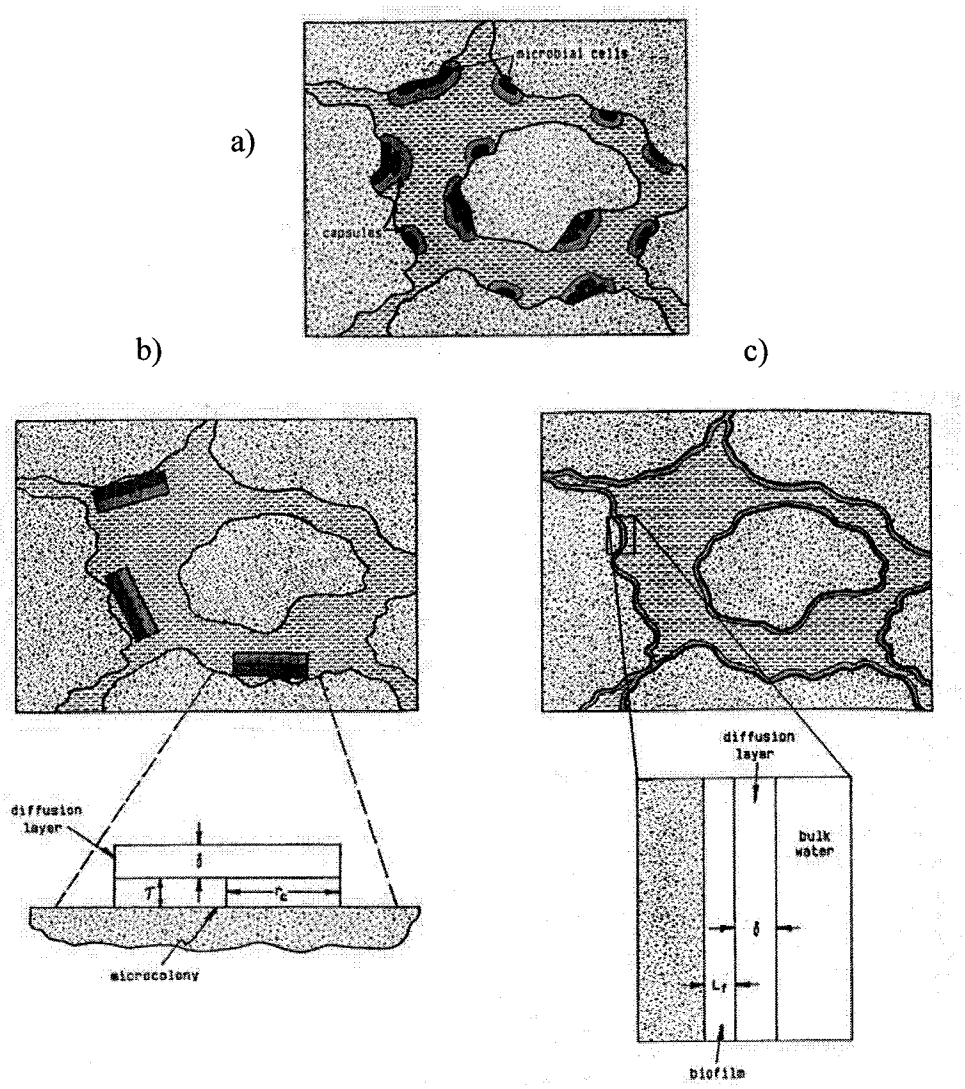

Figure 2-3: Representations of saturated porous medium as hypothesized in: a) Model I (Macroscopic Model); b) Model II (Microcolony Model); c) Model III (Biofilm Model); (Taken from Baveye and Valocchi 1989)

Clement et al. (1996) proposed a set of analytical expressions for the change in porosity, and permeability caused by biomass accumulation in unsaturated porous media. Their model does not assume any specific configuration for the microbial growth and is based on the Macroscopic Model. The reduction in porosity and permeability due to the bacterial growth is assumed to be caused by random accumulation of biomass in pore spaces. The model is based on either Van Genuchten or Brooks and Corey relationship

for the water saturation and capillary pressure head to obtain the pores size distribution. Clement et al. (1996) also compared the model result of their Macroscopic Model with the Biofilm Model of Taylor et al. (1990) and concluded that for the porous media with the pore size distribution index, λ, equal to 3, their model of porosity and permeability reduction agrees very well with Biofilm Model.

Taylor et al. (1990) proposed a model for permeability reduction due to microbial growth by manipulating the Biofilm Model and using the existing model for the relative permeability. They concluded that the permeability reduction based on the Mualem permeability model, and Kozeny-Carman permeability model predict realistic results to the problem of permeability reduction by a biofilm.

Molz et al. (1986) simulate microbial growth and degradation in saturated porous media by coupling five equations in developing the Microcolony Model. The five equations consist of two partial differential equations for substrate and oxygen transport governed by the advection-dispersion equation, and two nonlinear algebraic equations for substrate and oxygen consumption due to bacterial growth. The last equation is the modified Monod equation that considers the microbial growth, which is limited by a lack of either substrate, oxygen or both; and is expressed in terms of number of microcolonies per unit volume of porous media. The result of their model indicated that the highest amount of microbial growth always occurs at the substrate entrance to the porous media and the bacterial growth highly influences contaminant transport.

Thulliner et al. (2002) used pore network models as a tool to simulate the change of the hydraulic properties due to microbial growth in two different scenarios of bioclogging in pores. The first scenario assumed microbial growth in discrete colonies

clogging particular pores completely and the second one assumed microbial growth as a biofilm growing on the wall of each pore (Thulliner et al. 2002). In both scenarios, the hydraulic conductivity was reduced by at least two orders of magnitude, but for the colony scenario much less biomass was needed to reach the clogging and better agreement with previously published experimental data was found using the colony scenario model.

2.6 Modeling of Biological Growth Environment

Bazin et al. (1976) pointed out that most of the knowledge of the microbial interactions in soil is of their steady-state behaviour thus, there seems to be a need to study the transient phase more closely. Bazin et al. (1976) reviewed the existing microbial growth equations and suggested that the Monod equation is the most widely employed equation that can serve as a useful conceptual basis for the study of microbial growth. In the Monod equation, the biomass growth is modeled as follow:

$$\frac{\partial M_T}{\partial t} = M_T \mu_m \left(\frac{C}{K_s + C} \right) - b M_T \tag{2-6}$$

where, M_T is the biomass concentration, C is organic matter concentration, b is the first order biomass decay rate, and K_s is the half-velocity constant, defined as the substrate concentration at one-half the maximum specific substrate utilization rate and μ_m is the maximum specific growth rate of biomass. The maximum specific growth rate of biomass (μ_m) is related to the maximum specific substrate utilization rate (q_m) by the following equation.

$$\mu_m = Y q_m \tag{2-7}$$

where, Y is the yield coefficient for biomass and defined as cell mass produced per mass of substrate consumed.

The Monod equation can be modified according to the microorganism properties, the situation where more than one nutrient is available, and reaction type (e.g. substrate inhibition, non-competitive inhibition) (Bazin et al. 1976). The Monod parameters in the Monod equation are highly dependent to the bacterial species, the nature of growth, substrate and environmental conditions (Williamson and McCarty 1976a). Data collected in Table 1-1 indicates the variability of the Monod parameters that are used or suggested by researchers upon different growth conditions, environmental conditions and bacterial species.

Table1-1: Monod Kinetic parameters suggested and used by researchers

Reference	Summary of investigation	Contaminant or species	Monod kinetic parameters μ_m (1/ d)	Y	b (1/d)	K_S (mg/L)
Taylor and Jaffé (1990)	Used the Monod equation to model the transport of substrate and biomass in saturated porous media. Obtained from Literature.	----	7.7	0.0975	0.0275	0.799
El-Farhan et al.(1998)	Modeled transport and biodegradation of Toluene under unsaturated conditions. Monod parameters are calibrated to fit the experimental data	Toluene	3.22	0.35	1.43	1.95
Liu et al.(2005)	Investigated the aerobic granular sludge in a glass sequencing batch reactor	Synthetic wastewater (glucose as a primary carbon source)	13.2	0.183-0.25	0.023-0.075	275.8
Molz et al. (1986)	Developed a model for simulating microbial growth-degradation process in porous media. The Monod parameters are obtained from Literature.	---	4.34	0.278	0.02	120
Kurian et al. (2006)	Conducted respirometric aerobic experiments at 40° C to determine Monod kinetic parameters of aerobic biomass in a membrane-coupled bioreactor.	Acetate	13.1±0.68	0.29±0.02	0.23±0.01	180.6±14.2
		Propionic acid	7.53±1.99	0.29±0.03	0.23±0.01	271±32.6
		Rendering wastewater	4.11±0.57	0.2±0.01	0.14±0.02	806±192
Vogelaar et al.(2003)	Determined Monod kinetic parameters of mesophilic(30° C) and thermophilic(55° C) aerobic biomass in continious and batch experiments .	Mesophilic	11.52±2.64	0.096	0.5	9±2
		Thermophilic	17.04±2.16	0.408	0.5	3±2

2.7 SUMMARY

It appears that a greater understanding of the effect of bacterial growth on the hydraulic performance and treatment mechanism in biofilters as an unsaturated porous media is needed. In the literature review, many of the studies are undertaken in sandy media; obviously soils are highly variable and more research across a range of soil types would benefit our understanding of the hydraulic and clogging process occurring in biofilters.

Determining the appropriate values, of growth and decay parameters in the Monod equation, due to their dependence to the environmental conditions, is rather difficult. There is still a need for research to evaluate the effect of Monod parameters on the biomat development. This would be a useful advance in understanding the long-term performance of biofilters.

CHAPTER 3 -UNSATURATED FLOW MODEL DEVELOPMENT

3.1 VERTICAL DISTRIBUTION OF GROUND WATER

The soil which extends from the water table to the surface of the ground is divided into different zones in terms of the saturation level. Figure 3-1 indicates the main divisions of subsurface water. The capillary zone (capillary fringe) extends from the water table up to the limit of the capillary rise of water. Capillary rise of water varies inversely with the pore size and directly with the surface tension. In this zone the pores are practically saturated. Above the capillary zone, there is a gradual decrease in water content with elevation and this zone is referred to as unsaturated zone. The vadoze zone (aeration zone) is the soil zone above the water table where the pore water pressure is negative. The soil-water zone forms the top portion of the vadoze zone and extends from the ground surface down through the major root zone.

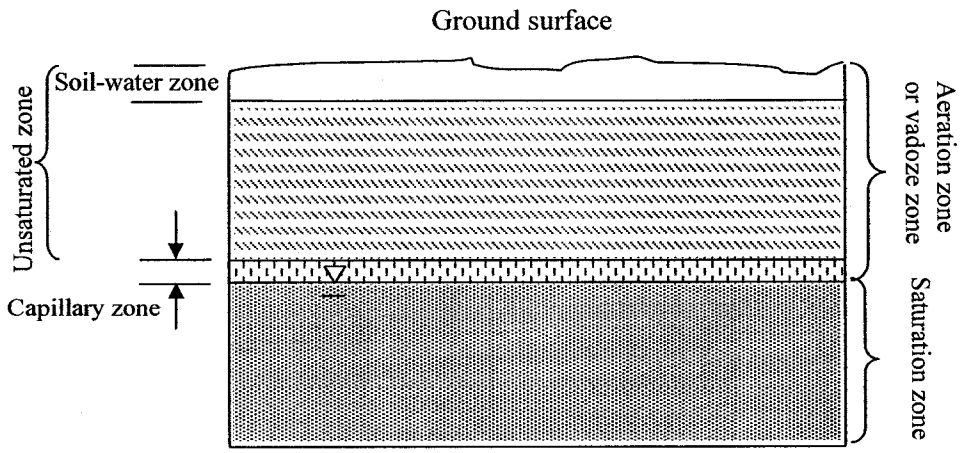

Figure 3-1: Vertical zone of subsurface water

3.2 SATURATED VS. UNSATURATED FLOW CONCEPT

Volumetric water content, θ, is defined as the volume of water per unit volume of soil. Since water saturation, S_w, is equal to the volume of water per unit volume of void space, the relationship between θ and S_w is:

$$\theta = \varphi S_w \tag{3-1}$$

where φ is the soil porosity.

In the saturated zone which occurs beneath the water table, the porosity, which is expressed as the ratio of the volume of voids to the total volume, is a direct measure of volumetric water content. The fundamental equation for flow in saturated porous media is based on Darcy's law. In 1856, Henry Darcy concluded that the rate of flow is directly proportional to the hydraulic head gradient and inversely proportional to the length of the column (Bear 1979).

$$q = \frac{Q}{A} = -K_{sat}\frac{\partial h}{\partial L} \tag{3-2}$$

where Q is the flow rate, A is the cross-sectional area, K_{sat} is the saturated hydraulic conductivity of the porous medium and h is the total head (piezometric head or hydraulic head), which is the sum of the elevation head (z) and the water pressure head (h_w):

$$h = z + \frac{P}{\gamma} = z + h_w \tag{3-3}$$

Where, P is the water pressure and γ is the specific weight of water. It is important to distinguish the specific discharge, q, with the average velocity (seepage velocity). In Eq.3-2, the Darcy velocity, q is actually a discharge per unit bulk area of porous media face, and is often referred to as specific discharge (Zheng and Bennett 1995). Since the flow takes place only through the porous part of the medium (pore volume) and the

remaining part is filled with the solid phase, the area available to flow is φ A. Therefore, the average velocity of the flow through the pores is:

$$V = \frac{Q}{\varphi \mathrm{A}} = \frac{q}{\varphi} \tag{3-4}$$

To help explain the flow in the unsaturated zone, the pores can be idealized as a series of capillary tubes with different radii representing different pore sizes. Water is held in the unsaturated zone mainly by surface tension or capillary pressure. Capillary pressure varies inversely with the pore size and directly with the surface tension and is defined as the difference between the pressure of air and water in the unsaturated zone.

$$P_c = -\frac{2\sigma}{\gamma \mathrm{r}} = h_a - h_w \tag{3-5}$$

Often air pressure (h_a) is assumed to be negligible in unsaturated soil and hence:

$$P_c = -h_w \tag{3-6}$$

where P_c is capillary pressure head, σ is the surface tension and r is the radius of capillary tubes.

The capillary pressure generally increases upward from the water table and results in a decrease in water content. Figure 3-2 is a typical soil moisture curve in the unsaturated zone where, under the static conditions, the water content decreases with the height above the water table.

Since, in a partially saturated porous medium, only the pores that contain some water can conduct fluid, the same flow equation can be applied to the unsaturated soil by taking into the account the effect of saturation on the hydraulic properties of the soil.

$$q = \frac{Q}{A} = -K(\theta)\frac{\partial h}{\partial L} \tag{3-7}$$

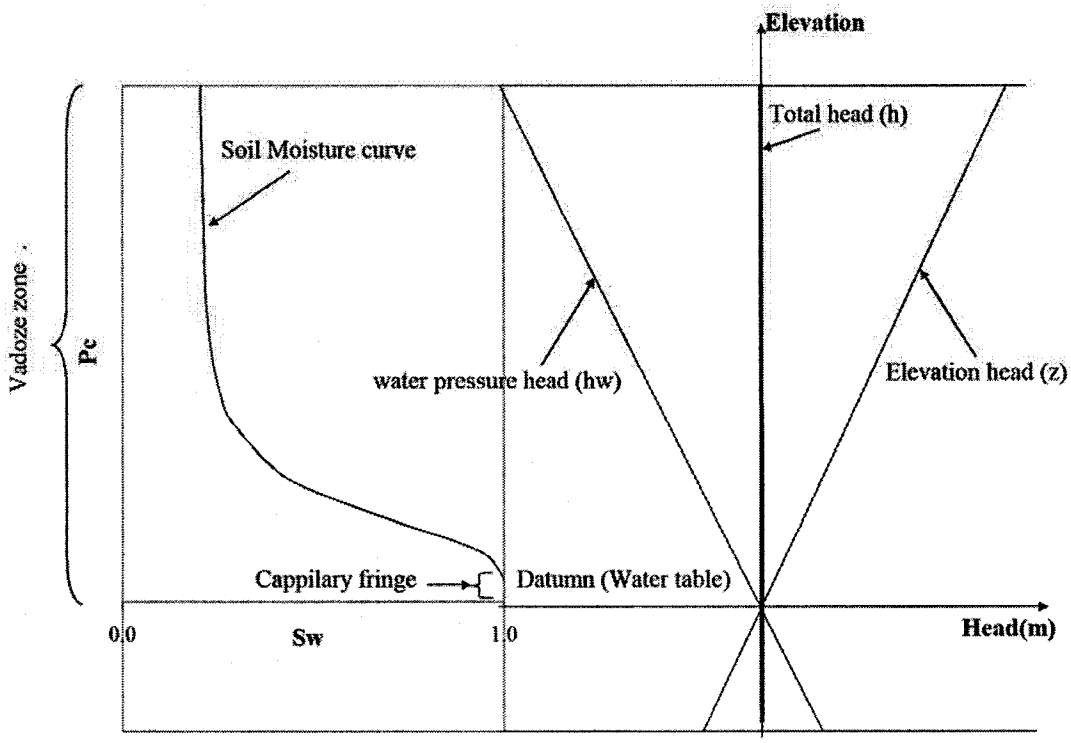

Figure 3-2: A typical soil moisture curve

$K(\theta)$ is the unsaturated hydraulic conductivity as a function of volumetric water content and can be expressed as:

$$K(\theta) = K_{sat}\, K_r \tag{3-8}$$

where K_r ($0 \le K_r \le 1$) is the relative permeability term and is a function of water content. The relative permeability of the medium follows a curve which is similar to the soil saturation curve. When drying or drainage of an initially saturated medium starts, first the largest pores start draining because the capillary pressure of these pores is lower than the other pores. As a result, the relative permeability experiences a sharp drop at first, followed by a more gradual decline with increasing values of suction head. The seepage velocity in unsaturated soil is also impacted by the water content as is given by:

$$V = \frac{q}{\theta} = \frac{q}{S_w \phi} \tag{3-9}$$

3.3 HYDRAULIC PROPERTIES OF UNSATURATED SOIL

The hydraulic properties of unsaturated soil are characterized by the soil water characteristic curve (soil moisture curve) and the hydraulic conductivity function. Soil water characteristic curve relates the saturation or volumetric water content to the capillary pressure and the hydraulic conductivity function expresses the dependence of unsaturated hydraulic conductivity on the saturation or capillary pressure. A number of equations for approximating these relationships, which can be found in the literature, are briefly described in the following text.

In 1953, Burdine developed a model for calculating the relative permeability from pore size distribution data. His model assumes the porous medium as a bundle of capillary tubes, and therefore the equation calculates the total flow by obtaining the flow of each tube using the Darcy and Poiseuille laws.

$$K_r(S_e) = S_e^2 \frac{\int_0^{S_e} \frac{dS_e}{P_c^2}}{\int_0^1 \frac{dS_e}{P_c^2}} \tag{3-10}$$

where $K_r(S_e)$ is the relative permeability, P_c is the capillary pressure and S_e is the effective saturation.

$$S_e = \frac{\theta - \theta_r}{\theta_{sat} - \theta_r} = \frac{S_w - S_r}{1 - S_r} \tag{3-11}$$

θ_r, S_r are the irreducible water content and irreducible saturation, respectively. The irreducible saturation represents a thin layer of water which covers the solid particles of soil and can not be extracted easily.

In 1976, Mualem proposed a new simplified model which was more reliable than the existing models at the time and improved the prediction of hydraulic conductivity.

$$K_r(S_e) = S_e^{\frac{1}{2}} \left[\frac{\int_0^{S_e} \frac{dS_e}{P_c}}{\int_0^1 \frac{dS_e}{P_c}} \right]^2 \tag{3-12}$$

The model proposed by Mualem can be easily reduced to a closed form solution using the P_c-θ relationship given as an analytical equation.

In 1964, Brooks and Corey proposed a relationship between P_c and S_e in order to obtain the closed-form expression for predicting the hydraulic conductivity. The schematic of their relationship is presented in Figure 3-4.

$$S_e = \left(\frac{P_c}{P_b} \right)^{-\lambda} \tag{3-13}$$

where λ is an index which characterizes the pore-size distribution and P_b, is the bubbling pressure which is a measure of the maximum pore size that can form a continuous network of flow paths within the medium (Brooks and Corey, 1964). λ is a number greater than zero. A small value represents a well graded porous media with a wide range of pore sizes and a large value represents a relatively uniform pore size. Figure 3-3 is the typical shape of P_c-S_e curve based on the Brooks and Corey approximation.

Based on Eq.3-13, Brooks and Corey (1964) utilized the Burdine formula and presented a close form expression for predicting the hydraulic conductivity.

$$K_r(S_e) = S_e^{\frac{2+3\lambda}{\lambda}} \tag{3-14}$$

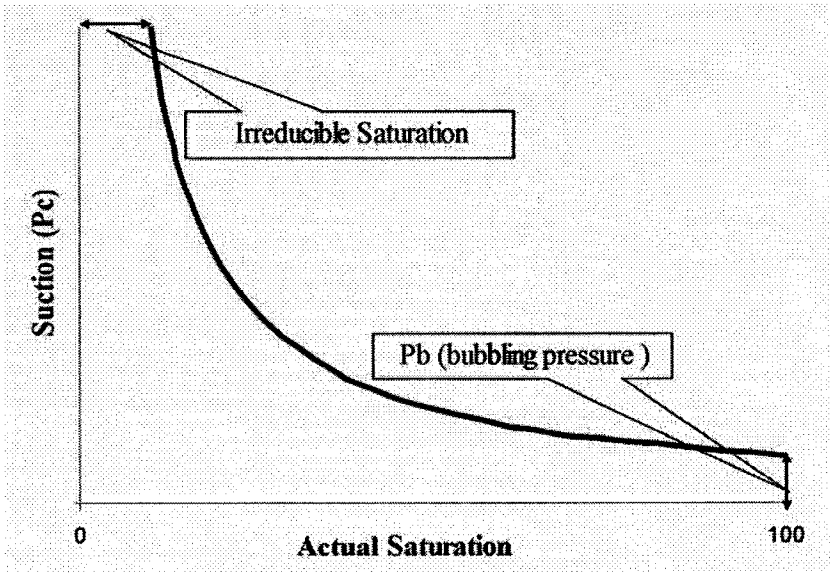

Figure 3-3: A typical P_c-Se approximation by Brooks and Corey

In 1980, Van Genuchten proposed a new analytical solution for P_c-S_e relationship which he indicated to be more accurate than Brooks and Corey relationship.

$$S_e = \left[1 + (\alpha \cdot P_c)^n\right]^{-m} \tag{3-15}$$

where P_c is always positive, α and n are fitting parameters. One can obtain α and n by fitting the equation on the experimental data. m is defined as follows according to the formula being used for the hydraulic conductivity prediction.

For Mualem model: $m = 1 - \frac{1}{n}$

For Burdine model: $m = 1 - \frac{2}{n}$

Equation 3-15 defines S_e and P_c relationship as a S-shape curve where n reflects the slope of the transition and α reflects the height of the curve (Figure3-4). The higher n value makes the transition part flatter, which represents uniformly graded sands or gravels, and the higher α shifts the curve downward, which would be the better representation of soils with larger pores.

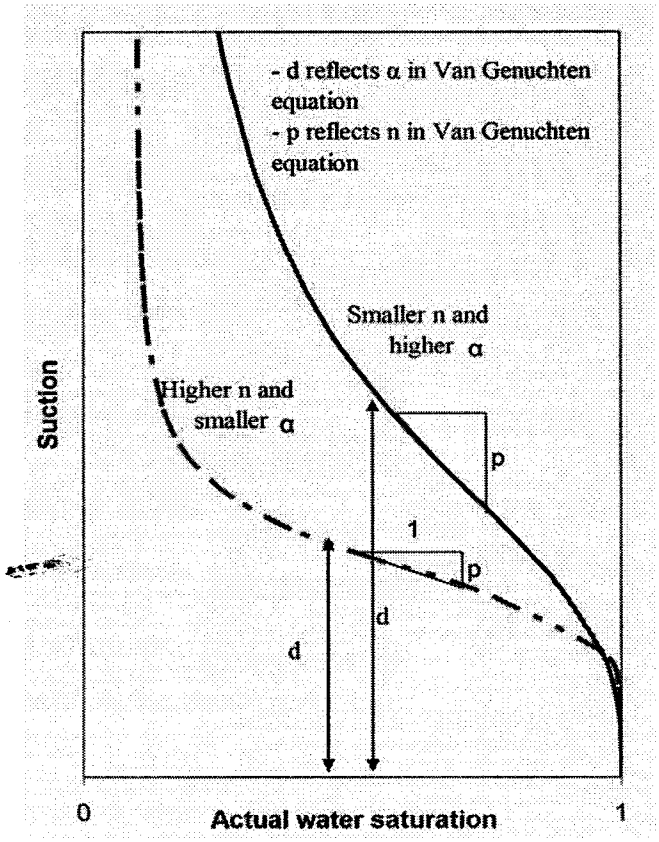

Figure 3-4: n and α relation with the shape of soil moisture curve

Van Genuchten also derived closed-form analytical expressions for the relative permeability, K_r, by using the predictive conductivity models of Burdine and Mualem using his P_c-S_e relationship (Eq.3-15).

Based on Burdine: $$K_r(S_e) = S_e^2\left(1-(1-S_e^{1/m})^m\right) \tag{3-16}$$

Based on Mualem: $$K_r(S_e) = S_e^{1/2}\left(1-(1-S_e^{1/m})^m\right)^2 \tag{3-17}$$

3.4 GOVERNING EQUATIONS

In a two dimensional problem Darcy velocity is expressed as a vector which has two components in x and y directions through the relation:

$$\mathrm{q} = q_x\,\hat{\mathrm{i}} + q_y\,\hat{\mathrm{j}} \tag{3-18}$$

where $\hat{i}$ and $\hat{j}$ are conventional unit vectors in x and y directions and:

$$q_x = -K_x(\theta)\frac{\partial h}{\partial x} \qquad \text{where, } K_x(\theta) = K_{x,sat}K_r \tag{3-19}$$

$$q_y = -K_y(\theta)\frac{\partial h}{\partial y} \qquad \text{where, } K_y(\theta) = K_{y,sat}K_r \tag{3-20}$$

For an isotropic medium, $K_{x,sat} = K_{y,sat}=K_{sat}$, so:

$$K_x(\theta) = K_y(\theta) = K_{sat}K_r \tag{3-21}$$

By using the basic Darcy's law and considering an equation of continuity that describes the conservation of fluid mass in a porous medium, the partial differential equation of flow can be obtained. The law of conservation of mass for transient flow requires that the net rate of fluid mass flow into any element be equal to the rate of change of fluid mass storage within the element (Figure 3-5).

Net rate of fluid mass flow element = Flow coming in –Flow going out

$$= -\frac{\partial(\rho q_x)}{\partial x} - \frac{\partial(\rho q_y)}{\partial y} \tag{3-22}$$

$$\text{Change in fluid mass storage within the element} = \rho\frac{\partial\theta}{\partial t} \tag{3-23}$$

where ρ is the water density. By substituting the Darcy flux in the Eq.3-22 and placing the net rate of mass flow equal to the rate of storage and dividing the equation by ρ, the unsaturated flow equation would be:

$$\frac{\partial(\theta)}{\partial t} = \frac{\partial}{\partial x}(K_r K_{sat}\frac{\partial h}{\partial x}) + \frac{\partial}{\partial y}(K_r K_{sat}\frac{\partial h}{\partial y}) \tag{3-24}$$

Eq.3-24 has two unknowns, total head (h) and volumetric water content (θ). By using the relationship between P_c and θ, and accounting for elevation head, Eq.3-24 will be converted into a form where the independent variable is either h or θ. It is noted that in

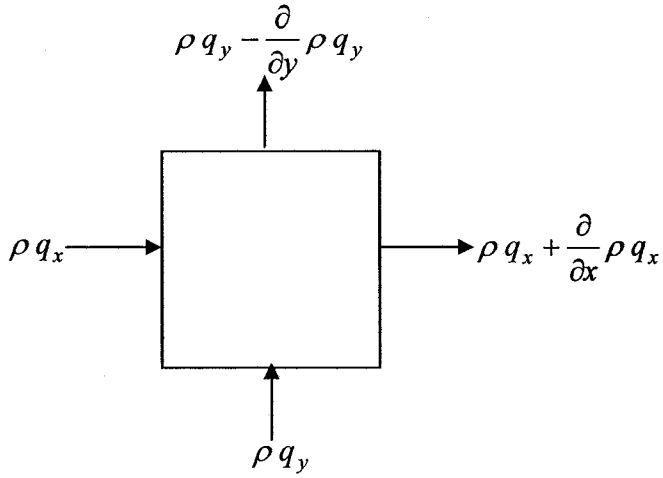

Figure 3-5: Element model for flow through porous media

this research the flow equation was solved based on the total head. Appendix A shows how the flow equation is converted into a form where the independent variable is the total head.

3.5 NUMERICAL SOLUTION

The finite element method (FEM) was used to find the approximate solution of the partial differential equation for the fluid flow. The partial differential flow equation is implemented in a two-dimensional time dependent finite element engine called Condur. Condur solves the generic boundary value problem described as:

$$E_x(\frac{\partial^2\Phi}{\partial x^2}) + E_y(\frac{\partial^2\Phi}{\partial y^2}) + \nu_x(\frac{\partial\Phi}{\partial x}) + \nu_y(\frac{\partial\Phi}{\partial y}) - G\Phi + R = f\,c\frac{\partial(\Phi)}{\partial t} \qquad (3\text{-}25)$$

where Φ is the field variable of interest and E_x, E_y, ν_x, ν_y, G, and R are the coefficients that are defined by considering the material properties of the domain and the actual partial differential equation. In terms of flow equation, total head, h, is the field variable; E_x and E_y are the hydraulic conductivity of soil; ν_x, ν_y, and G are zero, and f and c are

pre-transient terms that are defined in Appendix A. Condur reads an input file in a specific order that contains all the coefficients and provides an output file once the finite element analysis is complete.

3.5.1 Method of Solving Flow Equation

The analysis starts with the definition of the geometry of the problem, the specification of soil properties, such as n, α, φ and K_{sat}; and the introduction of the initial boundary conditions of the domain. The flow equation written based on the total head is a nonlinear equation. Generally, the solution scheme goes through a trial and error process in which the initial estimate of the solution will be refined through a series of iterations. Figure 3-6 represents the flowchart of a part of complete model for solving the flow equation.

3.5.2 Boundary and Initial Conditions

In order to use a numerical technique for solving the partial differential equation, an initial condition as well as a boundary condition has to be assigned to the domain. The initial condition is the value of the field variable at the starting time within the domain (in the case of flow equation, the magnitude of the total head at each node).

$$h(x,y,t=0)=h_i \tag{3-26}$$

For all x and y inside the domain, h is the known function.

Two types of boundary conditions are encountered for flow through porous media; prescribed head and flux boundary condition. In the case of a prescribed boundary, the head of h_i is prescribed for node i on that boundary.

$$h(x,y,t)=h_i \quad \text{on the boundary} \tag{3-27}$$

In terms of flux boundary condition, the flux normal to the boundary surface is prescribed for all nodes. It means that for the flow equation, the gradient of total head is known.

$$h(x,y,t) = -K(\theta)\, grad(h_i) = q_i \tag{3-28}$$

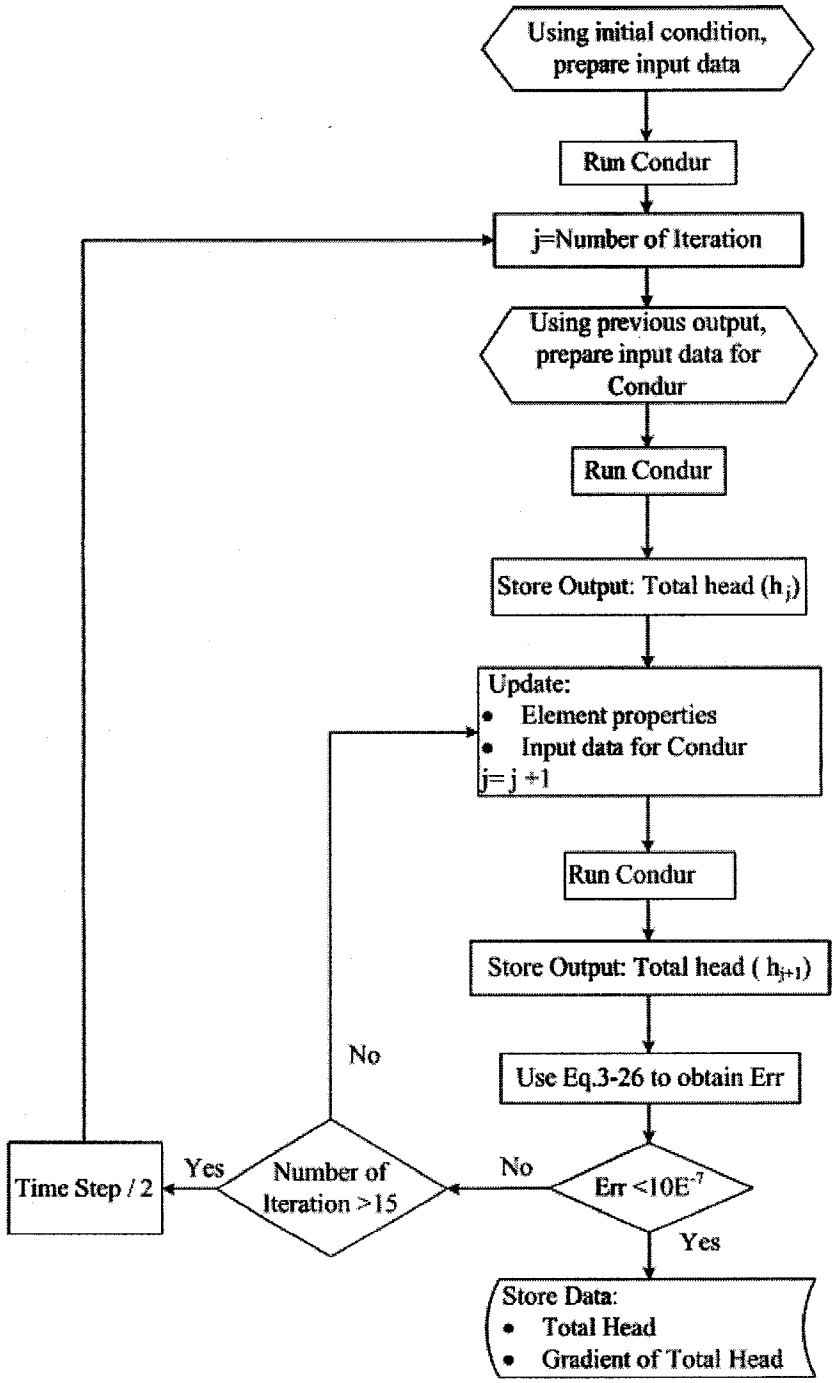

Figure 3-6 : Flowchart for solving flow equation

The developed model can incorporate several stress periods in which the value of the boundary condition can change. If the value for boundary condition changes, the model will enter a new stress period.

3.5.3 Convergence Criterion

Since the flow equation is a nonlinear equation, a solution technique is needed to refine the initial estimate of each iteration. There are several methods for attaining the convergence in the numerical solution of nonlinear differential equations including direct substitution method, modified direct substitution method, the Newton-Rapson method or modified Newton-Rapson method. Since the severity of nonlinearity is not known for the flow equation, first the modified direct method or direct method is tried for solving the flow equation. In the direct substitution method, a solution is calculated from the previous value assuming a linear system. At the end of each solution the material properties are updated based on the previous iteration results and the calculated nodal values are compared with the previous iteration by considering the convergence criterion. The iterations are terminated when the criterion is satisfied as follow.

$$\Delta_j h = \frac{\sum_{k=1}^{nodes} ({}_{j-1}h_k - {}_j h_k)^2}{\sum_{k=1}^{nodes} ({}_j h_k)^2} \le Err \qquad \text{where } Err=10^{-7} \tag{3-29}$$

where h is the total head, j is the iteration number and k is the node number. In the modified direct substitution method, the material properties are updated based on a portion of two previous solutions and the calculated values are compared with the previous calculation by using the same convergence criterion.

$$ {}_{j}h_k = \phi \ {}_{j-1}h_k + (\phi - 1) \ {}_{j-2}h_k \tag{3-30} $$

where ϕ is a factor ($0 \le \phi < 1$) that defines the contribution amount of the two previous iterations in obtaining the next value for the next iteration.

3.6 FLOW EQUATION CODE VERIFICATION

The flow equation code is verified by checking that the mass is conserved using a mass balance approach and also by comparing the model results against two sets of experimental data obtained from the literature (Touma and Vauclin 1986, Lenhard et al. 1991). Those two verification cases were selected because they include different boundary conditions. The verification simulations are conducted using the element size of 1cm by 1 cm for the entire soil column and time step and time marching of 10 and 1 second, respectively.

3.6.1 Mass Balance Approach

As it was discussed earlier, the flow equation is obtained by writing the equation of continuity or conservation of fluid mass in each element. Hence the accumulation of mass in the domain at any time should be equal to difference of mass coming into the domain and mass going out of the domain at that time:

Accumulation = Mass In- Mass Out

where, according to Figure 3-7 and considering element i, j for the formulation:

$$ \text{Accumulation} = \rho_w \left(\theta_{i,j}^{t+\Delta t} - \theta_{i,j}^{t}\right) \Delta x \, \Delta y \, \Delta z \tag{3-31} $$

Mass entering element i, j:

$$\Delta t\,(q_{In,x} + q_{In,y} + source) = \Delta t \left\{ K(\theta)_{i,j-1} \left(\frac{\Delta h}{\Delta x} \right)_{i,j-1} \Delta y\, \Delta z + K(\theta)_{i-1,j} \left(\frac{\Delta h}{\Delta y} \right)_{i,j-1} \Delta x\, \Delta z + q\, \Delta x\, \Delta y\, \Delta z \right\} \tag{3-32}$$

Mass exiting element i, j:

$$\Delta t\,(q_{Out,x} + q_{Out,y}) = \Delta t \left\{ K(\theta)_{i,j} \left(\frac{\Delta h}{\Delta x} \right)_{i,j} \Delta y\, \Delta z + K(\theta)_{i,j} \left(\frac{\Delta h}{\Delta y} \right)_{i,j} \Delta x\, \Delta z \right\} \tag{3-33}$$

The mass balance error, expressed as a percentage, that is given to the user for any time is calculated as follows:

$$\text{Mass balance error} = \frac{\text{Mass entering the domain - Mass exiting the domain - Accumulation}}{\text{Initial mass within the domain}} \times 100 \tag{3-34}$$

A lower mass balance error indicates improved model results in terms of conservation of mass.

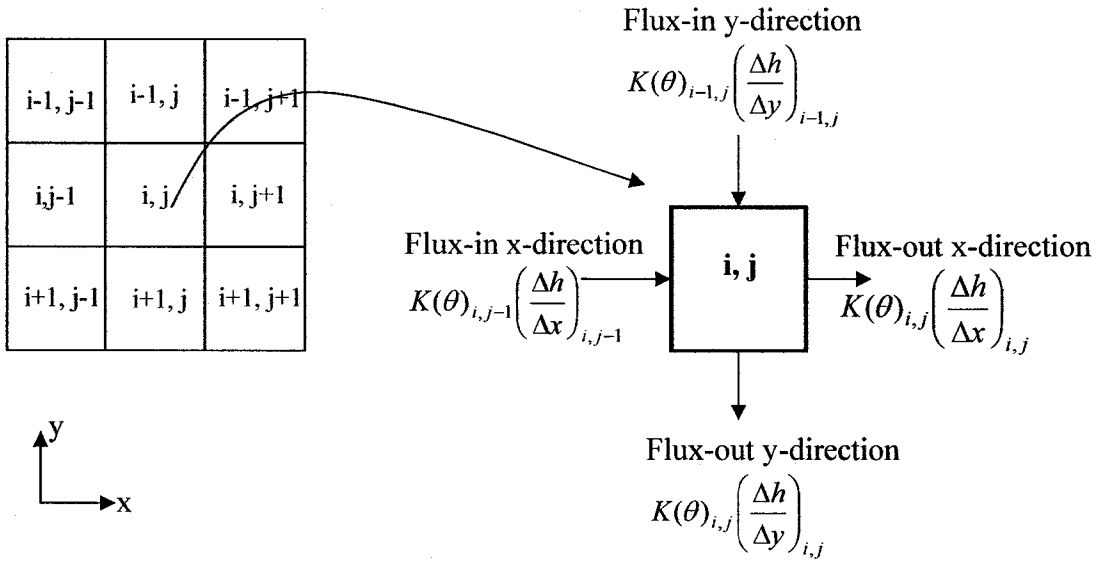

Figure 3-7: Schematic representation of element arrangement in a two-dimensional media

3.6.2 Case 1: Two-Phase Infiltration

The study of Touma and Vauclin (1986), on the effect of partially saturated soil on the process of water infiltration, is used to verify the developed flow equation code. Touma and Vauclin (1986) conducted several experiments on a sandy soil column to investigate how a constant flux infiltrates into a partially saturated soil. They also checked the validity of their developed finite difference code for two phase flow using their experimental data. The input data that were used in their model and are used for the verification of current code is shown in Table 3-1.

Table 3-1: Parameters used in the verification test of sand soil

Parameter	Value
θ_r	0.0265
K_{sat}(cm/s)	0.00428
φ	0.312
α	0.044
n	2.2
m	0.54
Column height (cm)	100
Flux top boundary condition-q $_w$ (cm/s)	0.00231
Prescribed bottom boundary (cm)	-9.9

Touma and Vauclin (1986) applied the relationship derived by Van Genuchten for the P_c-S_e relationship (Eq.3-15) and obtained relative permeability value by using the instantaneous profile method to the transient infiltration data. A slight difference is seen in the result of their model and the current model due to the slightly different way of calculating the hydraulic conductivity value. Mostafa (2004) and Kennedy (1998) have

also used the same soil properties listed in Table 3-1, in order to verify their respective codes with Touma and Vauclin (1986). They modeled unsaturated flow equation using the finite difference method and used the same approach to obtain hydraulic conductivity as is used in the present study. The result of Touma and Vauclin (1986), Mostafa (2004) and Kennedy (1998) are demonstrated in Figures 3-8, 3-9 and 3-10 respectively and the result of present code are illustrated in Figure 3-11. The good agreement between the results indicates that the present code was implemented properly.

Touma and Vauclin (1986) have indicated that the steady-state water content profile near the surface for their model agreed very well with the theoretical one by:

$$q_w(0,t) = K(S_{el}) \tag{3-35}$$

where S_{el} is the effective saturation at the steady state condition. Present model also validates the above statement by using the Van Genuchten relationship of the hydraulic conductivity (Eq.3-16 and Eq.3-17).

The results of mass balance for the above simulation is very close to zero, 0.075% after 2 hours, which also confirms that the flow equation is coded properly.

3.6.3 Case 2: Variable Water Table

Lenhard et al. (1991) conducted the air-water flow experiment in a 72-cm vertical soil column with the fluctuating water table (Figure 3-12). They measured the experimental water content and the water pressure at seven elevations in the column (i.e. 70, 60, 50, 40, 30, 20 and 10 cm, where 0 cm corresponds to the base of the column). They used their experimental data to validate their model for the two-phase permeability-saturation-pressure relations in unsaturated fluid flow. In their proposed model, the S_e-P_c relationship is described by the Van Genuchten soil retention function, and Mualem's

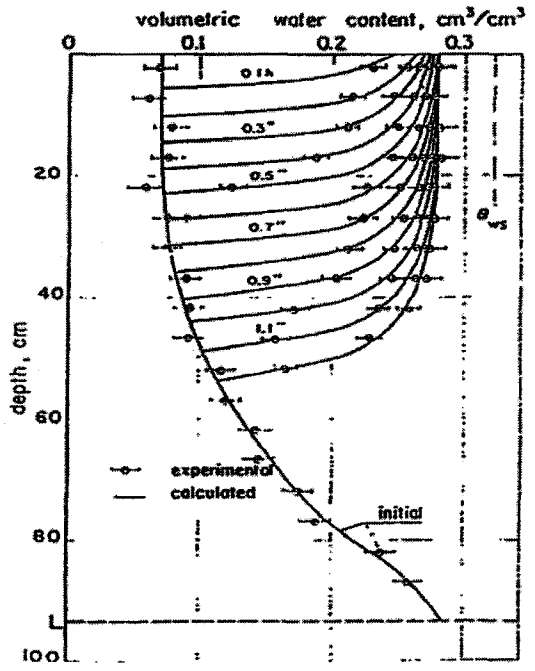

Figure 3-8: Saturation profile result using parameters given in Table 3-1 (Taken from Touma and Vauclin 1986)

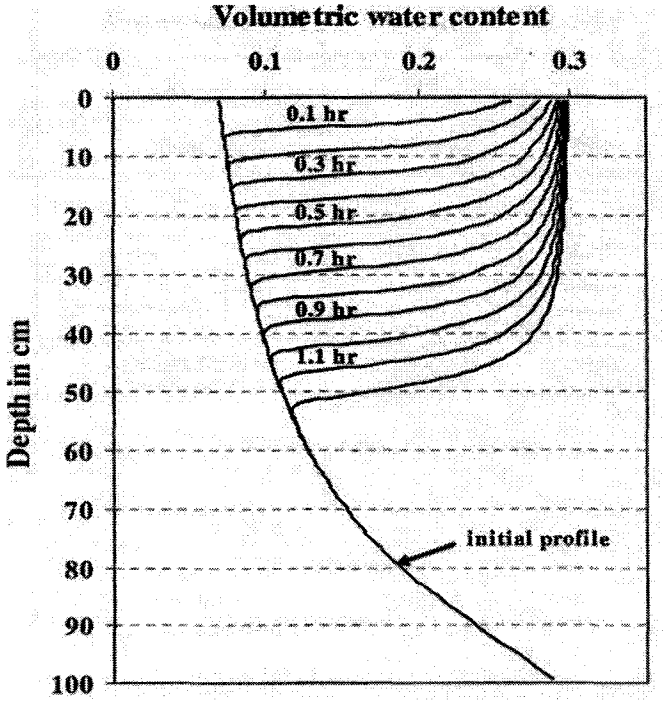

Figure 3-9 : Saturation profile result using parameters given in Table 3-1 (Taken from Mostafa 2004)

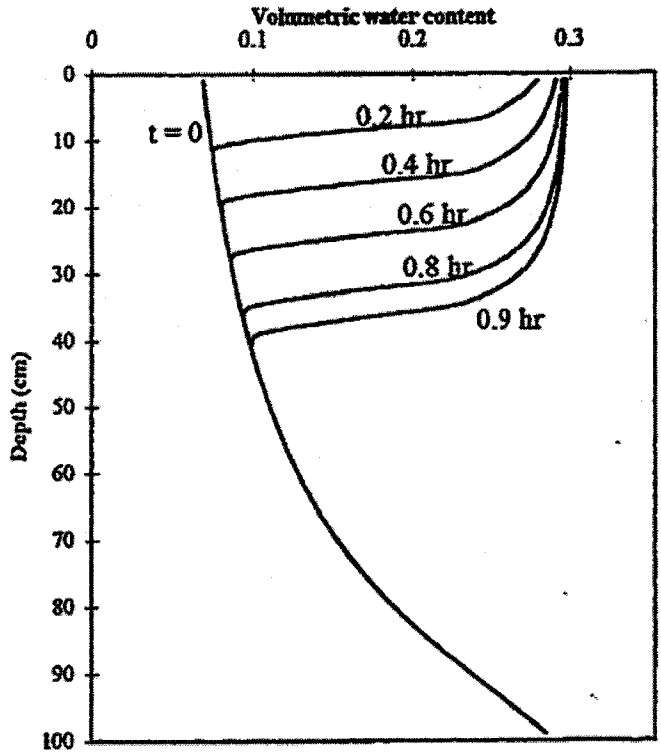

Figure 3-10: Saturation profile result using parameters given in Table 3-1 (Taken from Kennedy 1998)

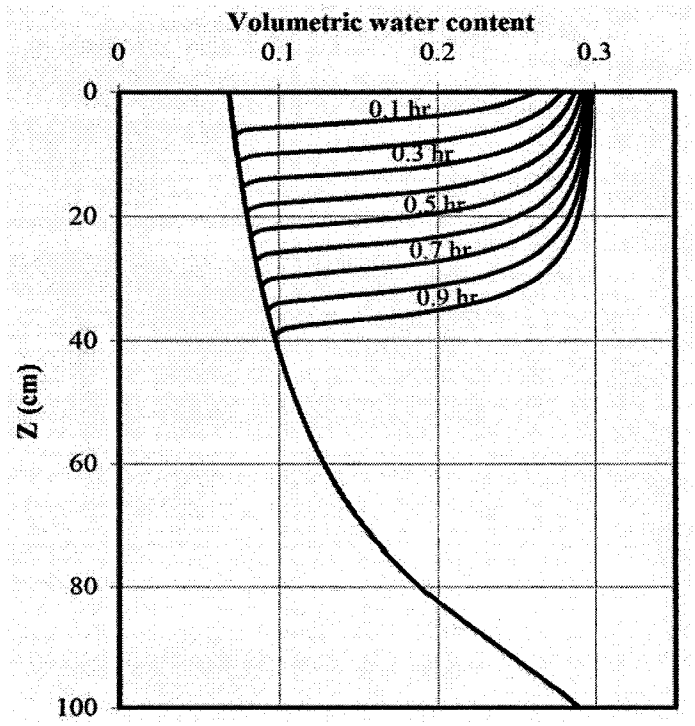

Figure 3-11: Saturation profile result of the present model using parameters given in Table 3-1

relative permeability model. Table 3-2 contains the values of the parameters they used for their simulation. The bottom boundary condition was a prescribed pressure that varied as indicated in the Figure 3-12.

The measured and predicted water saturation obtained by Lenhard et al. (1991) and the results from the model developed for this research can be found in Figures 3-13 and 3-14, respectively.

Table 3-2: Parameters used in Lenhard et al. (1991)

Parameter	Value
θ_r	0.0612
K_{sat}(cm/s)	0.00331
φ	0.36
α	0.042
n	5.25
Column height (cm)	72
Prescribed bottom boundary condition (cm)	Refer to Fig. 3-13

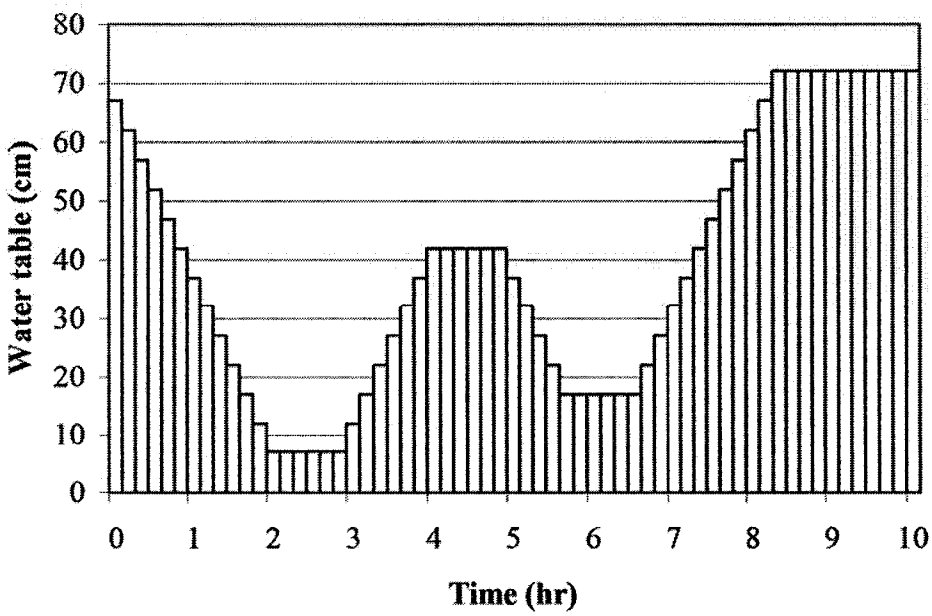

Figure 3-12: Water pressure at the base of column for the verification of case 2

Similarity of the non-hysteretic results reported by Lenhard et al. (1991) and the current model verifies that the equations were coded properly in the current study.

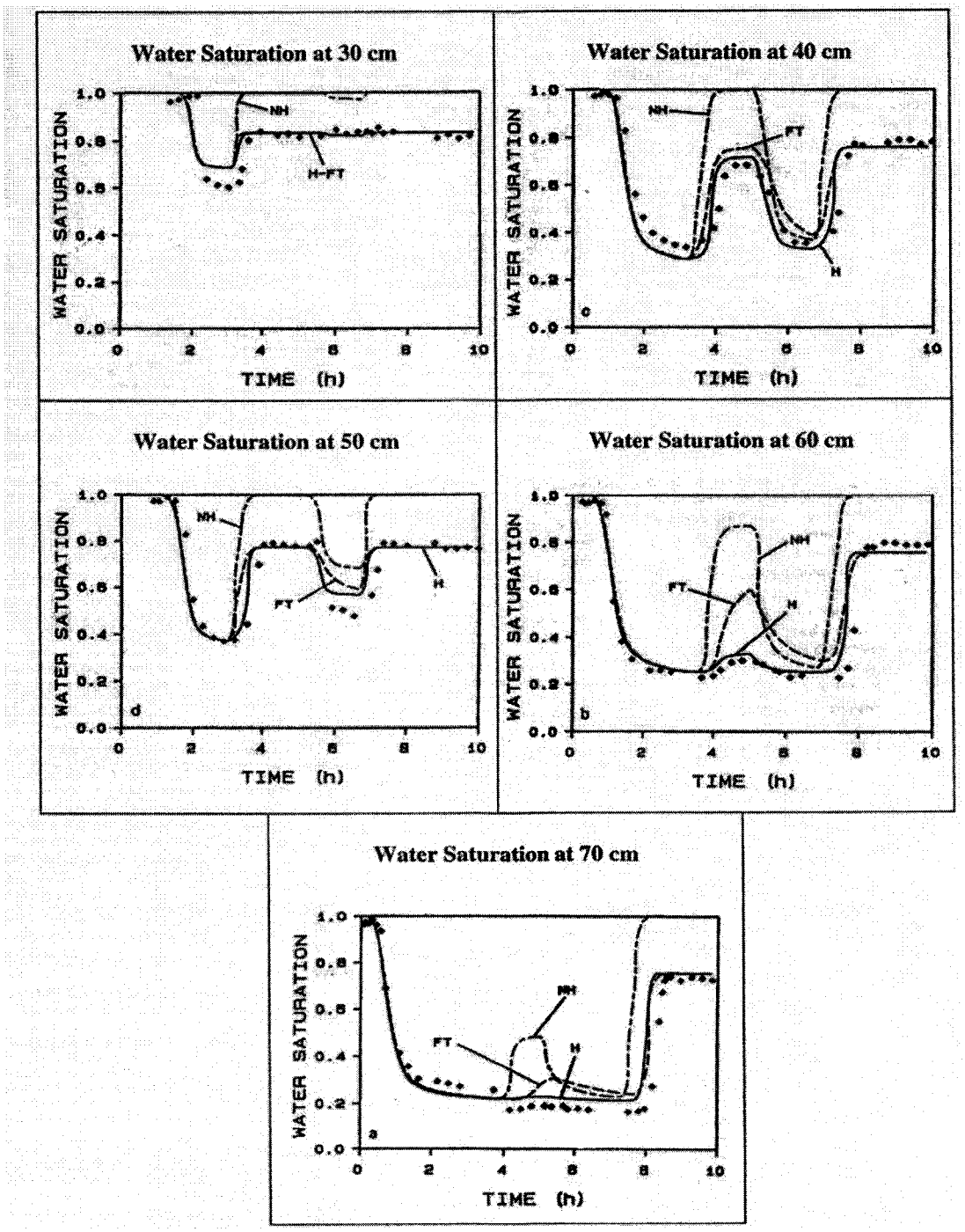

Figure 3-13: Water saturation results of Lenhard et al. (1991) for both non-hysteretic (NH) and hysteretic (H) solutions (Taken from Lenhard et al. 1991)

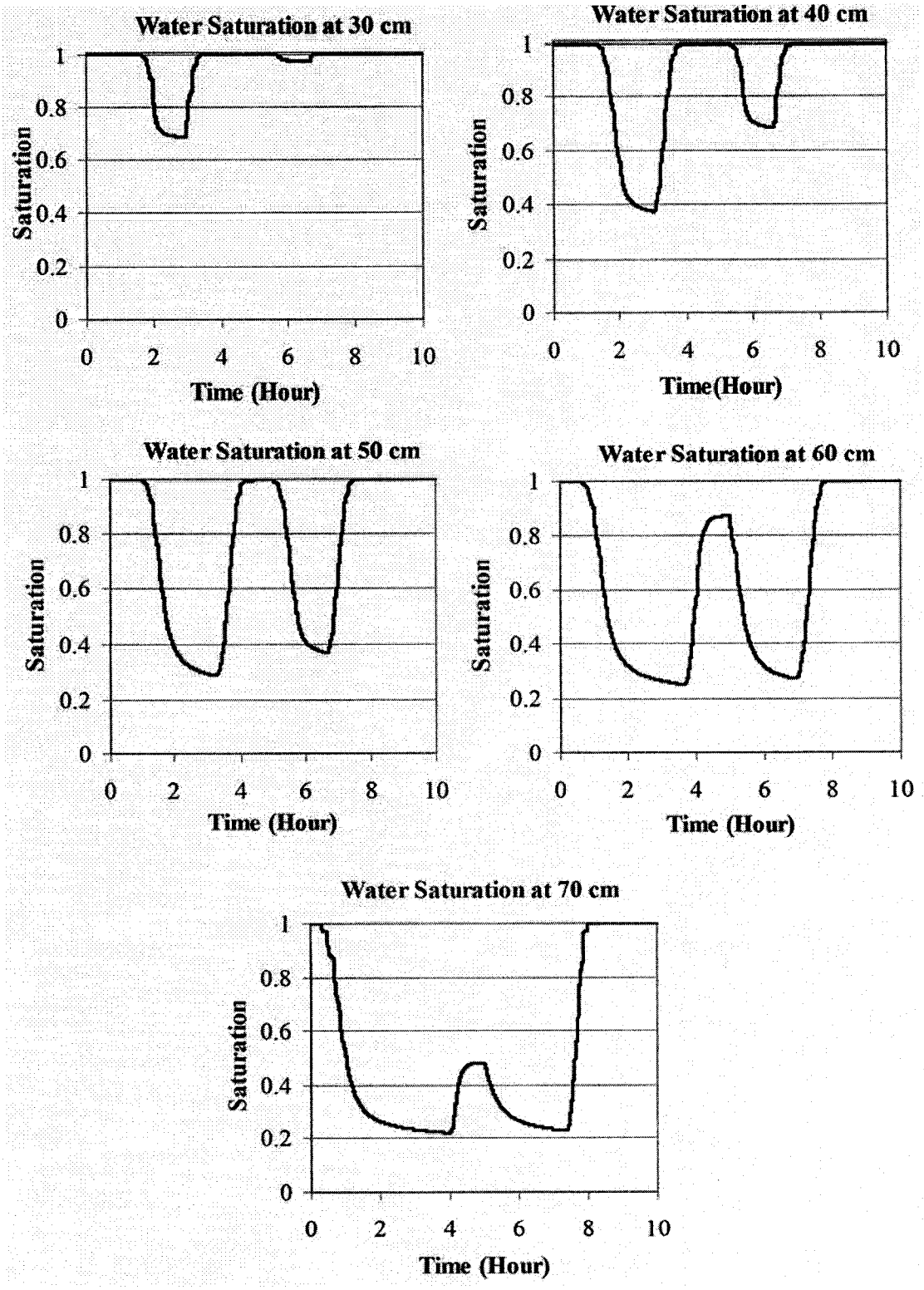

Figure 3-14: Water saturation results of the current model

CHAPTER 4 -CONTAMINANT TRANSPORT EQUATION AND COMPLETE MODEL DEVELOPMENT

4.1 CONTAMINANT TRANSPORT EQUATION

The advection-dispersion transport equation is applied to account for the transport of dissolved organic matter through porous media. When organic matter enters the porous media, it will migrate due to the movement of the water and disperses due to hydrodynamic mixing and molecular diffusion. The migration also may be impacted due to biodegradation. A complete transport equation can be written by adding the dispersive flux terms to the advective flux and a sink term. The sink term accounts for the reduction of organic matter due to the bacterial consumption or biodegradation. The two-dimensional advection-dispersion equation with decay in steady-state uniform flow is:

$$\frac{\partial C}{\partial t} = \frac{\partial}{\partial x}\left(D_x \frac{\partial C}{\partial x}\right) - V_x \frac{\partial C}{\partial x} + \frac{\partial}{\partial y}\left(D_y \frac{\partial C}{\partial y}\right) - V_y \frac{\partial C}{\partial y} - R_S \qquad (4\text{-}1)$$

where D_x and D_y are the dispersion coefficients in the x and y directions, respectively. V_x and V_y are the seepage velocities through the porous media which are equal to the Darcy flux divided by the area available for flow (Eq.3-9). C is the solute concentration and R_s is the sink term for the solute loss due to biodegradation. In the upcoming subsections, the development of the advective and dispersive terms in the two-dimensional advection-dispersion equation will be described separately.

4.1.1 **Advection**

Advection is the movement of solute with the average seepage velocity of the water. The rate of mass transported by advection is given by product of the solute concentration C and the components of the apparent flow fluxes, q_x, q_y, q_z, hence :

$$\vec{q}_m = \vec{q}\, C \tag{4-2}$$

where $\vec{q}_m$ is the mass vector of solute crossing the plane per unit time which has the direction of Darcy velocity and $\vec{q}$ is the Darcy velocity vector.

The net rate of advective inflow of the mass across the volume element with the dimension of Δx, Δy, Δz in the x direction will be

$$-\frac{\partial}{\partial x}(q_x C) \tag{4-3}$$

where q_x is the component of Darcy velocity in x direction. Similar expression can be written in the y direction, so the net rate of advective inflow of solute mass for a two-dimensional element is:

$$-\frac{\partial}{\partial x}(q_x C) - \frac{\partial}{\partial y}(q_y C) \tag{4-4}$$

Rate of accumulation of solute mass within the element is given by:

$$\theta \frac{\partial C}{\partial t} \tag{4-5}$$

Equating the rate of accumulation to the expression given in Eq.4-4 gives the advective transport equation as follow:

$$-\frac{\partial}{\partial x}(q_x C) - \frac{\partial}{\partial y}(q_y C) = \theta \frac{\partial C}{\partial t} \tag{4-6}$$

For solute transport in the porous media, Eq.4-6 should be divided by volumetric water content (θ), and the Darcy velocity components should be converted to the seepage velocity components:

$$-\frac{\partial}{\partial x}(V_x C)-\frac{\partial}{\partial y}(V_y C)=\frac{\partial C}{\partial t} \tag{4-7}$$

4.1.2 Dispersion (Molecular Diffusion and Hydrodynamic Dispersion)

Dispersion causes spreading of the solute in the transverse and longitudinal flow directions. This spreading is governed by two mechanisms; molecular diffusion and mechanical dispersion. Fick's law of diffusion describes the diffusive transport of substances by:

$$F_D=-D\frac{\partial C}{\partial x} \tag{4-8}$$

where, F_D represents the rate, in mass per unit time per unit area, C is the concentration of dissolved substance and D is the diffusion coefficient.

The heterogeneity in the porous media causes the fluid particles to follow a tortuous path around the sand grains and the velocity must therefore vary in direction and magnitude from one point to another (Zheng and Bennett, 1995). Hydrodynamic dispersion terms in the transport equation account for this heterogeneity in the porous media by introducing a dispersive coefficient in the dispersion coefficient. Hence, the dispersion coefficients, which include the molecular diffusion and hydrodynamic dispersion, are expressed in the longitudinal and the transverse directions as follows:

$$D_x=\alpha_L\frac{V_x V_x}{|V|}+\alpha_T\frac{V_y V_y}{|V|}+D^* \tag{4-9}$$

$$D_y = \alpha_L \frac{V_y V_y}{|V|} + \alpha_T \frac{V_x V_x}{|V|} + D^* \tag{4-10}$$

where $|V|$ is the magnitude of velocity, V_x and V_y are the seepage velocities in x and y direction, α_L and α_T are dispersivities in the longitudinal and transverse directions, respectively, and D^* is the effective diffusion coefficient in porous media.

Thus, assuming dispersion can be simulated using a form similar to the Fick's law of diffusion, the net rate of mass inflow due to the dispersion in two-dimension is described as:

$$\frac{\partial}{\partial x}\left(D_x \frac{\partial C}{\partial x}\right)\theta + \frac{\partial}{\partial y}\left(D_y \frac{\partial C}{\partial y}\right)\theta \tag{4-11}$$

Rate of mass accumulation within the element is:

$$\theta \frac{\partial C}{\partial t} \tag{4-12}$$

Equating the accumulation term to the sum of the two terms describing the difference between mass inflow and mass outflow due to the dispersion (Eq.4-11) and advection (Eq.4-4) will give the advection-dispersion transport equation.

$$\frac{\partial C}{\partial t} = \frac{\partial}{\partial x}\left(D_x \frac{\partial C}{\partial x}\right) - V_x \frac{\partial C}{\partial x} + \frac{\partial}{\partial y}\left(D_y \frac{\partial C}{\partial y}\right) - V_y \frac{\partial C}{\partial y} \tag{4-13}$$

Generally, the molecular diffusion has a limited effect on the dispersion of solute. However, at low seepage velocities, the diffusion may be a significant contributor to the dispersion coefficient. At a high velocity, mechanical mixing is the dominant dispersive process, in which case, the diffusion term in the dispersion coefficient equations (Eq.4-9, Eq.4-10) can be neglected.

4.1.3 Growth Rate Models (Sink or Source Term)

The reduction in organic material can be modeled by adding a sink term to the advection-dispersion transport equation. This reduction is due to the utilization of soluble substrate for biomass growth. The model proposed for the transport of substrate in porous media accounts for the growth and decay of biomass attached to the solid matrix as a biofilm. Many expressions can be implemented in the transport equation as the biomass growth rate and substrate utilization term [Metcalf and Eddy 2003]. The first order decay rate and Monod equation are two different types of sink term which are implemented in the developed model.

4.1.3.1 First Order Decay Rate

The substrate utilization rate in a biological system can be modeled with the first order decay rate as follow:

$$\frac{\partial C}{\partial t} = -kC \tag{4-14}$$

The negative sign of the equation is due to the decrease of substrate with time. In the above equation, k is the first order decay rate and C is the substrate or organic matter concentration. By substituting the first order decay rate as a sink term in the transport equation, the transport equation will be in the form of:

$$\frac{\partial(C)}{\partial t} = \frac{\partial}{\partial x}\left(D_x \frac{\partial C}{\partial x}\right) - \frac{\partial(V_x C)}{\partial x} + \frac{\partial}{\partial y}\left(D_y \frac{\partial C}{\partial y}\right) - \frac{\partial(V_y C)}{\partial y} - kC \tag{4-15}$$

An approximation to the steady-state one-dimensional advection-dispersion equation with the first order decay term can be given by:

$$C = C_0\, e^{-kt^*} \tag{4-16}$$

where t^* is the travel time.

4.1.3.2 Monod Equation

The most widely used expression for describing the rate of microbial growth as a function of substrate concentration is attributed to Monod (Monod 1949). In the Monod equation, the substrate utilization is modeled as follow:

$$\frac{\partial C}{\partial t} = R_s = (M_T)(q_m)\left(\frac{C}{K_s + C}\right) \tag{4-17}$$

where, M_T is the biomass (microorganism) concentration (g/m^3), K_s is the half-velocity constant, substrate concentration at one-half of the maximum specific substrate utilization rate (g/m^3), q_m is the maximum specific substrate utilization rate, (g substrate/g biomass ·d), and R_s is the rate of substrate concentration change due to utilization (g/m^3·d).

The complete transport equation by using the Monod equation for the substrate utilization will be simplified to:

$$\frac{\partial(C)}{\partial t} = \frac{\partial}{\partial x}\left(D_x \frac{\partial C}{\partial x}\right) - \frac{\partial(V_x C)}{\partial x} + \frac{\partial}{\partial y}\left(D_y \frac{\partial C}{\partial y}\right) - \frac{\partial(V_y C)}{\partial y} - M_T q_m \left(\frac{C}{K_s + C}\right) \tag{4-18}$$

The biomass growth is proportional to the substrate utilization rate by the synthesis yield coefficient (Y), and biomass decay is proportional to the biomass present and the decay rate (b).

$$\frac{\partial M_T}{\partial t} = Y M_T q_m \left(\frac{C}{K_s + C}\right) - b M_T \tag{4-19}$$

The equation describing specific growth rate is limited by substrate concentration. At low concentrations, the rate is first order with respect to substrate concentration (Monod 1949). Hence, the organisms still have a significant reaction potential, and an increase in the substrate supply will cause an increase in the growth rate.

For $C << K_s$

$$\frac{\partial C}{\partial t} \approx \frac{M_T q_m}{K_s} C \tag{4-20}$$

At high concentrations, the rate is independent of the concentration (zero order) because uptake by the microorganism is no longer limited by the substrate.

For $C >> K_s$

$$\frac{\partial C}{\partial t} \approx M_T \, q_m \tag{4-21}$$

For estimating the microbial saturation, the user must prescribe an initial microbial concentration over the entire domain and boundary conditions. The boundary conditions for the Monod growth rate equation (Eq.4-19) are zero flux of microbial mass into or out of the domain.

4.2 INITIAL AND BOUNDARY CONDITIONS FOR TRANSPORT EQUATION

The initial condition of the transport equation is the organic matter concentration and must be specified before the solution of the mathematical model. The initial condition in two-dimensional form can be written as:

$$C(x, y, 0) = c_0(x, y) \qquad \text{on entire domain} \tag{4-22}$$

where $c_0(x, y)$ indicates a known concentration distribution in the entire domain.

Generally, there are three types of boundary conditions for the transport equation:

1- Concentration is specified along the inlet boundary for a specified time period (Drichlet condition):

$$C(x, y, t) = c_i(x, y) \qquad \text{on the boundary for t>0} \tag{4-23}$$

where $c_i(x, y)$ indicates a known concentration along the boundary.

2- Concentration gradients are specified across a boundary which implies that the dispersive flux is specified (Neumann condition):

$$-D_{ij}\frac{\partial C}{\partial x_j} = f_i(x,y) \qquad \text{on the boundary for } t>0 \tag{4-24}$$

where $f_i(x,y)$ is a function representing the dispersive flux normal to the boundary.

3- Both concentrations along a boundary and concentration gradients across the boundary are specified which means that both dispersive and advective flux across that boundary are specified (Cauchy condition):

$$-D_{ij}\frac{\partial C}{\partial x_j} + V_i C = g_i(x,y) \qquad \text{on the boundary for } t>0 \tag{4-25}$$

where $g_i(x,y)$ is a function representing the total flux (dispersive and advective) normal to the boundary.

A free exit boundary condition is another type of Cauchy boundary condition, in which the gradient of the field variable immediately inside the boundary is assumed to be equal to the gradient immediately outside the boundary. Implementing this type of boundary condition will introduce small errors in the last three elements; however, these errors can be eliminated using smaller size elements close to the boundary. In this type of boundary condition, the finite–domain numerical solution ignores the existence of the boundary and behaves as an infinite domain solution (Frind 1988).

4.3 CONVERTING MICROBIAL CONCENTRATION TO MICROBIAL SATURATION

The conceptual models for relative permeability, which consider the bacterial growth and biomat formation, require the evaluation of the microbial saturation. The microbial saturation can be calculated by using the microbial concentration obtained from the Monod equation as follows:

$$\text{Microbial Mass} = \overbrace{M_t}^{\text{Concentration}} \quad \overbrace{\Delta x\, \Delta y\, \Delta z\, \varphi\, S_w}^{\text{Water volume in voids}} \tag{4-26}$$

Using the density of bacteria, microbial mass can be converted to the microbial volume.

$$\text{Microbial Volume} = \frac{\text{Microbial mass}}{\rho_{\text{dry density}}}$$

Thus, the actual and effective saturation of bacteria would be as follow:

$$S_{am} = \frac{\text{Microbial Volume}}{\text{Void Volume}} = \frac{M_t \Delta x\, \Delta y\, \Delta z\, \varphi\, S_w}{\rho_{\text{dry density}} \underbrace{\varphi\, \Delta x\, \Delta y\, \Delta z}_{VoidVolume}} = \frac{M_t\, S_w}{\rho_{\text{dry density}}} \tag{4-27}$$

$$S_{em} = \frac{S_{am}}{(1 - S_r)} \tag{4-28}$$

where S_{am} and S_{em} are actual and effective microbial saturations, respectively.

4.4 CONCEPTUAL MODELS FOR RELATIVE PERMEABILITY

Under unsaturated conditions, water fills the small pores as the largest pores are the first to drain when a suction is applied to a soil sample. In unsaturated flow, the water is flowing through the saturated smaller pores and hence one can assume the microbial mass is growing in these pores. For this reason, the smaller pores clog, reducing the relative permeability and causing the water to displace to the larger pores to increase the

relative permeability. This process continues until the pores become saturated with biomass and water. This process will reduce the permeability such that water starts to pond on the surface to increase the hydraulic gradient to allow flow through the biomat that has formed.

A conceptual model for the relative permeability is required to relate the decrease of the relative permeability to the biomass formation. Mostafa and Van Geel (2007) proposed three conceptual models to relate the microbial growth to the reduction of the relative permeability term for the unsaturated flow equation. These conceptual models are implemented in the current code to account for the impact of microbial growth on unsaturated flow.

4.4.1 **Model#1**

This model is based on the proposed relative permeability term for three-phase flow systems such as water, air and immiscible fluid by Lenhard and Parker (1987). Lenhard and Parker (1987) modified Mualem's equation for relative permeability (Eq.3-12) to account for an entrapped air phase in the water phase as follow:

$$K_r(S_e) = S_e^{\frac{1}{2}}\left[\frac{\int_0^{\bar{\bar{S}}_w}\frac{dS_e}{P_c} - \int_0^{S_{ea}}\frac{dS_e}{P_c}}{\int_0^1\frac{dS_e}{P_c}}\right]^2 \tag{4-29}$$

where $\bar{\bar{S}}_w$ is the apparent water saturation, and S_{ea} is the effective trapped air saturation. The above equation reduces the relative permeability of the water phase due to the presence of an entrapped air. The same concept can be applied to the microbial growth as

the presence of microbial population reduces the relative permeability of the water phase by the following equation proposed by Mostafa and Van Geel (2007):

$$\text{For Burdine: } K_r(S_e) = S_{et}^2 \frac{\int_0^{S_{et}} \frac{dS_e}{P_c^2} - \int_0^{S_{em}} \frac{dS_e}{P_c^2}}{\int_0^1 \frac{dS_e}{P_c}} \tag{4-30}$$

$$\text{For Mualem: } K_r(S_e) = S_{et}^{\frac{1}{2}} \left[\frac{\int_0^{S_{et}} \frac{dS_e}{P_c} - \int_0^{S_{em}} \frac{dS_e}{P_c}}{\int_0^1 \frac{dS_e}{P_c}} \right]^2 \tag{4-31}$$

where S_{et} is the effective total saturation and is defined as the sum of the effective water and microbial saturations. Also, the close form of the integral equations (4-30) and (4-31) are given as:

$$\text{Burdine equation: } K_r(S_e) = S_{et}^2 \left((1 - S_{em}^{1/m})^m - (1 - S_{et}^{1/m})^m \right) \tag{4-32}$$

$$\text{Mualem equation: } K_r(S_e) = S_{et}^{1/2} \left((1 - S_{em}^{1/m})^m - (1 - S_{et}^{1/m})^m \right)^2 \tag{4-33}$$

4.4.2 **Model #2**

The second proposed model considers the relative permeability reduction by a factor of one minus the effective microbial saturation, S_{em}.

$$\text{Burdine equation: } K_r(S_e) = S_{ew}^2 \left(1 - (1 - S_{ew}^{1/m})^m \right) \times (1 - S_{em}) \tag{4-34}$$

$$\text{Mualem equation: } K_r(S_e) = S_{ew}^{1/2} \left(1 - (1 - S_{ew}^{1/m})^m \right)^2 \times (1 - S_{em}) \tag{4-35}$$

In this model, it is assumed that the bacteria will grow in the saturated pores and fill the saturated pores. Hence, as the microbial saturation increases, the water saturation

decreases and based on the above equations (Eq.4-34 and 4-35) the relative permeability decreases.

4.4.3 Model #3

The third model is based on considering the soil as a bundle of capillary tubes, in which the capillary tube radii are uniformly reduced by the development of a biofilm on the walls of the capillary tubes. This model assumes that the capillary tubes are categorized into a user-defined number of groups with the equal radius. The soil moisture retention curve is divided into the user-defined number of equal incremental volumes to obtain the representative saturation of groups. The mid-point saturation of each increment in the soil moisture curve is used as the saturation representing that group of capillary tubes (Figure 4-1). The Van Genuchten capillary pressure–saturation relationship is used to find the capillary pressure corresponding to the saturation of each tube (division). Using the capillary pressure of each group, the radius of each group is obtained by Eq.3-5. A schematic visualization of this calculation for model #3 with four user-defined divisions is shown in Figure 4-1.

Once the distribution of capillary tubes is known, the microbial volume can be distributed evenly within the capillary tubes and the thickness of biofilm formed in tubes is obtained by using the following equation:

$$\sum_{i=1}^{n(\#\text{ of division})} (\#\text{of Tubes})_i \cdot \pi \cdot r_i^2 - (\#\text{of Tubes})_i \cdot \pi \cdot (r - t_b)_i^2 = V_m \qquad (4\text{-}36)$$

where t_b is the estimated thickness of biofilm.

Accordingly, the reduction factor for flow due to the bacterial growth is determined assuming laminar flow and using Hagen-Poisseuille's law. The reduction factor is the

ratio of the flow passing through the tubes with a layer of biofilm over the flow passing though the tubes without biofilm and is given as,

$$\frac{Q_{\text{tube filled by biofilm}}\Big|_0^{\varphi}}{Q_{\text{tubes}}\Big|_0^{\varphi}} = \frac{\sum_{l=1}^{\#\text{ofdivisions}}\left[(\#\text{of Tubes})_i \cdot (r_i - t_b)^4\right]}{\sum_{l=1}^{\#\text{ofdivisions}}\left[(\#\text{of Tubes})_i \cdot r_i^4\right]} \tag{4-37}$$

Multiplying the reduction factor by the relative permeability terms will give the relative permeability terms that accounts for the presence of the bacteria.

$$\text{Burdine equation: } K_r = S_{ew}^2\left(1-(1-S_{ew}^{1/m})^m\right)\times\frac{Q_{tube\ filled\ by\ biofilm}\Big|_0^{\varphi}}{Q_{tubes}\Big|_0^{\varphi}} \tag{4-38}$$

$$\text{Mualem equation: } K_r = S_{ew}^{1/2}\left(1-(1-S_{ew}^{1/m})^m\right)^2\times\frac{Q_{tube\ filled\ by\ biofilm}\Big|_0^{\varphi}}{Q_{tubes}\Big|_0^{\varphi}} \tag{4-39}$$

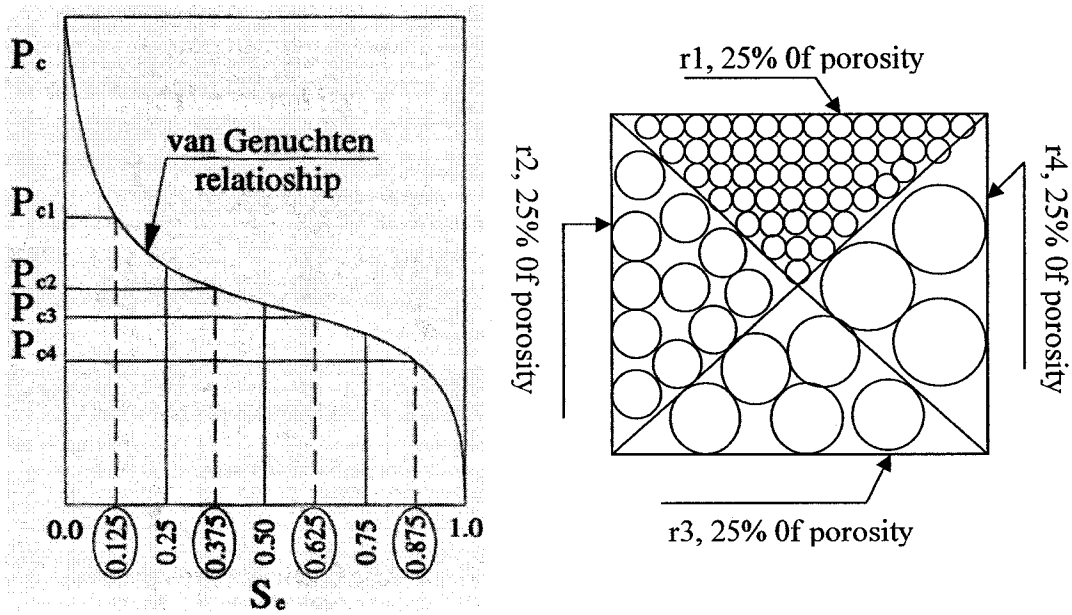

Figure 4-1: Schematic visualization of model three, in which soil is divided into four groups, each has the same void volume (Taken from Mostafa 2004)

4.5 NUMERICAL SOLUTION

The biological clogging models introduced in the previous sections, require the solution of the flow equation, transport equation and biological growth equation (Monod equation). The first two equations, flow and transport equations, are a form of the general transient quasi-harmonic equation which is represented in Eq.4-36.

$$E_x(\frac{\partial^2\Phi}{\partial x^2}) + E_y(\frac{\partial^2\Phi}{\partial y^2}) + v_x(\frac{\partial\Phi}{\partial x}) + v_y(\frac{\partial\Phi}{\partial y}) - G\Phi + R = f\,c\frac{\partial(\Phi)}{\partial t} \tag{4-40}$$

E_x and E_y are the material properties in x and y direction. In the transport equation, the Φ term represents the concentration of solute and E_x and E_y represent the dispersion coefficient in x and y direction, respectively. v_x and v_y are the seepage velocity in x and y direction, respectively. If the first order decay rate is used as a sink term, G represents the first order decay rate coefficient. Considering the Monod equation as the sink term, R is the substrate utilization rate and is obtained by Eq.4-17. f and c are pre-transient terms equalling one in the case of transport equation. The flow and transport equations are solved by using the finite element solver, Condur.

The last equation is the Monod equation that is an ordinary differential equation and can be solved as follow:

$$\frac{dM_T}{dt} = YM_t q_m\left(\frac{C}{K_s + C}\right) - bM_t \tag{4-41}$$

By moving dt to the other side and taking the integral of both sides:

$$\int_{M_{t1}}^{M_{t2}} \frac{dM_T}{M_t} = \int_{t=t_1}^{t=t_2}\left(Yq_m\left(\frac{C}{K_s + C}\right) - b\right)dt$$

Assuming that the solute concentration is constant in which C is the value of concentration at the previous time step:

$$M_T^{t_2} = M_T^{t_1} \times \exp\left\{\left(Yq_m\left(\frac{C}{K_s + C}\right) - b\right) \times (t_2 - t_1)\right\} \tag{4-42}$$

Thus, having the initial microbial concentration, $M_T^{t_1}$, the microbial concentration at each time step will be obtained by Eq.4-42.

4.5.1 **Complete Model Procedure**

The developed code consists of the three main functions which solve the flow, transport and Monod equations. The program commences by reading an input data file that includes the boundary and initial values, soil properties, method of solution (e.g. Model #1 vs. #2 and #3, Mualem Based vs. Burdine based) as well as the dimensions of the domain.

Then, the user should define an appropriate mesh for the domain dimensions. For all the verification simulations in chapters three and four, the column is divided into the square elements with 1cm by 1cm element size. To reduce the simulation time, a spatial discretization that is implemented for all the simulations in chapter five, has been suggested for one and two dimensional domains (subsection 5.1.1).

To improve the efficiency of the numerical solution, two time steps have been defined. A larger time step over which the flow and transport equations are coupled and the material properties updated, and a smaller time step (defined here as the marching time step) to handle the transient nature of the flow equation at early times in the solution. At later times in the solution, the flow approaches steady state and hence the number of iterations is reduced. The time step and marching time step were constant

throughout the simulations conducted in chapters three and four were equal to 10 and 1 second, respectively. However, increasing the introduced flow rate to the system, especially in the case of pulse simulations requires the selection of smaller time steps for the duration of high flow. Hence, a time step and marching time step selection scheme has been considered for all the simulations in chapter five.

Afterward, the following steps are taken in each time step for the implementation of the complete model:

1. Solve Monod equation using Eq.4-38 and the initial microbial concentration and initial solute concentration.
2. Convert the microbial concentration to a microbial saturation (Eq.4-27).
3. Update the relative permeability terms based on the microbial saturation and using one of the conceptual models (Model #1, #2 or #3)
4. Solve flow equation using flow equation function (Figure 3-6).
5. Solve transport equation (Eq.4-18) by creating an input data set for Condur.

The flowchart for the complete model procedure is given in Figure 4-2.

4.5.2 **Comparison between Flow and Transport Boundary Condition**

There is an analogy between the transport model boundary condition and the flow model boundary condition, and understanding the influence of each type of boundary condition on the respective simulation is very important. The specified-head boundary condition of the flow equation is equivalent to a specified-concentration boundary condition of transport equation; however, it influences solute mass inflow in a very

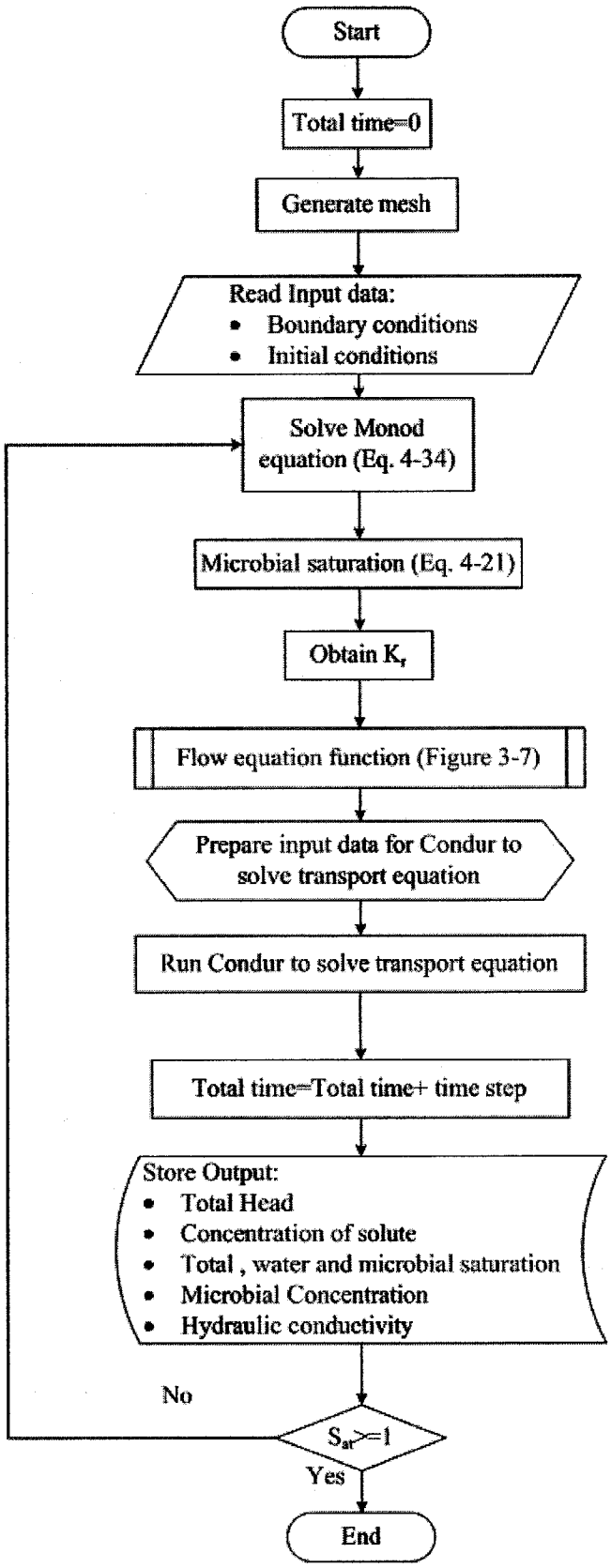

Figure 4-2: Complete model procedure

different way than the specified-head boundary influences water inflow. In the case of the flow equation, when the hydraulic gradient is determined, the inflow and outflow of water is determined. However, in the transport equation, determining the gradient concentration only considers the relatively small dispersive component of solute mass flux. "In order to generate a transport model boundary for which the solute mass flux is exactly and fully determined, a specified-flow boundary condition of the flow equation should be accompanied with the specified-concentration and concentration gradient of transport equation" (Zheng and Bennet 1995).

4.6 CONTAMINANT TRANSPORT MODEL VERIFICATION

The contaminant transport code is verified by two means; with and without decay. The results of simulation with no decay and first-order decay rate are compared to analytical solutions of the one-dimensional advection-dispersion equation (Bear, 1979). Bear (1979) proposed an analytical solution for the 1-D partial differential equation which governs the solute transport with a constant velocity and dispersion coefficient. Being able to compare the results of the current simulation to the analytical solution, a uniform velocity along the 1-D profile is needed. The uniform velocity is provided by maintaining the steady-state flow condition. Considering one-dimensional uniform flow along the x-axis, the governing equation for the solute transport is:

$$\frac{\partial C}{\partial t} = D_x \frac{\partial^2 C}{\partial x^2} - V_x \frac{\partial C}{\partial x} - kC \qquad (4\text{-}43)$$

Accordingly, the initial and boundary conditions are:

t =0 : x≥0, C=0

t >0 : x=0 , C=C_0

x= ∞, $C=0$

The analytical solution of one-dimensional transport equation (Eq.4-35) is given by Bear, 1979 as:

$$C(x,t)=\frac{C_0}{2}\exp\left\{\frac{V_x x}{2D}\right\}\cdot\left[\exp(-x\beta)\,erfc\left(\frac{x-[V_x^2+4kD_x]^{\frac{1}{2}}t}{2[D_x t]^{\frac{1}{2}}}\right)\right.$$
$$\left.+\exp(x\beta)\cdot erfc\left(\frac{x+[V_x{}^2+4kD]^{\frac{1}{2}}t}{2[Dt]^{\frac{1}{2}}}\right)\right] \tag{4-44}$$

$$\text{where } \beta=\frac{V_x^2}{4D_x^2}+\frac{k}{D_x} \tag{4-45}$$

For k=0 when there is no decay, Eq.4-44 will be simplified as follows:

$$C(x,t)=\frac{C_0}{2}\cdot\left[erfc\left(\frac{x-Vt}{2[Dt]^{\frac{1}{2}}}\right)+\exp(x\beta)\cdot\left[erfc\left(\frac{x+Vt}{2[Dt]^{\frac{1}{2}}}\right)\right]\right. \tag{4-46}$$

4.6.1 Case 1: Verification against Analytical Solution without Decay for Sand and Peat Filter

Using the developed computer code, the soil columns of the sand and peat were simulated using the properties listed in Table 4-1. A contaminant with a concentration of 2000 (mg/L) was added to the column after the column reached a steady-state flow condition (after 6 hours for each case) by infiltrating a water flux at the top of column. Figure 4-3 and Figure 4-5 illustrate the steady state condition for the flow through the sand soil and peat soil, respectively. Table 4-2 shows the contaminant properties, and boundary and initial conditions for the transport equation.

Table 4-1: Soil properties for running the verification cases

Parameter	Peat filter	Sand filter
θ_r	0.08736	0.0265
K_{sat}(cm/s)	0.079	0.00428
φ	0.8	0.312
α	0.18	0.044
n	1.3	2.2
m	0.23	0.54
Column height	100	100
Top boundary condition (Flux -cm/s)	0.00231	0.00231
Bottom boundary condition (prescribed-cm)	-9.9	-9.9

Table 4-2: Contaminant properties, boundary and initial conditions for the transport equation

Parameter	Value
Effective diffusion coefficient D^* (cm^2/s)	0.00001
Longitudinal dipersivity α_l (cm)	1
Initial concentration (mg/L)	0
Top boundary: Prescribed (mg/L)	2000
Bottom boundary condition	Free exit boundary

Comparison of the model results with the analytical solution (Eq.4-46) is presented in Figure 4-4 and Figure 4-6 for sand and peat, respectively. As illustrated in Figure 4-4, the advective front moves with the flow such that the C/C_0 equalling 0.5, which in this case 1000 mg/L, reflects the advective front. After 0.5 hours of injection in the sand filter, the advective front should be at 13.93 cm from the top of the column as the porosity of sand is 0.312, Darcy flux is 0.00231 cm/s and the saturation is 0.957. For both the sand and peat column simulations, there is good agreement between the model results and the corresponding analytical solutions.

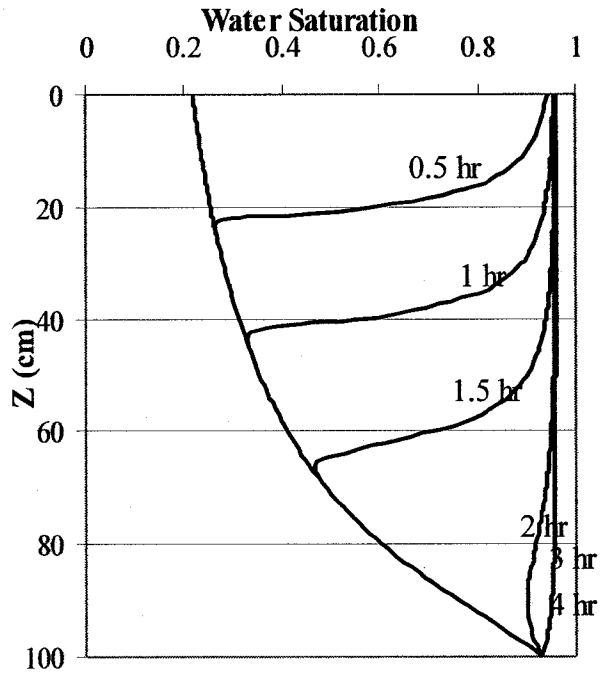

Figure 4-3: Flow through sand filter at the steady state condition

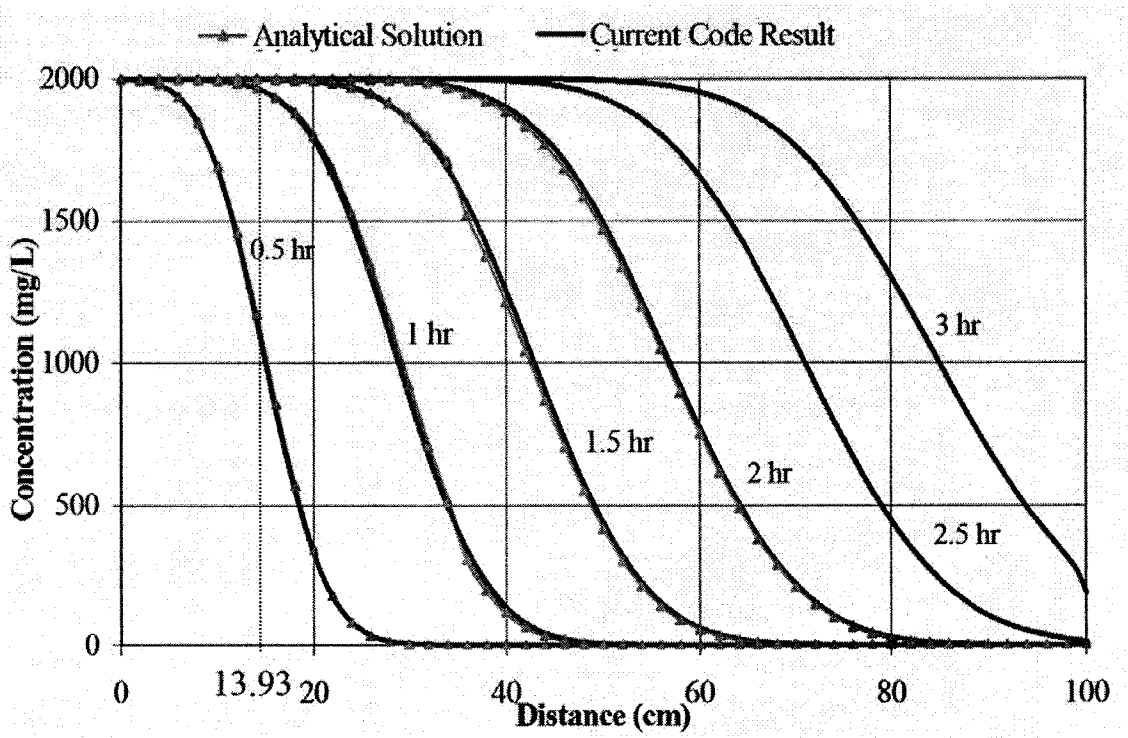

Figure 4-4: Conservative contaminant transport in sand (comparison of the current code with the analytical solution)

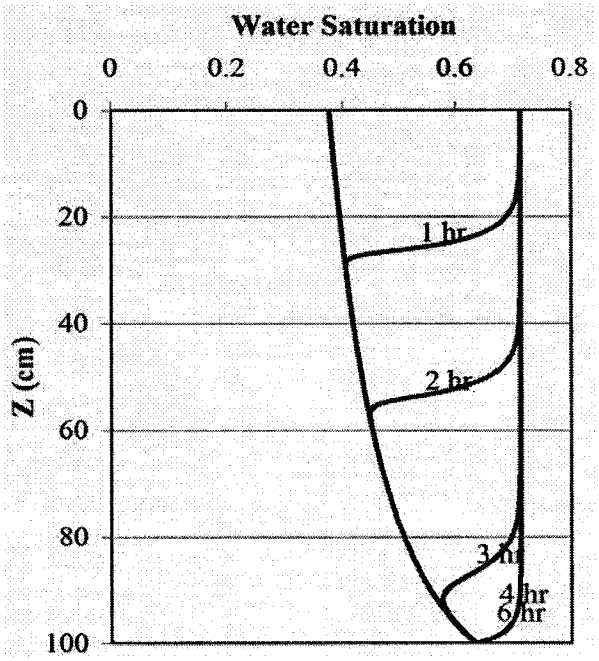

Figure 4-5: Flow through peat filter at the steady state condition

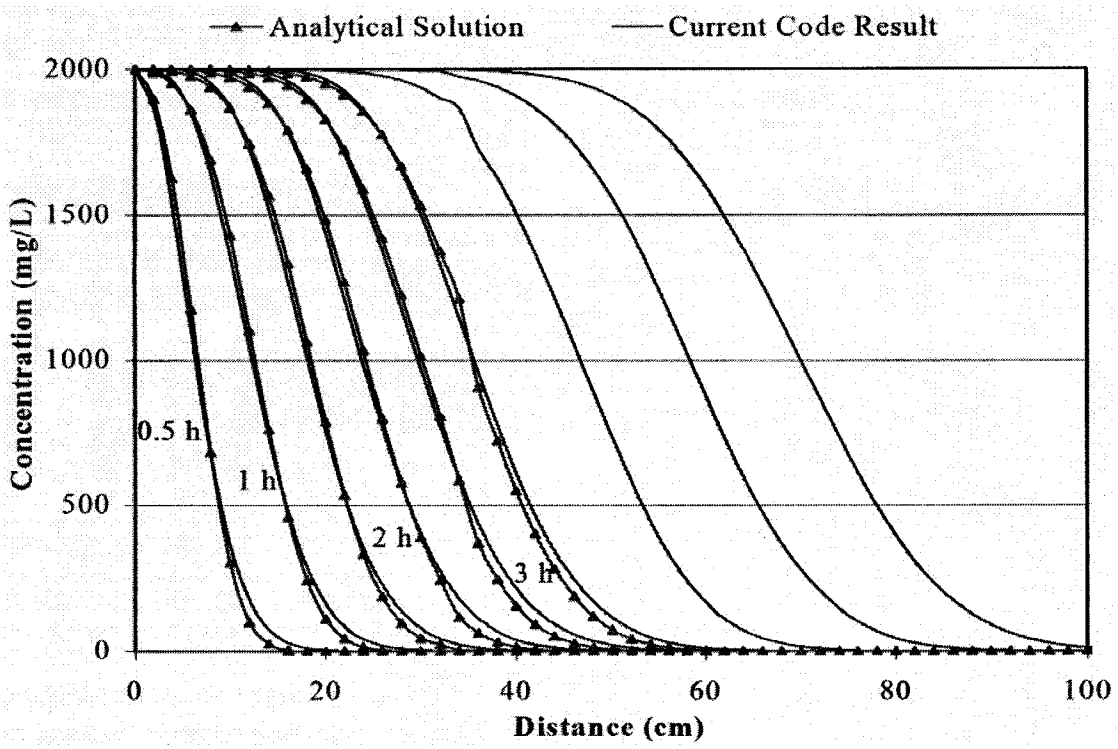

Figure 4-6: Conservative contaminant transport in peat (comparison of the current code with the analytical solution)

4.6.2 Case 2: First-order Decay Rate Verification by Analytical solution

For the sand and peat column simulations in Table 4-1, a first-order decay rate of 6.93 ($days^{-1}$) was applied to verify the contaminant transport equation with first-order decay as a sink term. These simulations were compared with the analytical solution, Eq. 4-44. Comparison of the concentration profiles obtained from the current code with the analytical solution with respect to time is shown in Figures 4-7 and 4-8 for sand and peat, respectively. As expected, the steady-state concentration decreases as the travel time within the column increases. Again, there is good agreement between the model simulations and analytical solutions.

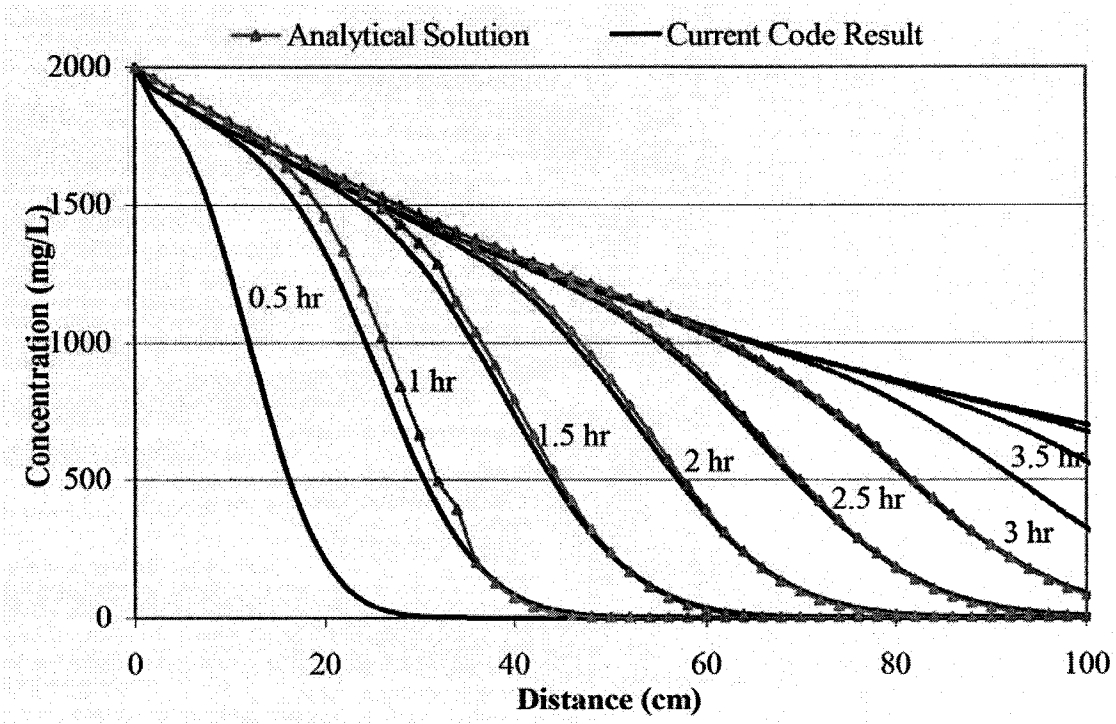

Figure 4-7: Contaminant transport with decay in sand (comparison of the current code with the analytical solution)

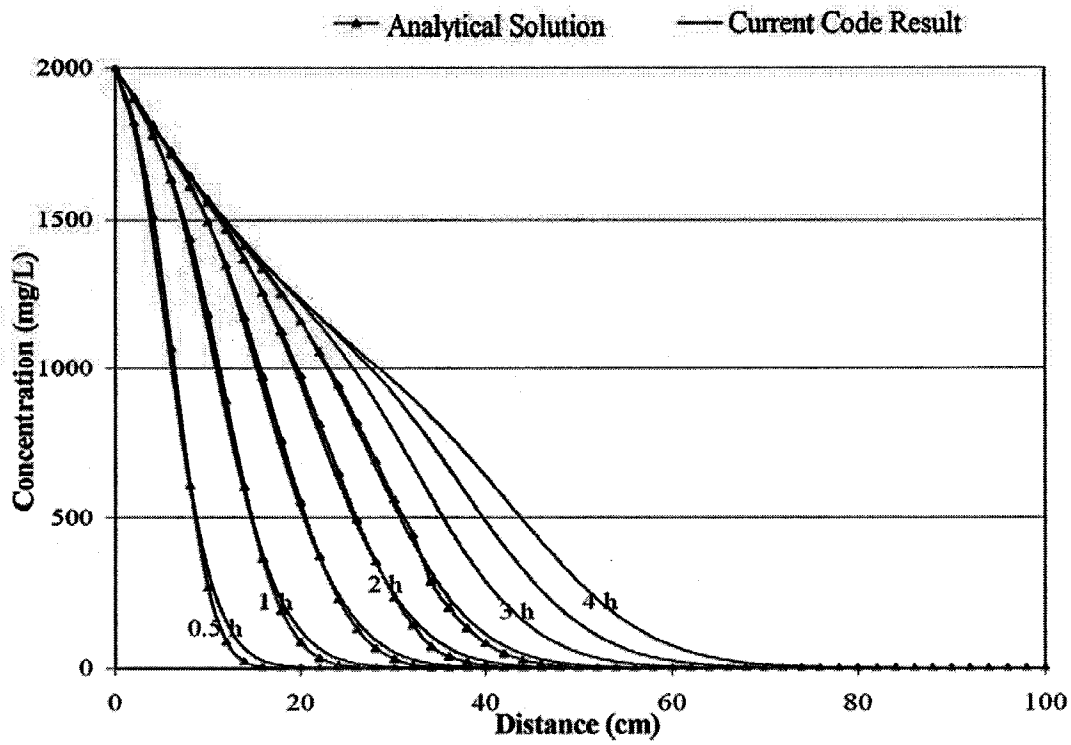

Figure 4-8: Contaminant transport with decay in peat (comparison of the current code with the analytical solution)

4.7 COMPLETE MODEL VERIFICATION

Due to the lack of experimental data for the validation of the complete model (i.e. model with the coupled solution of the flow, transport and Monod equations), the complete model is verified by checking the mass balance to ensure mass is conserved and by comparing the model result against the one-dimensional finite difference model results presented by Mostafa (2004).

4.7.1 Mass Balance Approach

To verify the complete biological clogging scenario using a mass balance approach, the mass balance equations for the flow and transport equations are considered separately. Using the same concept for the flow equation mass balance (Section 3-6-1), transport equation mass balance is considered to check if the transport equation code is

implemented correctly. The mass balance for the transport equation considers the Monod relationship for substrate utilization as a sink term. The resultant mass balance for the transport equation is calculated for each time step and element as follows (Figure 4-9),

Accumulation = Mass In- Mass Out – Degradation

where,

Accumulation = mass in the domain at time (t+Δt) - mass in the domain at time (t)

$$=\left(C^{t+\Delta t}-C^{t}\right)\theta\,\Delta x\,\Delta y\,\Delta z \tag{4-47}$$

mass entering element i, j:

$$\Delta t\theta\,(q_{In,x}+q_{In,y})=\Delta t\,\theta\left\{V_{x_{i.j-1}}C_{i,j-1}\Delta y\,\Delta z-D_{x_{i.j-1}}\left(\frac{\Delta C}{\Delta x}\right)_{i,j-1}\Delta y\,\Delta z\right.$$
$$\left.+V_{y_{i-1.j}}C_{i-1,j}\Delta x\,\Delta z-D_{x_{i-1.j}}\left(\frac{\Delta C}{\Delta y}\right)_{i-1,j}\Delta x\,\Delta z\right\} \tag{4-49}$$

Mass exiting element i, j:

$$\Delta t\,\theta\,(q_{Out,x}+q_{Out,y})=\Delta t\,\theta\left\{V_{x_{i,j}}C_{i,j}\;\Delta y\,\Delta z-D_{x_{i,j}}\left(\frac{\Delta C}{\Delta x}\right)_{i,j}\Delta y\,\Delta z\right.$$
$$\left.+V_{y_{i,j}}C_{i,j}\;\Delta x\,\Delta z-D_{y_{i,j}}\left(\frac{\Delta C}{\Delta y}\right)_{i,j}\Delta x\,\Delta z\right\} \tag{4-50}$$

If the Monod equation is used as a sink term the degradation will be calculated as follows:

$$\text{Degradation} = M_T\,q_m\frac{C}{K_s+C}\;\theta\,\Delta x\,\Delta y\,\Delta z\,\Delta t \tag{4-51}$$

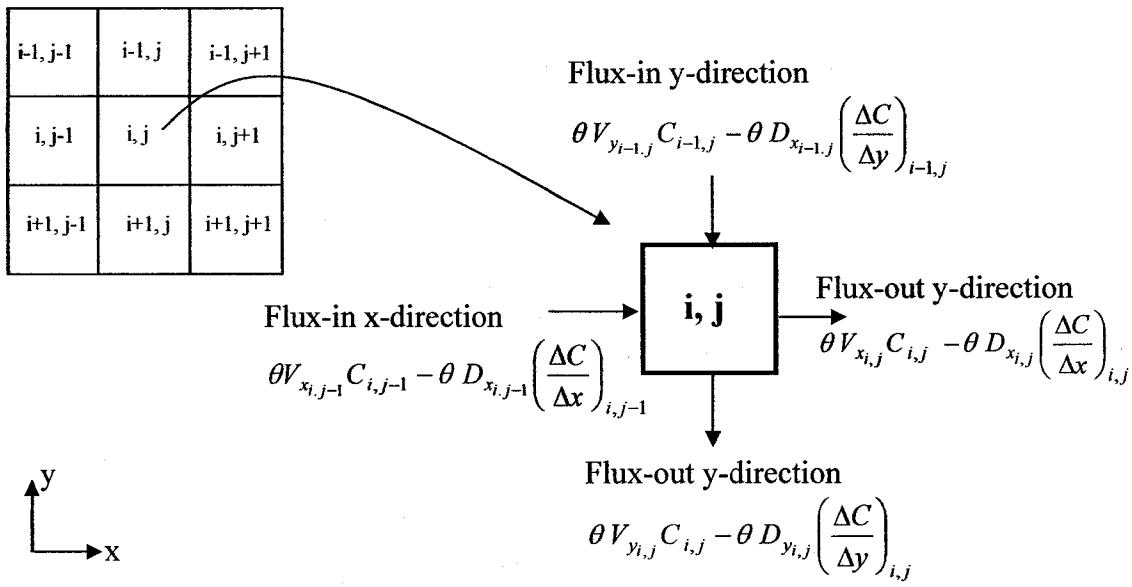

Figure 4-9: Two-dimensional representation of mass balance for an element

The solute mass balance error, expressed as a percentage, that is given to the user for any time is calculated as follows:

$$\text{Mass balance error} = \frac{\text{Mass entering - Mass exiting - Accumulation - Degradation}}{\text{Mass entering the domain}} \times 100 \qquad (4\text{-}52)$$

So that, the smaller the mass balance error indicates the more accuracy in the results.

4.7.2 Comparison with Mostafa's (2004) Model Results

The scientific literature dealing with the transport of solute in unsaturated porous media accounting for solute consumption due to the biodegradation of bacteria is limited. Hence, the complete bioclogging model is compared with the numerical simulations presented by Mostafa (2004) who developed a finite difference code to simulate the transport of solute under unsaturated conditions with the impacts of microbial growth and decay. Another advantage of comparing the current model with Mostafa (2004) is that his

model was based on the same conceptual models that relate the relative permeability reduction to the microbial growth.

Three simulations are conducted for three different hydraulic conductivity models on the peat filter using the properties of peat (Table 4-1); Monod input parameters, and boundary and initial conditions listed in Table 4-3. The results of developed model are based on the prescribed boundary condition for transport equation that is assigned at one extra imaginary element at the top of the column. Hence, the results were sensitive to the size of top element.

The results of the current code for model #1, #2 and #3 are presented in Figures 4-10, 4-12 and 4-14, respectively and the results of Mostafa (2004) are illustrated in Figures 4-11, 4-13, and 4-15 for model #1, #2, and #3, respectively. For the comparison of these simulations, clogging was assumed to occur once the total saturation of an element (grid block in the case of Mostafa, 2004) reached one. For model #1, clogging occurs after 45 days with a cumulative flow mass balance error of 0.0757 percent of initial mass and transport mass balance error of 0.11 percent of flux entering the domain. For model #2, clogging occurs faster at 40.4 days with a cumulative flow mass balance error of 0.035 percent of initial mass and transport mass balance error of 0.49 percent of flux entering the domain. Clogging in model #3, occurs almost at the same time as model #2 at 41 days and the cumulative flow mass balance error is given as 0.0369 percent of initial mass and transport mass balance error of 0.47 percent of flux entering the domain. The results of mass balance for flow and transport equations also supported that the developed code is implemented correctly.

Table 4-3: Monod input parameters used for three verification simulations

Monod kinetic parameters	**value**	**Boundary and initial conditions**	
$Y\ (\frac{mg_{biomass}}{mg_{substrate}})$	0.5	Flow equation	Top: flux =0.000231 cm/s Bottom: prescribed head = -9.9 cm
$q_m\ (\frac{mg_{substrate}}{mg_{biomass} \cdot s})$	5E-6	Transport equation	Top: prescribed concentration =2000 mg/L Bottom: exit boundary
$b\ (s^{-1})$	5.78E-7		
$\rho_{dry\ density}\ (mg/cm^3)$	1.39	Monod initial condition	$M_T = 1500\ (\frac{mg_{biomass}}{L})$
$K_s\ (\frac{mg_{substrate}}{L})$	100	Column height	100 cm

As the boundary condition for the transport equation is not clearly defined in Mostafa (2004), it is believed that the slight differences in the developed code results and the results of Mostafa (2004) is due to either considering the different type of boundary conditions or different method of solution. However, both results show the same patterns in reducing the hydraulic conductivity and water saturation, and increasing the microbial saturation and total saturation over time. The trend of hydraulic conductivity reduction along with the trend of actual saturation change versus time is demonstrated in Figure 4-15, 4-17 and 4-19 for current code and Figure 4-16, 4-18 and 4-20 for Mostafa's (2004) code.

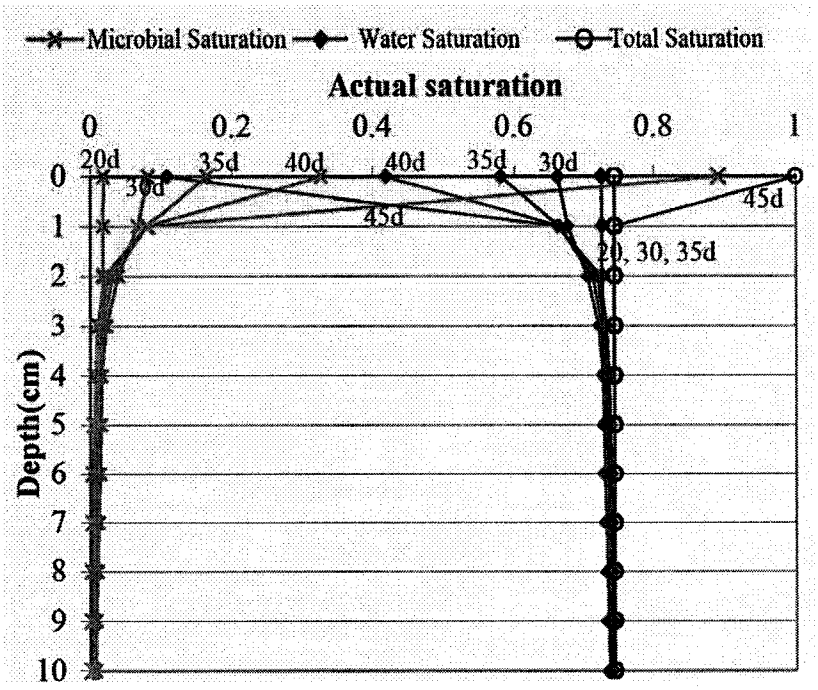

Figure 4-10: Actual saturation profile for model #1; current model

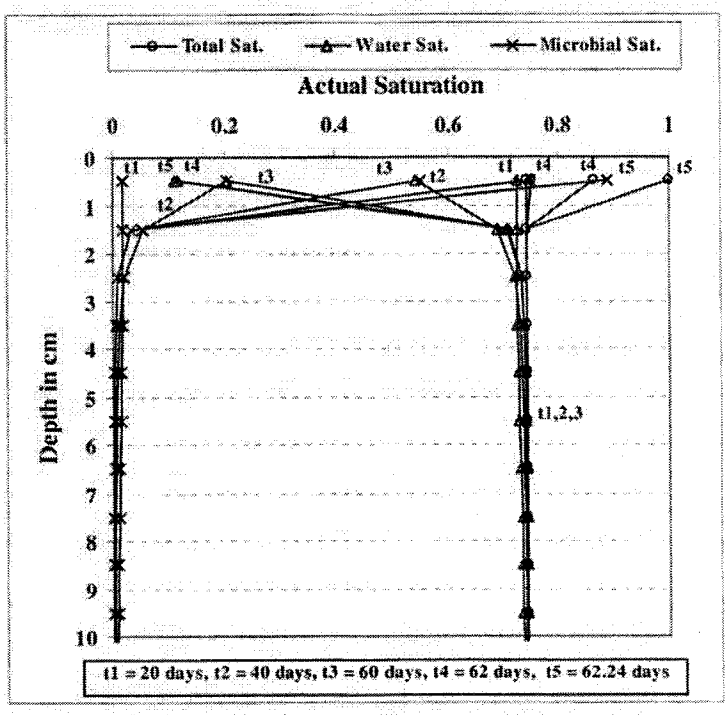

Figure 4-11: Actual saturation profile for model #1 (Mostafa 2004)

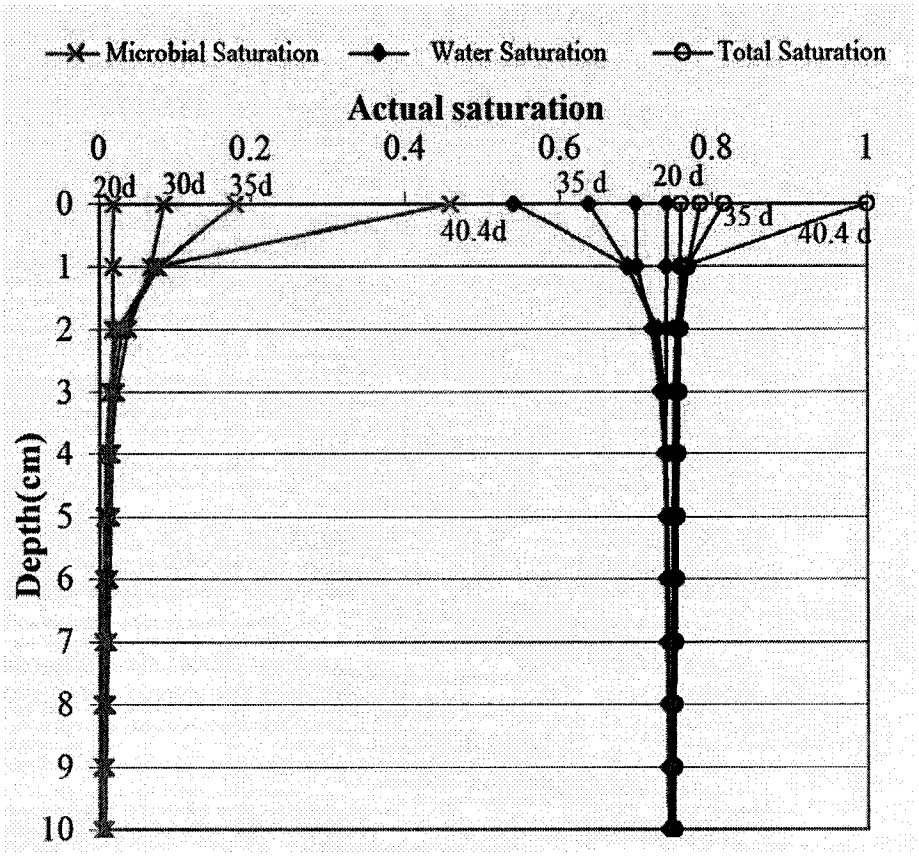

Figure 4-12: Actual saturation profile for model #2; current model

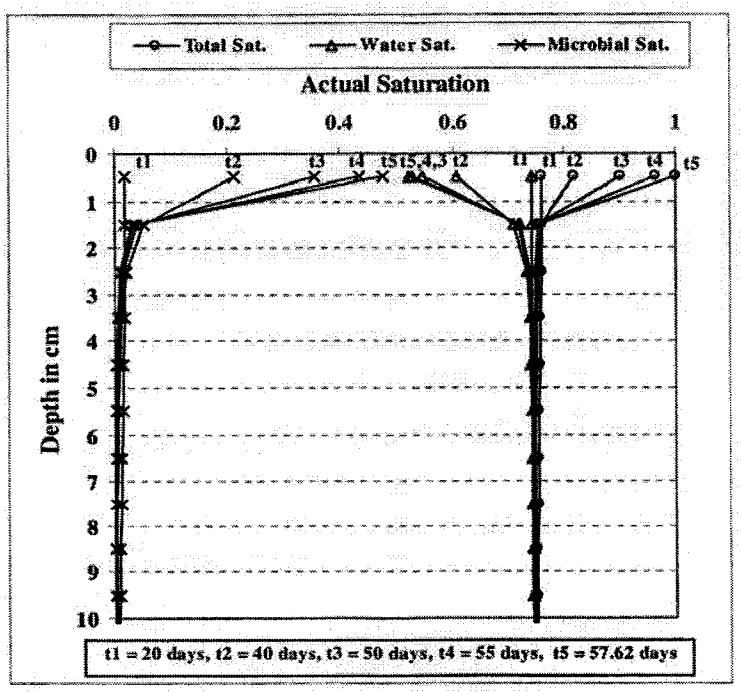

Figure 4-13: Actual saturation profile for model #2 (Mostafa 2004)

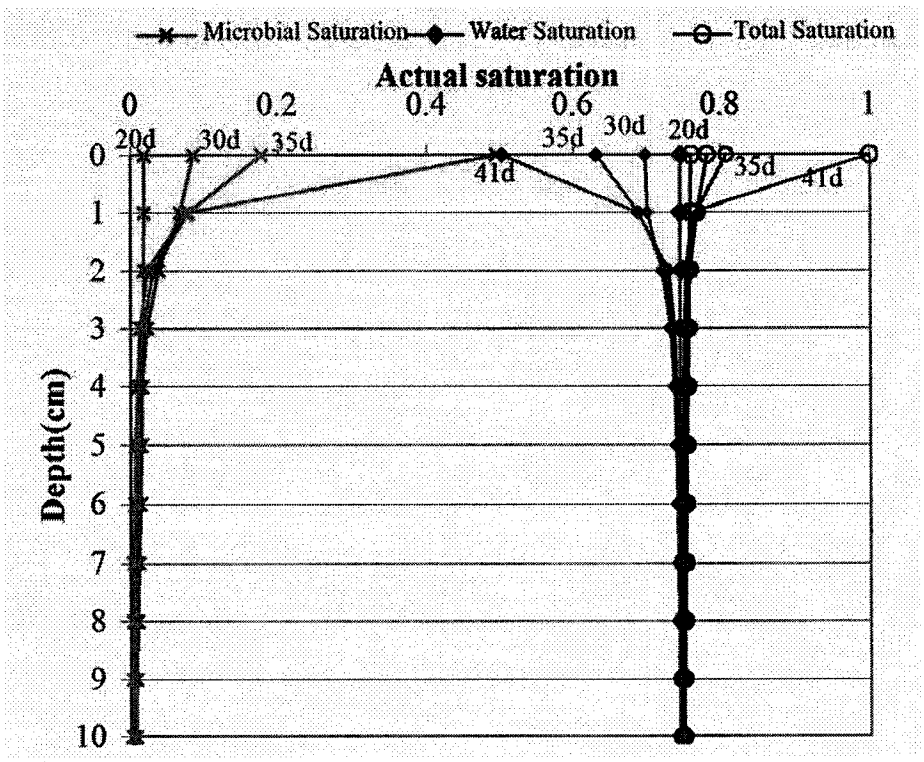

Figure 4-4-14: Actual saturation profile for model #3; current model

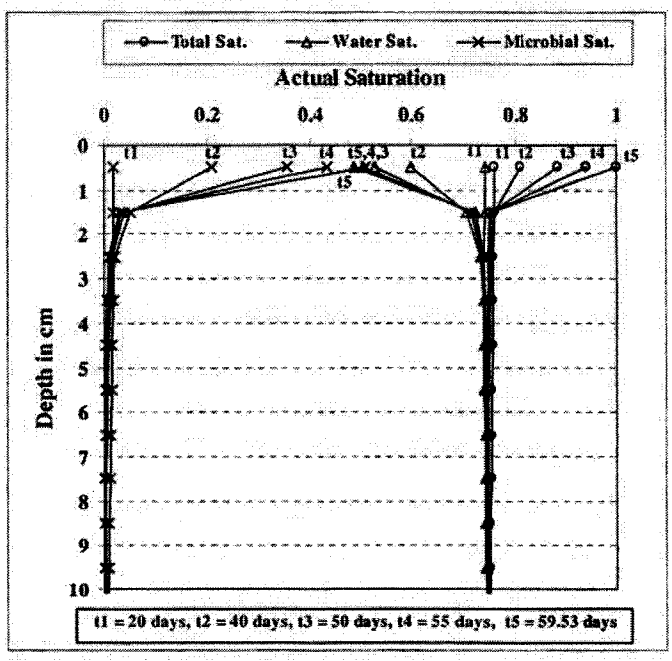

Figure 4-15: Actual saturation profile for model #3 (Mostafa 2004)

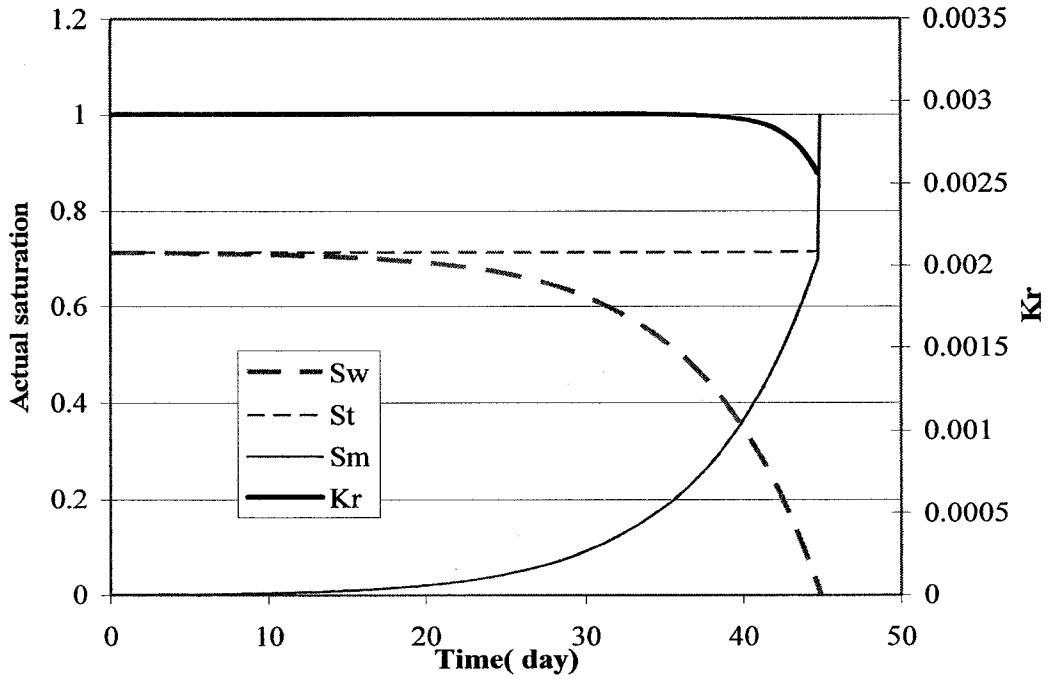

Figure 4-16: Relative permeability, actual total, water and microbial saturation versus time for the top of column for model #1

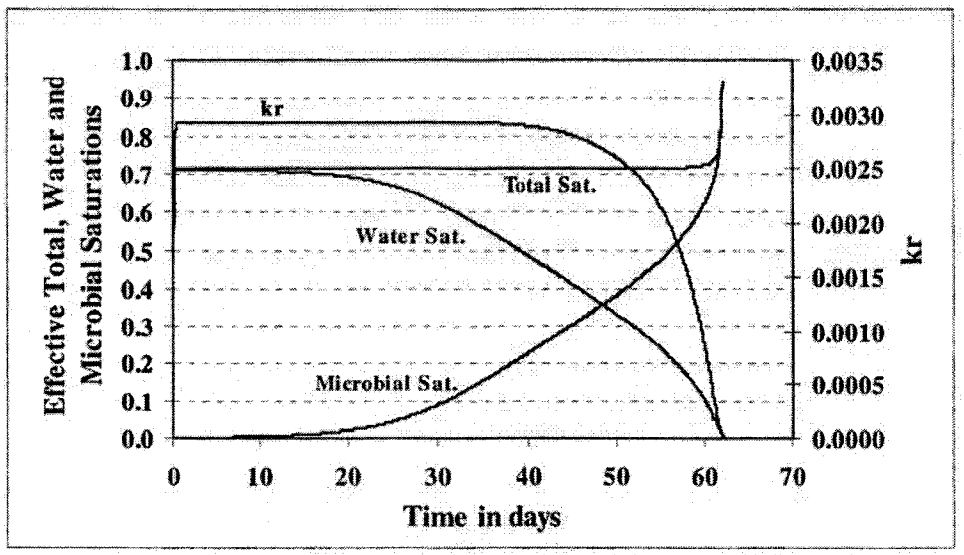

Figure 4-17: Relative permeability, effective total, water and microbial saturation versus time for the top of column for model #1(Mostafa 2004)

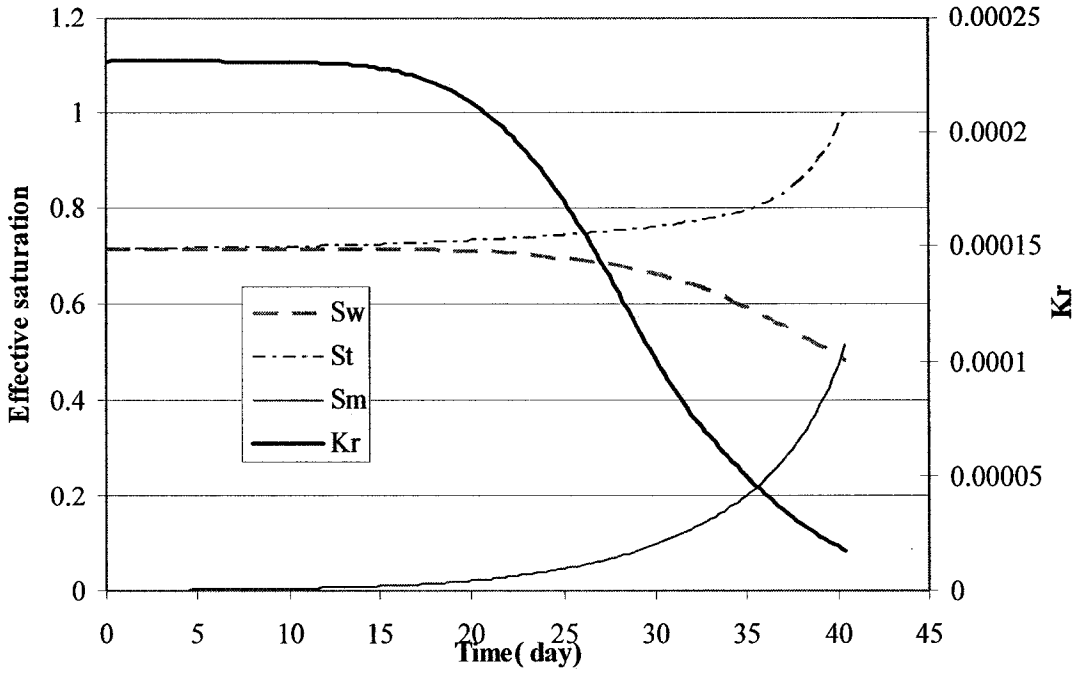

Figure 4-18: Relative permeability, actual total, water and microbial saturation versus time for the top of column for model #2

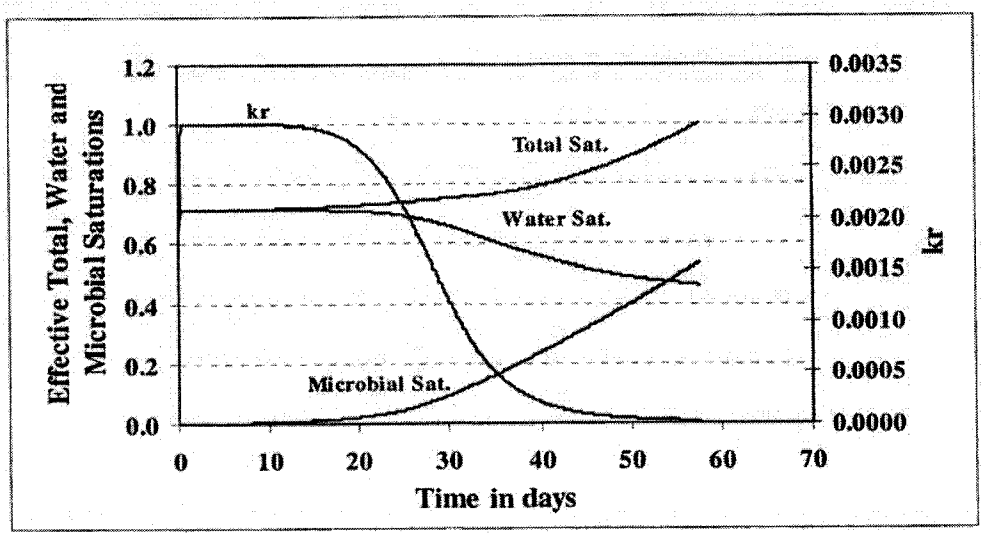

Figure 4-19: Relative permeability, effective total, water and microbial saturation versus time for the top of column for model #2(Mostafa 2004)

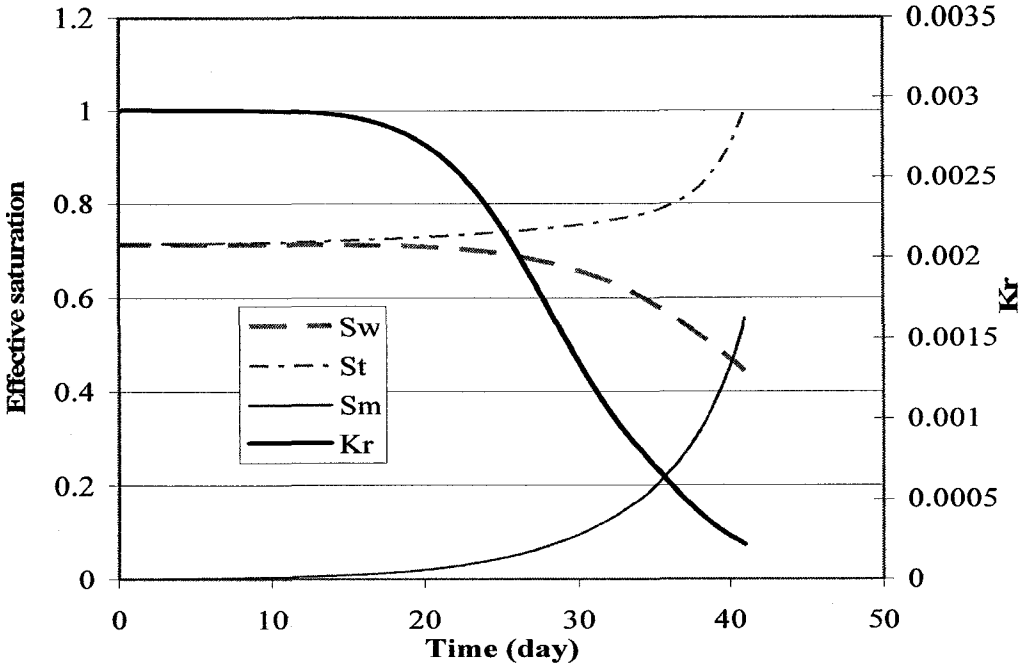

Figure 4-20: Relative permeability, actual total, water and microbial saturation versus time for the top of column for model #3

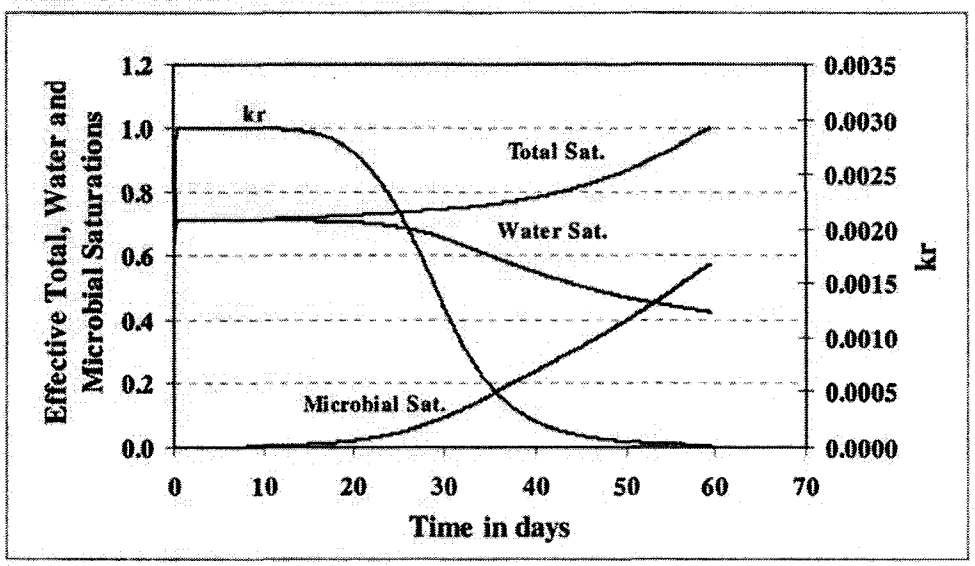

Figure 4-21: Relative permeability, effective total, water and microbial saturation versus time for the top of column for model #3(Mostafa 2004)

CHAPTER 5 -APPLICATION OF MODEL

5.1 MODEL APPLICATIONS

This chapter outlines three applications of the numerical model that was developed in this research. The first application illustrates the effect of pulse loading versus continuous loading on the clogging process. The second application illustrates the influence of a number of input parameters on the depth of the clogging zone and clogging time as well as comparing the results of different relative permeability models. These parameters can be either soil properties or the Monod kinetic parameters such as maximum growth rate, decay rate or bacterial density. The last application illustrates the progressive clogging of a two-dimensional septic bed in which wastewater discharges at the up-gradient end of the septic bed and the clogging progresses toward the down-gradient of the septic bed.

Six soils consisting of three peats and three sands with different hydraulic properties are considered for the simulations conducted in this chapter. Table 5-1 lists the hydraulic properties of each soil including the irreducible saturation, saturated hydraulic conductivity, porosity and Van Genuchten parameters. The hydraulic properties of the three different peats with different density were obtained from literature (Shibchurn et al. 2005). The density of the peats varied from low to high for peat 1 through peat 3. Three different sands were selected based on their application. Sand 1 is a filter media bed sand which is a uniform sand with a relatively high porosity. Sand 2 is a concrete sand which is a well graded sand with 1.7 percent fines. Sand 3 is a septic bed sand, which is a well graded sand but with a higher amount of fines (13.8% fines) than the concrete sand. The

hydraulic properties of sands were obtained from laboratory experiments conducted by Mohamed Mostafa.

Table 5-1: Hydraulic properties of soils assigned in the simulations

	θr	K_{sat} (cm/s)	Porosity	α	n
Peat 1	0.251	0.4779	0.93	0.75	1.5
Peat 2	0.255	0.1823	0.91	0.33	1.4
Peat 3	0.387	0.038	0.86	0.09	1.4
Sand 1	0.13	0.1430	0.478	0.15	4
Sand 2	0.15	0.0310	0.386	0.045	3.4
Sand 3	0.14	0.00504	0.366	0.021	4.6

It should also be noted that the Mualem-based equations for the relative permeability were used for all the simulations presented in this chapter.

5.1.1 Temporal and Spatial Discretization for Simulations

Several simulations were conducted to determine the appropriate temporal and spatial discritization for model. The flow equation proved to be more critical in terms of the allowable spatial and temporal discritization. The flow equation is a highly nonlinear equation and requires a very small time step to converge to the proper solution. However, as the system reaches the steady-state condition, the higher time step values also provide the accurate results.

The small enough time step and accordingly smaller marching time step provides a more accurate result for calculating the results for the next iteration. As a result a more rapid convergence is achieved; however due to the selection of the small time steps, the simulation time normally increases. On the other hand, longer time steps result in a solution with lower accuracy. However, a longer time step will generally decrease the

simulation time. Hence, the optimum time step and marching time step values was selected on the basis that the program will start with the time step and time marching equalling 1 and 0.1 second, respectively, and based on the number of iterations in that time period, the time step for the next time period will be adjusted as follows:

If number of iteration ≤ 5 and time step < 200 s time step= time step + 1

If number of iteration ≥ 15 time step = time step /2

After setting the new time step for the next iteration, the marching time step will be adjusted as follows:

If time step < 10 marching time step =0.1

If time step > 10 marching time step =1

It should be noted that the very small time steps (1 and 0.1 second, respectively) which are selected for the beginning of the simulations are assigned mostly for the simulations with a high flow such as pulse simulations. For the other simulations (simulations with lower flow), the initial time step will rapidly increase to the normal time step, which was about 20 to 100 seconds based on the flow rate and soil types, until the steady-state condition is reached. After the steady-state condition, the time step is maintained at 200 seconds

Based on the above algorithm for selecting the time step, some simulations have been performed to evaluate the optimum element size. For these simulations, a continuous flow of 20cm/day was added to a 100 cm column of sand 3 for a duration of 4 hours. Figures 5-1 illustrates the effect of varying element size (1, 2, 5, and 10 cm) on the simulated water saturation profile. As indicated in Figure 5-1, there is negligible difference between the model result for element size of 1 and 2 cm (maximum difference

of 0.003) and a small difference between element size of 1 cm and 5 cm (maximum difference of 0.013). As the element size increases to 10 cm the inaccuracy of the results increases (maximum difference of 0.019). However, at 4 hr when the infiltration front reaches the lower section of the column and the gradient of the total head is no longer sharp, the predictions based on the 10 cm element size may be acceptable.

For each of the above simulations, after the sand reached the steady-state conditions, a conservative contaminant with a concentration of 2000 mg/L was added to column. Figure 5-2 compares the results of the solute transport model considering element sizes of 1, 2, 5, and 10 cm with the analytical solution. As shown in Figure 5-2, there are small differences in the model results with element sizes of 1, 2, 5 cm and analytical solution (maximum concentration differences of 138, 39, and 163 mg/L for 1, 2, and 5 cm element sizes). The differences increase with an element size of 10 cm (maximum concentration differences of 466 mg/L).

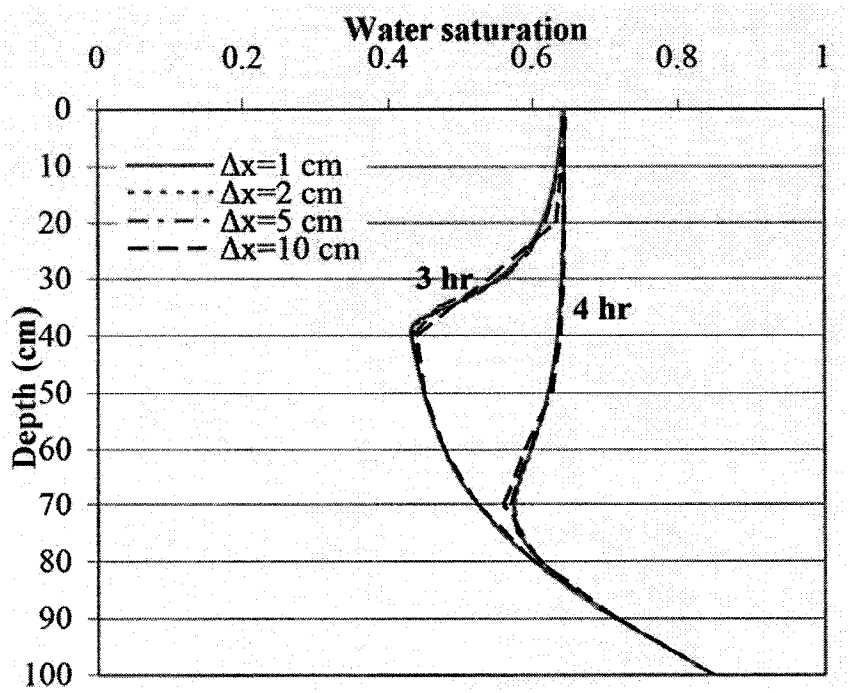

Figure 5-1: Effect of element size on the simulated water saturation profile

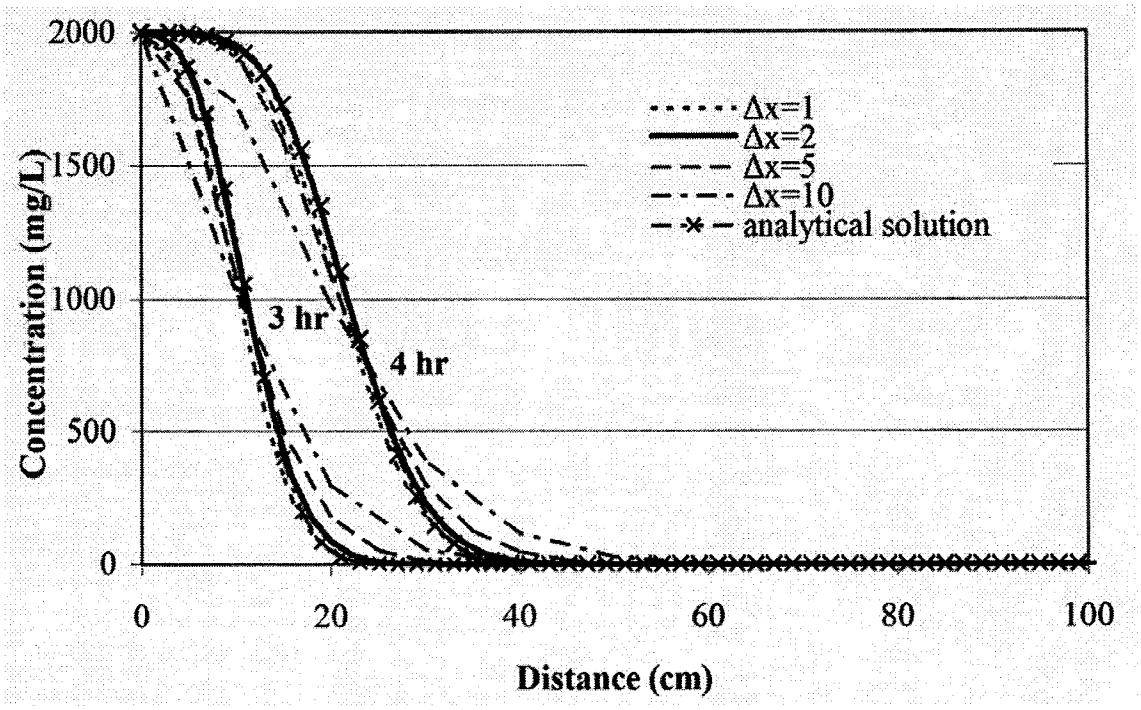

Figure 5-2: Effect of element size on the solute transport model results

The optimum element size that can be selected is the largest value below which further decreases no longer cause a significant change in results. Condur has a built-in mesh generation algorithm, which can produce one, and two dimensional meshes with four node quadrilateral elements, or three node triangular elements. The program allows the user to create transitional elements to refine the mesh in zones where the gradients are sharp.

As it was indicated earlier, for solving flow and transport equations an input data file should be generated that contains the element and node properties. Hence, the increase in the number of nodes and elements increases the simulation time. In order to optimize the simulation time with a good accuracy, the one–dimensional simulations conducted in this chapter have an element size of 1cm for the top 20 cm of the column and 2 cm for the rest of the column. In the two-dimensional simulation, an element size

of 2.5 cm was selected for the top 20 cm of the domain, a 5 cm element size for the centre 50 cm of the domain, and an element size of 10 cm was selected for the bottom 30 cm of the domain. The schematic of generated mesh for one and two-dimensional domain is illustrated in Figure 5-3. Using this element sizes for the one and two-dimensional simulations, the simulation time for simulating 30 days of a one-dimensional 100 cm column was about 3 and half hours, and simulation time for simulating 30 days of a two-dimensional septic bed with the dimension of 100 cm by 100 cm was about 22 hours. These simulations are conducted using a dual core processor 2.66 GHz with 4 MB of RAM.

5.2 COUNTINUOUS VS. PULSE SIMULATIONS

Peat 2 was simulated as a 1-D column with 100 cm height for comparison of pulse versus continuous loading. A constant total head of -40 cm was maintained at the bottom of column for the flow equation. A free exit boundary was maintained at the

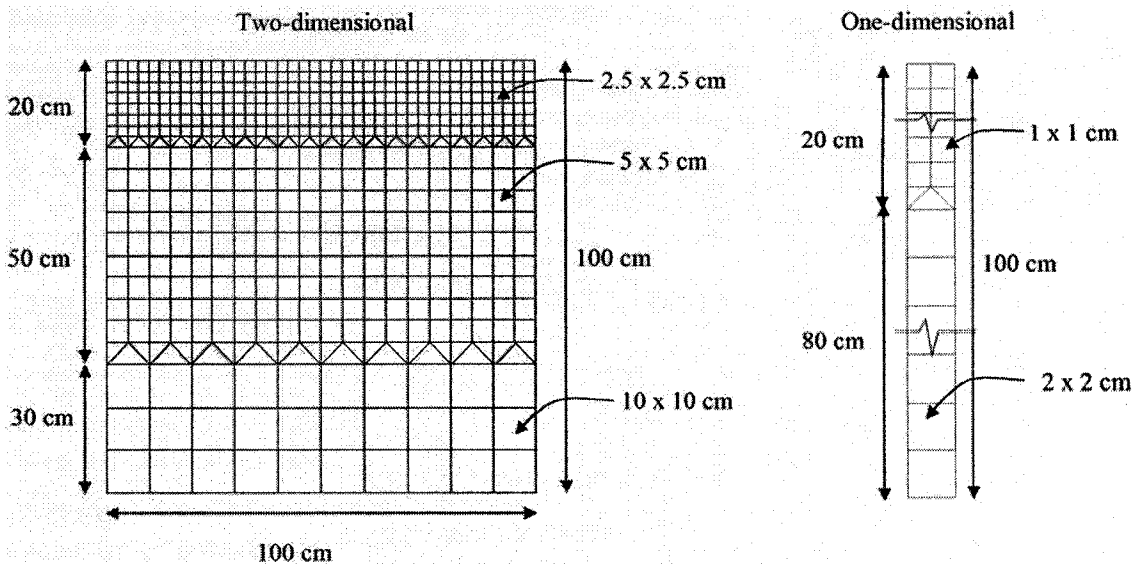

Figure 5-3: Schematic of the element sizes used for the simulations

bottom of column for the transport equation. The Monod parameters for the continuous and pulse simulations, Y, q_m, b and K_s were taken from Mostafa (2004) to be $0.5\left(\frac{mg\ bio}{mg\ sub}\right)$, $5\ E^{-6}\left(\frac{mg\ sub}{mg\ bio.\ s}\right)$, $5.78\ E^{-7}$ (s^{-1}) and $100\left(\frac{mg\ sub}{L}\right)$, respectively. Clogging was assumed to occur once the total saturation of an element reached one, which indicates that the microbial growth caused ponding on top of the column. In all the simulations, the relative permeability term is obtained using model #2 based on the Mualem's equation.

5.2.1 Continuous Loading

The simulation under continuous loading is beneficial as it gives an indication of how a biomat will form and impact the clogging. A constant wastewater flux with a continuous hydraulic loading of 20 cm/day and constant organic loading of 2000 mg/L was applied to the top of column. A high organic loading was simulated because preliminary experimental work at Carleton University used a high organic load to accelerate the clogging process in the laboratory. In addition, the high organic load accelerates the clogging time and reduces the simulation time for the model simulations presented here.

An initial microbial concentration of 1500 mg/L and an initial total head of -40 cm was assigned anywhere in the column. The saturation and concentration profile for the 1-D simulation are given in Figures 5-4 and 5-5, respectively.

Results show that the microbial concentration has a major effect on contaminant transport. As indicated in Figure 5-5, at early times, due to the limited amount of microbial mass, the organic matter could easily migrate to the end of column. As the microbial mass increases, the rate of removal of organic matter increases, and results in

the reduction in concentration downstream in the column. At the time of clogging, the organic matter concentration reaches zero almost anywhere in the column. This is due to

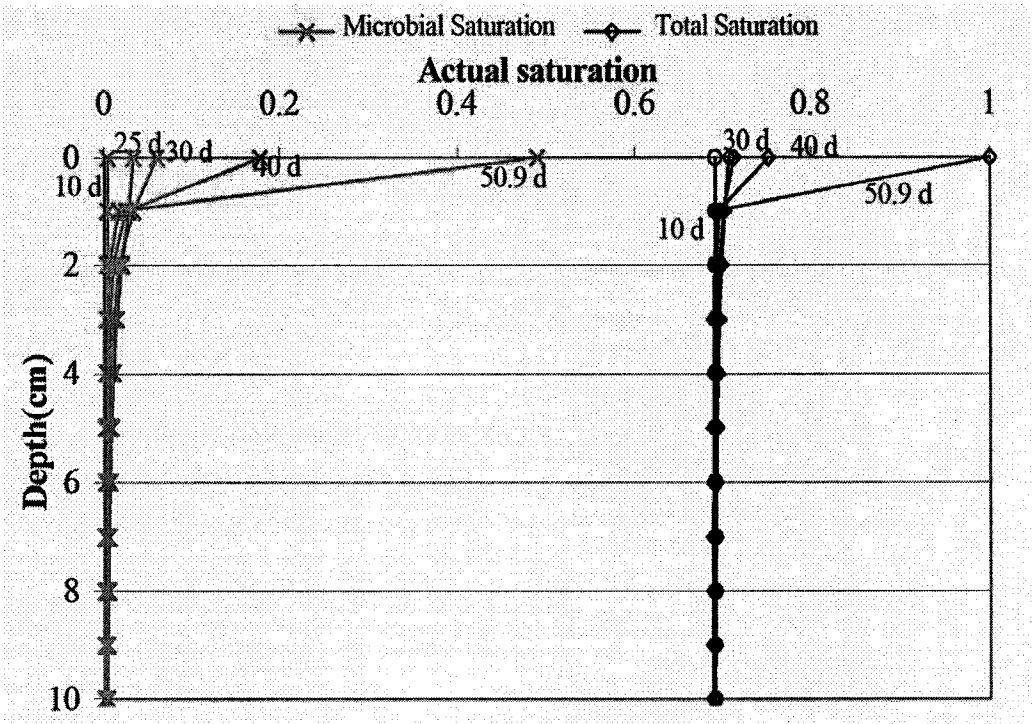

Figure 5-4: Actual saturation profile for peat 2 considering continuous loading

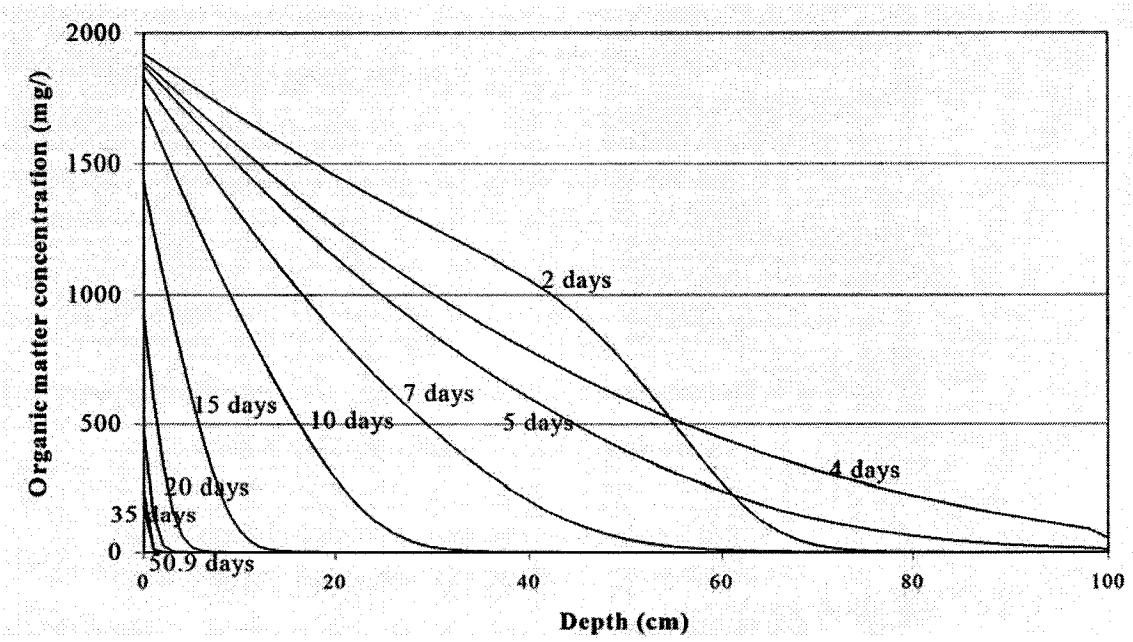

Figure 5-5: Concentration profile for peat 2 considering continuous loading

the consumption of organic matter by the large amount of biomass that is formed at the top of the column. Figure 5-4 illustrate that the most rapid microbial growth occurs at the influent boundary where the organic matter concentration is the highest. Hence, the microbial saturation increases at that boundary and leads to clogging over time.

5.2.2 Pulse Loading

In order to compare pulse loading with the continuous loading results, the same hydraulic and organic loading were simulated. Hence, 10 cm of water was pulsed twice a day over a duration of 30 minutes creating a hydraulic loading of 0.0055 cm/s during each 30-minute pulse. In this case, the total added flux for two pulses per day is equal to 20 cm/day. Accordingly, the simulation consists of a series of stress periods in which the boundary condition for the flow equation was changed from the flux boundary condition of 0.0055 cm/s for 30 minutes to a no flux boundary condition for 11.5 hours. The saturation profile for this type of boundary conditions is given in Figure 5-6. In this figure, the initial saturation profile at t=0 is based on the prescribed total head of -40 cm everywhere in the column. The influent pulse is applied for 30 minutes and increases the saturation to a maximum of 0.87, which is higher than the steady-state saturation for the continuous loading which was 0.69. After the influent pulse is stopped, the water that entered the column continues to move downward and distributes itself within the column. After 11.5 hours and prior to the next pulse, the saturation profile was not reached its original static profile at t=0 and hence downward flow is still occurring prior to the next pulse.

To evaluate the impact of pulse loading on the saturation and concentration profile, two pulse simulations were conducted. In the first simulation, the 20 cm/day of

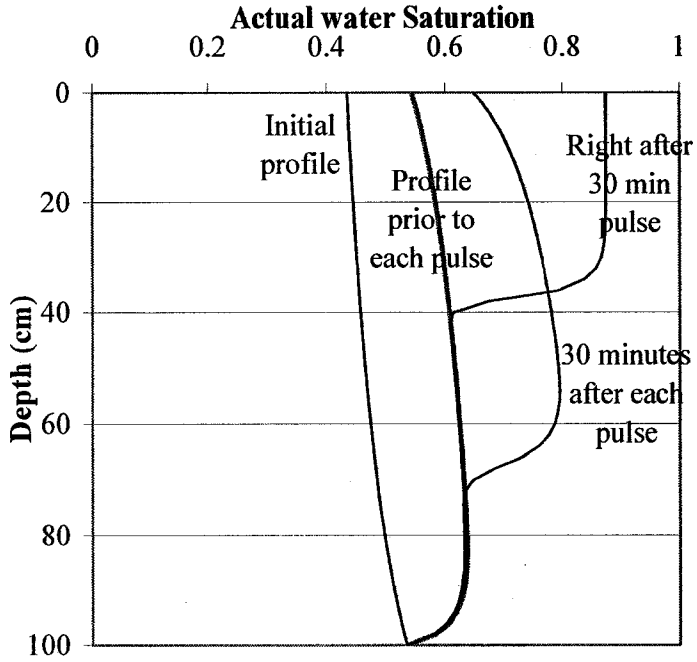

Figure 5-6: Water Saturation profile for the pulsing scenario on peat 2

wastewater contained with the same organic loading (2000 mg/L for the duration of flow) as the continuous condition. Accordingly, the boundary condition for the transport equation was prescribed at 2000 mg/L during the pulse period and no flow boundary for the other times. According to the saturation profile presented in Figure 5-7, clogging was not achieved after 250 days of simulation. The total saturation in this case never reached one, even though the water saturation at the top of the column after each pulse was higher than the steady-state saturation in case of continuous loading. Having a higher seepage velocity during the 30 minute pulse allows the organic matter to penetrate deeper into the peat column. Hence, the local accumulation of microbial mass at the top of column is prevented, and the depth over which microbial mass is distributed increased from 1.5 cm in the case of continuous loading to 21 cm for the pulse loading simulation. Considering the initial microbial saturation of 0.0005, the microbial saturation reached 0.49 after 50.9 days for the continuous loading scenario, which resulted in the clogging. The maximum

microbial saturation reached after the same simulation time for the pulse system was 0.025. The microbial volume that was accumulated in the entire column after the clogging (in 50.9 days) in the case of continuous loading was 0.61 m^3 which was higher than the microbial volume in the case of pulse loading equalling 0.43 m^3. The smaller amount of microbial volume in the case of pulse loading is due to the fact that the organic matter reaches zero everywhere in the column during the no pulse which limits the growth of microorganisms and results in the decay of microbial mass during that period.

To be able to evaluate the influence of pulse loading on clogging, a second pulse simulation was conducted with a higher organic loading (5000 mg/L). In the second pulse simulation, the column was pulsed with hydraulic loading of 20 cm/day, with the same pulse pattern as before, and an organic loading of 5000 mg/L during the pulse period.

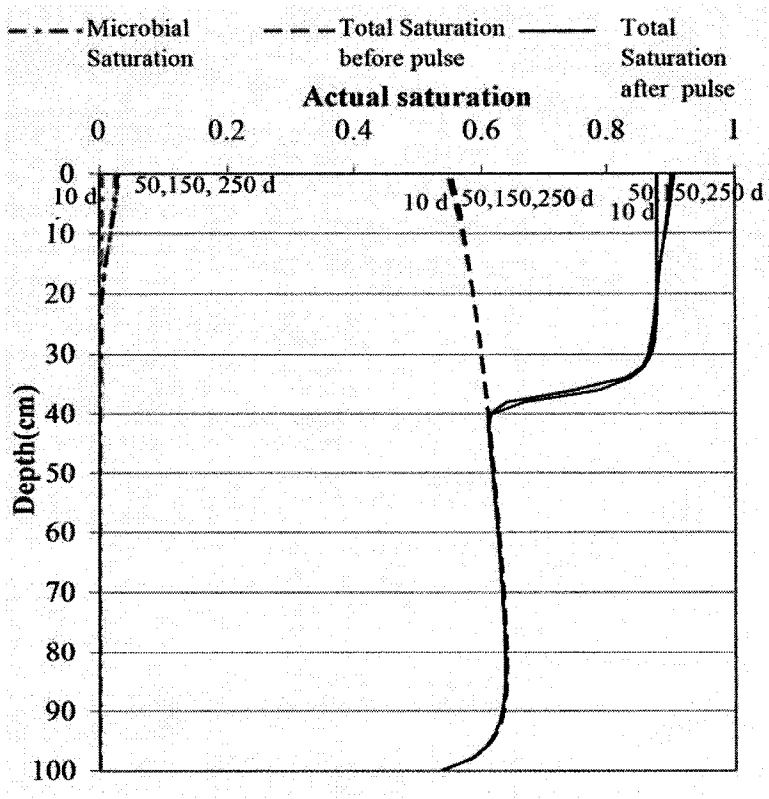

Figure 5-7: First pulse scenario of peat 2 with organic loading of 2000 mg/L

The saturation and concentration profiles for the second pulse simulation are provided in Figures 5-8 and 5-9, respectively. Figures 5-8 and 5-9 indicate that after 80 days, the microbial saturation profile approaches steady-state conditions and hence, the amount of microbial mass that was produced during the pulse period was almost equal the amount of microbial mass that decayed due to the lack of organic matter during no pulse periods. As indicated in Figure 5-9, after 20 days, the concentration profile at the end of the no pulse period prior to the next pulse reached zero indicating that sufficient microbial mass had been established to degrade the entire organic load before the application of the next pulse.

Increasing the organic matter by a factor of 2.5 increased the maximum microbial saturation from 0.031 to 0.081 but did not significantly change the thickness of biomat (approximately 21 cm). Hence, it can be concluded that the change in the biomat thickness in pulse and continuous loading is preliminary due to the seepage velocity of wastewater allowing the organic matter to infiltrate to a depth close to 21 cm and not the concentration of the organic matter.

5.3 INFLUENCE OF MONOD PARAMETERS ON CLOGGING PROCESS

A 25 cm column of Sand 3, septic bed sand, under a continuous hydraulic loading of 20 cm/day and organic loading of 2000 mg/L is simulated with different Monod kinetic parameters to evaluate the impact of Monod parameters on the clogging process. Two performance indicators were considered to compare the simulation results. The first indicator was the time that the clogging occurs, which was defined as the time that the actual microbial saturation reached 0.4. The second indicator is the depth of the clogging

zone (biomat thickness) which was described as the depth with a microbial saturation of more than 0.05.

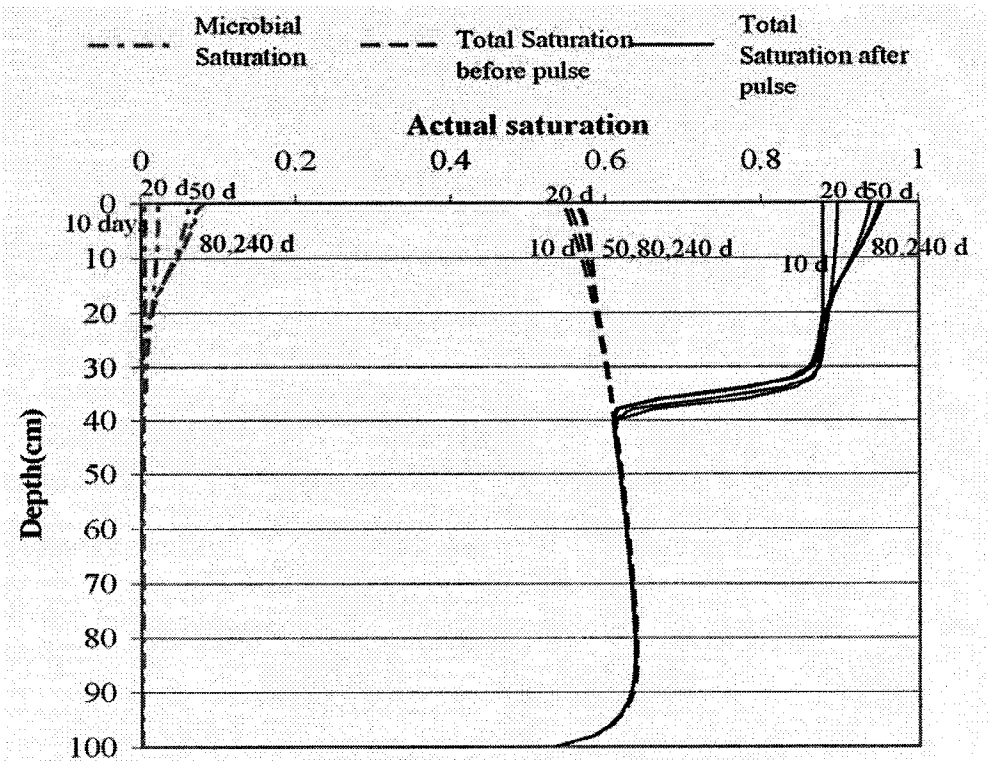

Figure 5-8: Saturation profile for the second pulse simulation for peat 2 with organic loading of 5000 mg/L

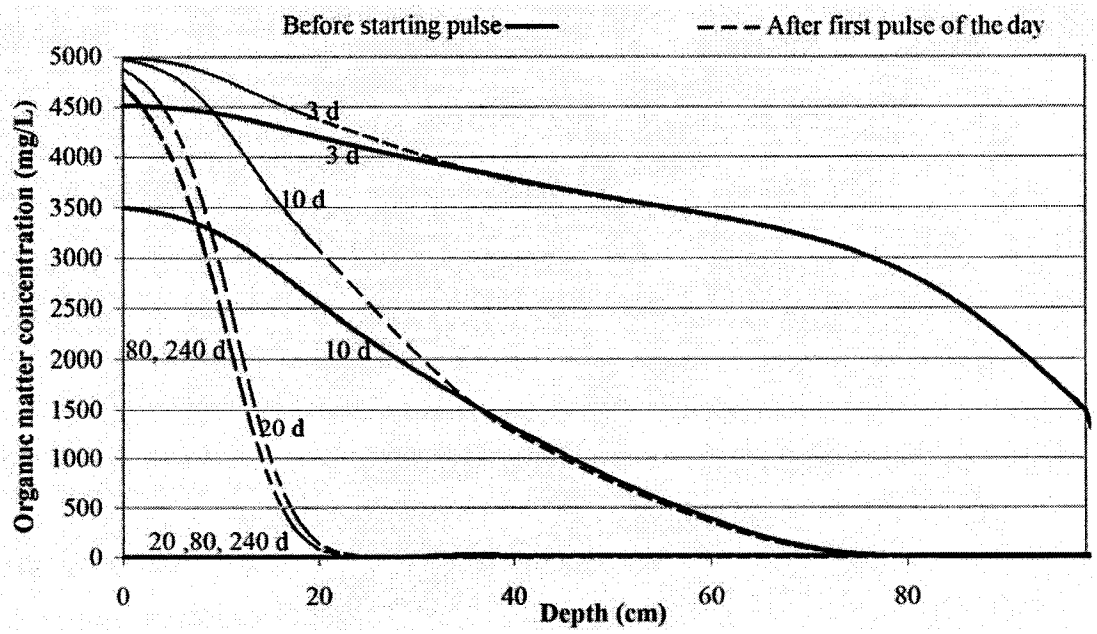

Figure 5-9: Concentration profile for the second pulse simulation for peat 2 with organic loading of 5000 mg/L

A summary of the reported values for the kinetic constants of the Monod equation corresponding to growth and degradation of a variety of bacteria was provided in Table 1-1. A comparison of kinetic values is difficult due to the variability in the environmental and operational conditions. In the absence of experimentally derived kinetic constants specific to the system modeled, the kinetic values of Mostafa (2004) were initially utilized, and a reasonable range was assigned to each parameter to compare the impact of the parameters on the biological clogging process. Table 5-2 lists the initial estimate of these parameters (Mostafa, 2004) and the range of values used for comparison. The kinetic parameters will be varied one by one to assess the sensitivity of

Table 5-2: Monod kinetic parameters used in the simulations

	Description		q_m $\left(\frac{mg\ sub}{mg\ bio.\ s}\right)$	b (s^{-1})	$\frac{Yq_m\ C}{b\ C+K_s}$	initial M_T $\left(\frac{mg\ bio}{L}\right)$	ρ_m $\left(\frac{mg}{cm^3}\right)$
case 1	Initial values (Mostafa, 2004)		5.0E-06	5.78E-07	4.12	1500	1.39
case 2	Reduction in ρ_m		5.0E-06	5.78E-07	4.12	1500	1.0
case 3	Change in q_m	20% decrease	4.0E-06	5.78E-07	3.30	1500	1.39
case 4		50% decrease	2.5E-06	5.78E-07	2.06	1500	1.39
case 5	Change in b	20% decrease	5.0E-06	4.62E-07	5.15	1500	1.39
case 6		50% decrease	5.0E-06	2.89E-07	8.24	1500	1.39
case 7	High decay		5.0E-06	2.30E-06	1.04	1500	1.39
case 8	Smaller initial M_T		5.0E-06	5.78E-07	2.06	1000	1.39
case 9	Smaller initial M_T and q_m		2.5E-06	5.78E-07	2.06	1000	1.39
case 10	Smaller initial M_T, ρ_m, q_m		2.5E-06	5.78E-07	2.06	1000	1.0
case 11	no decay		5.0E-06	0	---	1500	1.39
case 12	50% decrease in q_m and b		2.5E-06	2.89E-07	4.12	1500	1.39

the model to each parameter separately. In order to evaluate the impact of varying the parameters, all the simulations were performed using model #1 for relative permeability and considering constant K_s, and Y equalling $100\left(\frac{mg\ sub}{L}\right)$, $0.5\left(\frac{mg\ bio}{mg\ sub}\right)$, respectively.

The estimated clogging time, and the depth of clogging zone for different cases using model#1 for relative permeability is visualized in Figures 5-10 and 5-11, respectively. As indicated in Figure 5-10, a reduction in the microbial density (case 2) reduces the clogging time. This is expected as a lower density results in a greater microbial volume and hence less amount of microbial mass is needed to fill the same void space. As a result, the time to generate the same microbial saturation for clogging will be reduced. Similarly, the lower microbial density created a slightly thicker biomat based on the biomat thickness defined for this comparison (S_{em}>0.05). Generally, a reduction in the growth rate by 20 % and 50 % in cases 3 and 4, respectively, increased the time to clogging by reducing the microbial mass that is produced over time. Moreover, the reduction of the microbial mass at the top of the column facilitates the transport of the organic matter further into the column so that the depth of clogging zone increased by 1 cm and 1.5 cm, respectively, for the growth rate reduction of 20 % and 50 %.

A decrease in the microbial decay rate, in case 5 and 6, reduced the time of clogging and increased the depth of clogging zone by increasing the net rate of biomass formation. In case 7, a very high decay coefficient did not allow bacteria to grow at a rate greater than the decay so that after 700 days no clogging occurred. In case 8, reducing the initial microbial concentration by 500 mg/L increased the clogging time slightly from 40.3 days to 43 days but did not noticeably change the biomat thickness. It is also

indicated that 50 percent reduction in the microbial growth rate has a more significant impact on the clogging time and biomat thickness than 500 mg/L reduction in the initial microbial concentration.

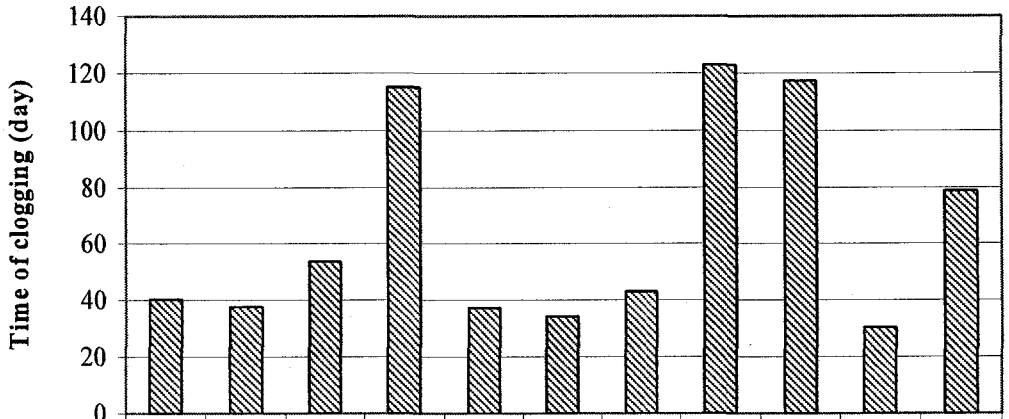

	case 1	case 2	case 3	case 4	case 5	case 6	case 8	case 9	case 10	case 11	case 12
Time of Clogging (day)	40.3	37.6	53.6	115.3	37.2	34.1	43	123	117.4	30.3	78.9

Figure 5-10: Estimated time of clogging for different cases listed in Table 5-2, using Model#1 of relative permeability

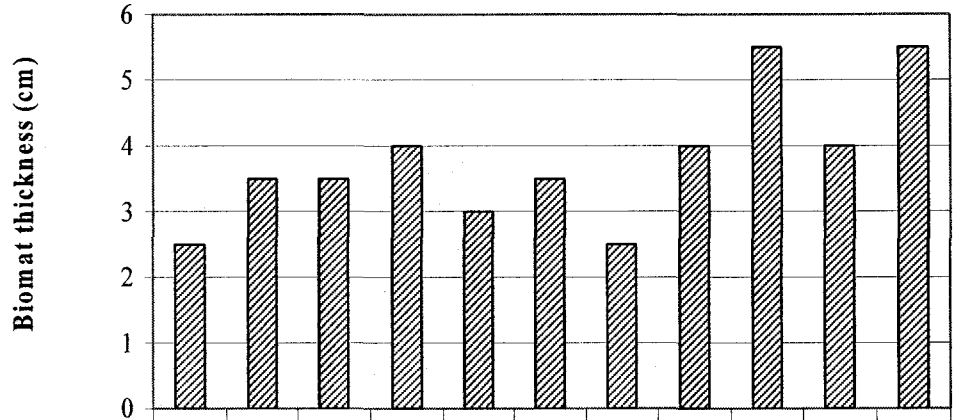

	case 1	case 2	case 3	case 4	case 5	case 6	case 8	case 9	case 10	case 11	case 12
Biomat thickness (cm)	2.5	3.5	3.5	4	3	3.5	2.5	4	5.5	4	5.5

Figure 5-11: Estimated depth of clogging zone for different cases listed in Table 5-2, using Model#1 of relative permeability

Starting the simulation in case 4 with a smaller microbial concentration in case 10, again increase clogging time slightly. However, reducing M_T had higher impact in case 4 with a lower q_m than in case 1. As it is indicated, reducing M_T in case 8 with the higher q_m increased clogging time by almost 3 days but reducing M_T in case 9 with a lower q_m increased clogging time by almost 8 days. Case 10 is a combination of case 2 and case 9, in which a reduction in microbial density is considered along with a reduction in initial microbial mass and microbial growth rate. It has been concluded that the reduction in the microbial density reduces the clogging time and reduction in microbial mass and growth rate increase the clogging time. In case 10, the clogging time was increased but it was less than the clogging time in case 9 due to the reduction in microbial density. It seems that q_m has a more significant impact on the clogging time than the microbial density.

No decay in case 11, reduced the clogging time as the reduction in the microbial mass due to the decay of microorganisms was not considered. Likewise, the thickness of biomat increased in case 11. Case 12 is a combination of case 4 and case 6. In this case, having a lower growth rate than case 1 increased the clogging time however, the smaller decay rate also reduced the time to clogging relative to case 4. Both reduction in the growth rate and the decay rate coefficient in case 4 and 6 increased the biomat thickness 1.5 cm and 1 cm, respectively. Hence, considering cases 4 and 6 together in case 12 increased the biomat thickness by 3.0 cm.

The coefficient of $\left(\frac{Yq_m}{b}\frac{C}{C+K_s}\right)$, which represents the ratio of the growth rate over the decay rate, is a good representative of the clogging time; since, the highest value for

$\left(\frac{Yq_m}{b}\frac{C}{C+K_s}\right)$ shows the lowest clogging time and the lowest value represents the highest clogging time. No relationship between biomat thickness and clogging time has been observed as the biomat thickness is mostly related to the hydraulic loading and the amount of biomass present in the column.

Cases 1, 4, 6 and 12 are chosen to evaluate the performance of model #2 and model #3 for the relative permeability using the different kinetic parameters. The results of the estimated clogging time and biomat thickness for model #2 and model #3 are presented in Figures 5-12 and 5-13, respectively. The simulated differences in the biomat thickness are small and a slight decrease in the clogging time was simulated for model #2 and model #3for relative permeability.

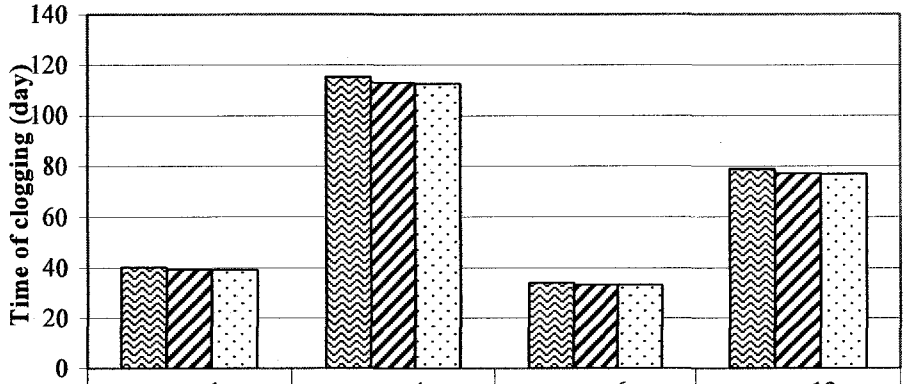

	case 1	case 4	case 6	case 12
Model # 1	40.3	115.3	34.1	78.9
Model # 2	39.4	112.9	33.4	77.3
Model # 3	39.3	112.6	33.3	77.1

Figure 5-12: Comparison of three models for relative permeability on the clogging time for some cases listed in Table 5-2

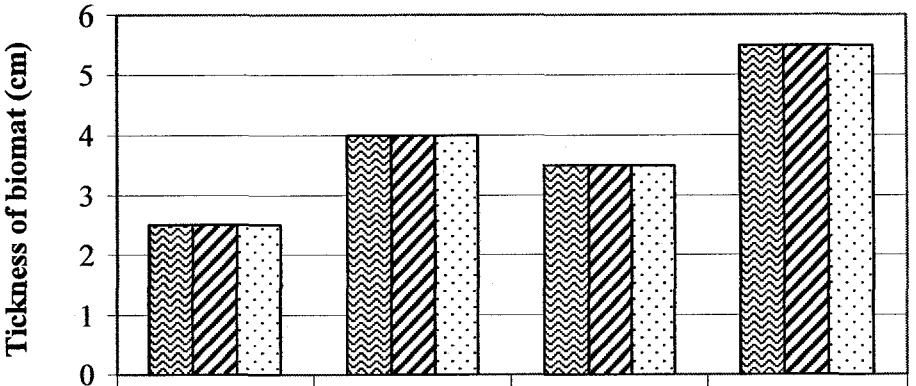

	case 1	case 4	case 6	case 12
Model # 1	2.5	4	3.5	5.5
Model # 2	2.5	4	3.5	5.5
Model # 3	2.5	4	3.5	5.5

Figure 5-13: Comparison of three models for relative permeability on the biomat thickness for some cases listed in Table 5-2

It should be noted that the simulated biomat thickness is sensitive to the spatial discretization at the top of the column. Because the element size of 1 cm was used at the top, the biomat thickness was reported in the 0.5 cm increment. Hence, in some cases the depth of the node with the microbial saturation close to the 0.05 was reported as the biomat thickness, and if microbial saturation of 0.05 was between two depths, the middle of the two depths was reported as the biomat thickness.

Since, varying the Monod parameters caused the simulated clogging time for the same soil to vary from 37.2 days to 117.4 days, it can be concluded that the model is highly sensitive to the Monod kinetic parameters.

5.4 DIFFERENT SOIL TYPES

To evaluate the clogging process in different soil types with different hydraulic parameters, six different soils listed in Table 5-1 are simulated using model #2 for relative permeability. The simulations are conducted using the Monod parameter values

taken from Mostafa (2004) and the initial and boundary conditions listed in Table 5-3. To evaluate the results of the model, the clogging time is defined as the time when the total saturation reaches one.

Table 5-3: Initial and boundary conditions for simulations on different soils

Boundary and initial conditions	
Flow equation	Top: flux =0.000231 cm/s Bottom: prescribed head = -40 cm
Transport equation	Top: prescribed concentration =2000 mg/L Bottom: exit boundary
Initial Microbial concentration	M_T= 1500 ($\frac{mg_{biomass}}{L}$)
Column height	100 cm

Figures 5-14 contains a comparison of the clogging time for the six soils, and indicates that the clogging occurs later in a less dense peat with higher porosity (peat 1) and as the density of peat increases, the time to clogging reduces. It also illustrates that the clogging time in sands is less than peats since sands have smaller porosities.

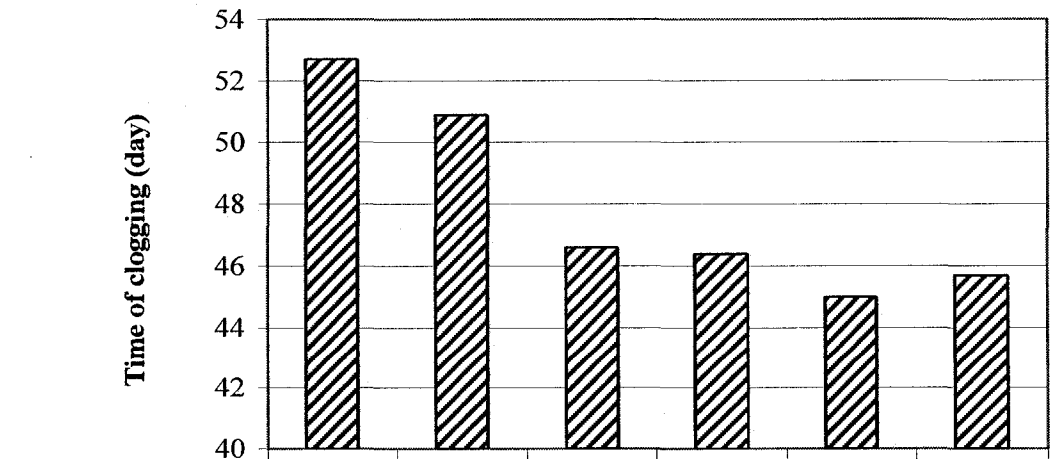

Figure 5-14: The estimated time of clogging for different soil types

Figure 5-15 illustrates the saturation profiles at the time of clogging for peats, and reveals that the clogging time for a peat with a lower steady-state saturation and higher porosity (less dense peat) is longer than for a peat with higher steady-state saturation and smaller porosity. In this figure, the clogging time is reduced from 52.7 days for peat 1 to 50.9 days for peat 2 and 46.6 days for peat 3 as the steady-state saturation increases from 0.58, to 0.69 and 0.83, for peat 1, peat 2 and peat 3 respectively. Similar profiles for the sands are presented in Figure 5-16. According to Figure 5-16, the steady-state saturation for sand 1 (filter media bed sand), sand 2 (concrete sand) and sand 3 (septic sand) are 0.39, 0.56, and 0.65, respectively. The smaller porosities and smaller hydraulic conductivities of the sands decrease the clogging time compared to the peats. In the sands, sand 1 with the highest porosity, highest hydraulic conductivity, and uniform grain size provides a better situation in terms of the time to clogging.

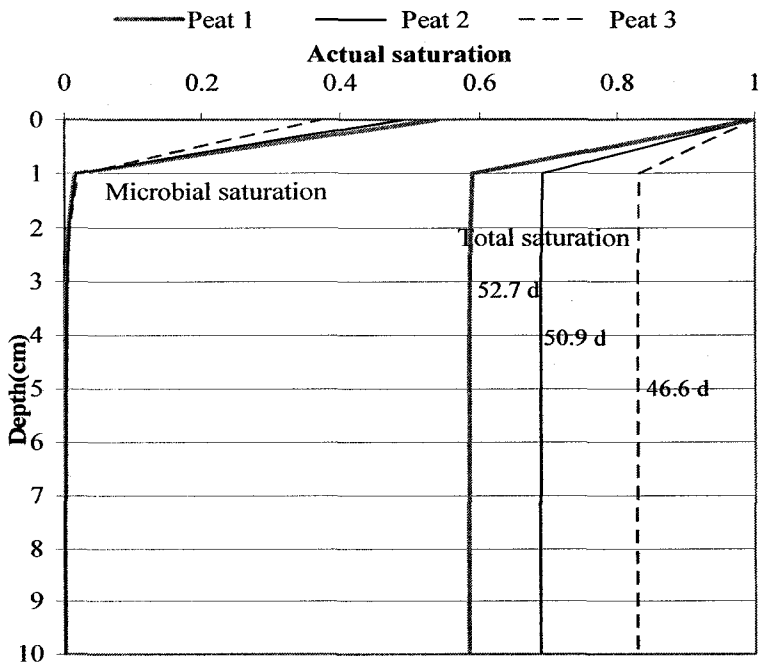

Figure 5-15: Saturation profiles at the clogging time for peat1, peat2 and peat3

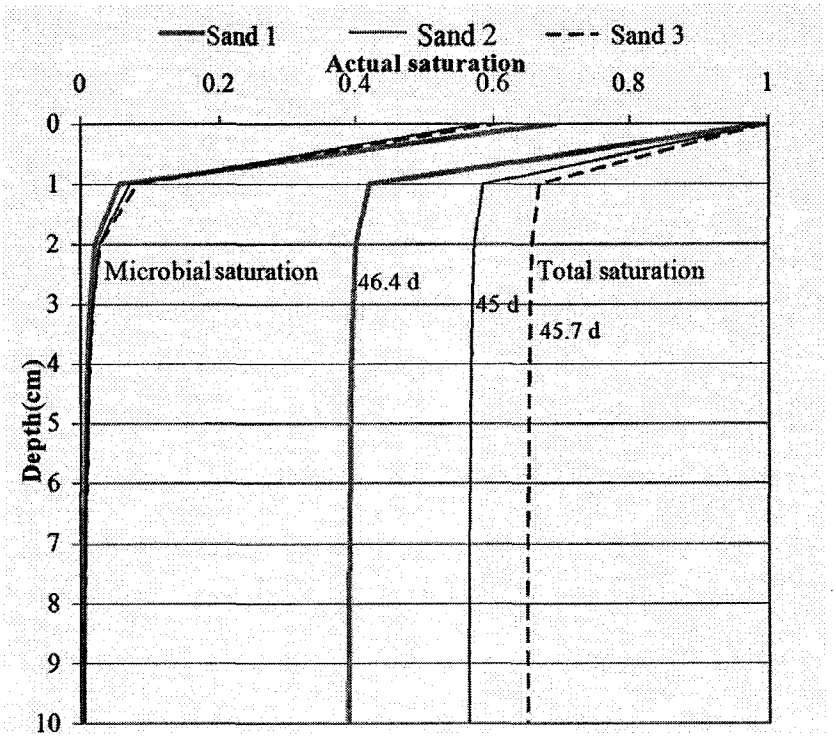

Figure 5-16: Saturation profiles at the clogging time for sand1, sand2 and sand3

As indicated in Figures 5-15 and 5-16, the depth of biomat zone increased from 1 cm in the peats to 2.5 cm in the sands. Having a higher seepage velocity in sands increased the biomat thickness by allowing the organic matter to penetrate further into the column.

5.5 APPLICATION IN SEPTIC BED CLOGGING

To illustrate the progressive clogging of a septic bed, a two-dimensional simulation was conducted. In order to increase the efficiency of the model and reduce the simulation time, only part of a septic bed was considered for 2-D simulation. The septic bed sand (sand 3) with the properties given in Table 5-1 was simulated as a 2-D septic bed with the dimension of 100 cm by 100 cm, to simulate the initial up-gradient section of a septic bed. Considering the hydraulic loading of 20 cm/day over the entire area of the

septic bed, the hydraulic loading for the simulated part of the bed was estimated based on a typical septic bed length of 15 m. The flow was simulated to enter the up-gradient end of the bed by applying a flux to the first three elements, each 2.5 cm in length. The flow calculation is as follows:

$$q = 20\frac{cm}{day}\left(\frac{1500cm}{7.5cm}\right) = 4000\frac{cm}{day} = 0.046\frac{cm}{s}$$

Accordingly, the organic loading was considered as a prescribed concentration of 2000 mg/L for the elements where the flow is entering. In order to simulate the perforated PVC distribution pipe that is typically used in a septic bed to distribute the septic tank effluent, clogging was neglected in the top row of elements. Hence, as the soil clogged below the up-gradient elements, the septic tank effluent could migrate laterally and infiltrate into the down-gradient areas with less microbial growth. The Monod input parameters were taken from Mostafa (2004) and are listed in Table 4-3. The initial condition for total head and organic matter concentration were at -40 cm and zero, respectively, everywhere in the filter bed.

The simulated total head, total saturation and microbial saturation for the 2D simulation are presented in Figures 5-17, 5-18 and 5-19, respectively. As expected, the wastewater starts to infiltrate at the up-gradient end of the distribution pipe. At 20 days the flow is mostly infiltrating between x=0 to x= 20 cm. At 40 days the flow is mostly infiltrating within the first half of the simulated domain (i.e. first 0.5 meter of a septic bed). The infiltration of wastewater within the first half of the domain will support the growth of the microbial mass in that area. As the biomat starts to form at that location (from day 1 to day 40) flow will continue to follow a path of least resistance and as indicated at day 43, the flow is shifting down-gradient in the bed. After 43 days, the

biomat established in the first half of the domain is mature enough to restrict the vertical flow and limited septic tank effluent can enter the bed from the first half of the bed so that the saturation under the biomat zone decreases (Figure 5-18). Profile of total head (Figure 5-17) also confirms that after 43 days flow is mostly entering from the down-gradient half of the domain (x=50 cm to x=100 cm) resulting in the water saturation reduction in the first half of the domain and the increase in the water saturation for the down-gradient areas. The profile of microbial saturation at day 50 (Figure 5-19) shows that the mature biomat has covered almost the entire top of the septic bed where the wastewater is entering. The formation of a mature biomat almost everywhere in the top elements at day 50, results in an increase in the total head within the entire PVC pipe to increase the driving force (hydraulic gradient) to force septic tank effluent through the biomat. By day 56, the total saturation for the top elements reaches one, which means that the wastewater starts to pond up, and complete clogging has occurred. Hence at 56 days, the flow beneath the biomat is largely vertical as indicated by the equal potential lines (Figure 5-17) and water saturation profile (Figure 5-18).

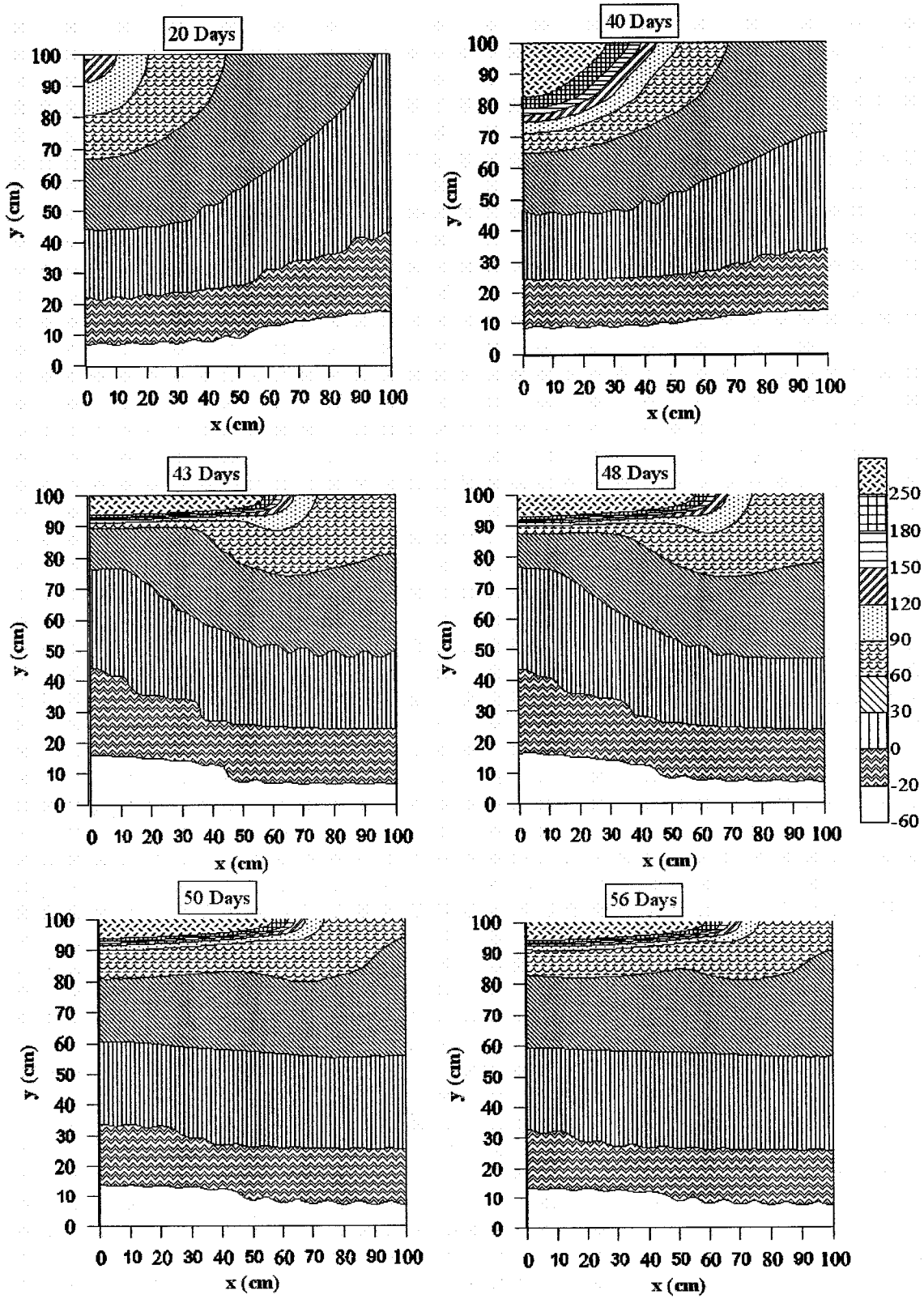

Figure 5-17: Total head in a two-dimensional septic bed sand media

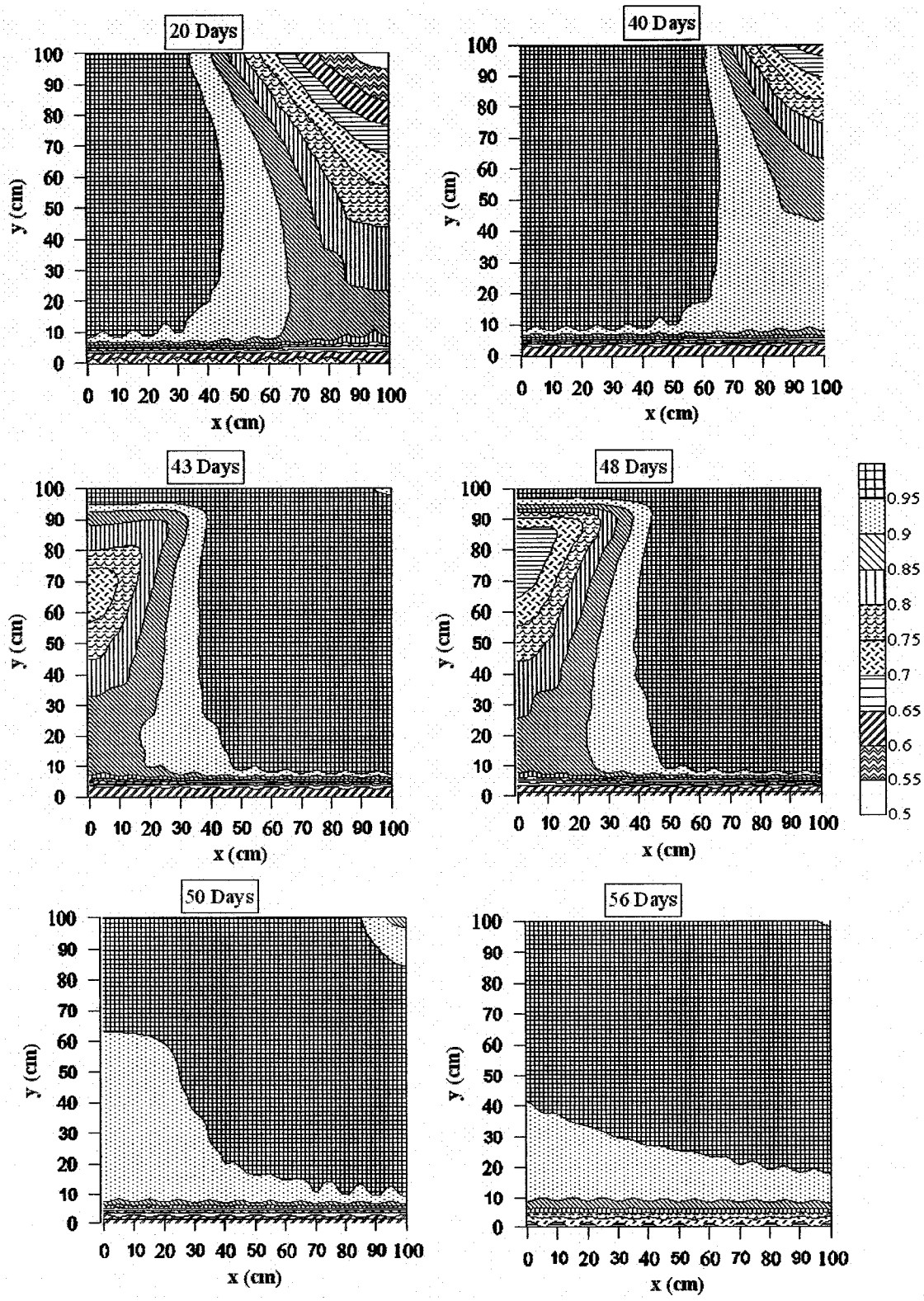

Figure 5-18: Total saturation in a two-dimensional septic bed sand media

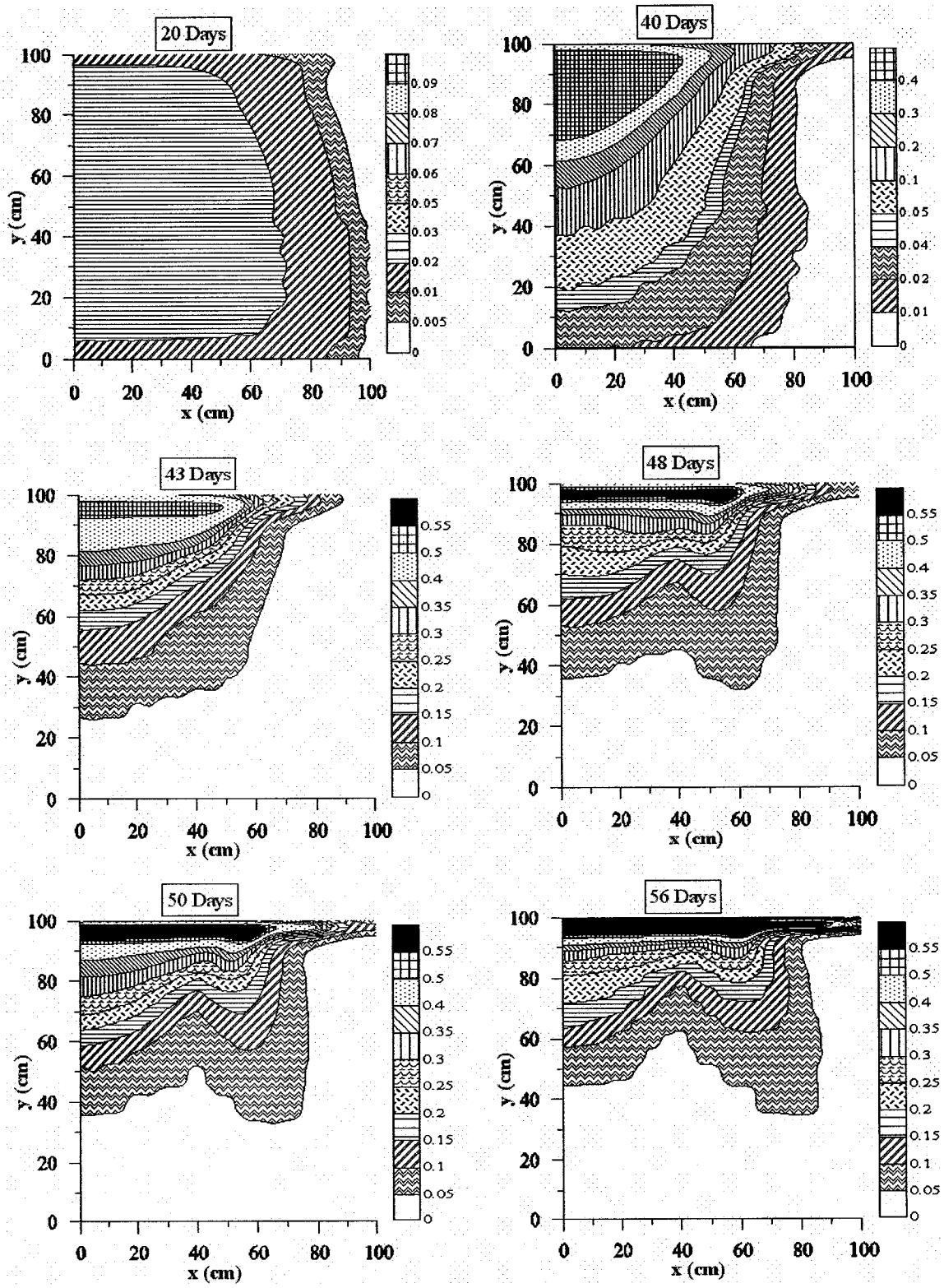

Figure 5-19: Microbial saturation in a two-dimensional septic bed sand media

CHAPTER 6 - CONCLUSIONS AND RECOMMENDATIONS

6.1 CONCLUSIONS

A two-dimensional model was developed to simulate biological clogging due to microbial growth under unsaturated soil conditions applicable to biofilters. The model assumes that the microbial growth occurs in the aqueous phase and is attached to the surface of the soil grains so that it reduces the available pore space for fluid flow. The model incorporates three relative permeability relationships proposed by Mostafa and Van Geel (2007) which relate the relative permeability to microbial growth. The model is also used to illustrate how the clogging will progress in a two-dimensional septic bed system.

The model is capable of simulating the formation of a biomat at the filter surface. The simulation results showed that due to the presence of the highest concentration of organic matter at the top of the column, where the wastewater is introduced into the filter, the highest microbial growth occurred at the top resulting in the formation of a biomat at that location. It was also shown that pulse loading of wastewater (high flow in a short period of time) will allow the wastewater to infiltrate further into the filter and hence reduce the accumulation of microbial mass at the top surface of the column. Therefore, pulse loading causes microbial growth to occur over a greater depth preventing the formation of a thick biomat and increasing the longevity of biofilters.

The model was used to simulate three sands (filter media sand, concrete sand, and septic bed sand) and three peats at three different densities. The simulations confirm that soils with higher porosity and hydraulic conductivity increase the time to clogging. The greater porosity requires more biomass to form the biomat. Therefore, the peat soils took longer to clog. The biomat for the sands was thicker than the biomat formed in the peats since the seepage velocity was greater in the sand soils with lower porosity. Among peats, the less dense peat, and among sands, the sand with the highest porosity and hydraulic conductivity performed better in terms of the time to clogging.

The model is also used to investigate the influence of the Monod kinetic parameters on the time to clogging and biomat thickness. Reasonable ranges for the Monod parameters, as reported in the literatures, have been selected to perform the Monod parameter sensitivity analysis. The results show the high sensitivity of the model results to the Monod kinetic parameters. Simulations conducted for a peat column with the constant hydraulic and organic loading, illustrated that for the specified range of values of Monod parameters, the clogging time varied from 37.2 days to 123 days and the biomat thickness varied from 2.5 cm to 5.5 cm.

Through a 2-D simulation of a septic bed, the model was able to simulate the progressive clogging of a septic bed. The up-gradient section of a septic bed was simulated. To simulate the lateral flow within the perforated PVC distribution pipe, microbial growth was not simulated in the top row of elements allowing the wastewater to migrate laterally as the biomat formed below the top row of elements. It was shown that the clogging will start from the inlet location at the up-gradient end resulting in the formation of the biomat at that location. The biomat formation will continue toward the

down-gradient end of the septic bed. Once the biomat formed along the entire length of the simulated section, the total head built up in the top row of elements to generate a large gradient for flow through the biomat.

6.2 FUTURE RESEARCH

Great insight has been obtained in this study regarding the phenomenon of bioclogging in biofilters by developing a model which considers the transport of organic matter in unsaturated conditions considering its biodegradation. However, the validation of the model should be conducted by comparison with experimental data that measure the spatial distribution of the organic matter along the column and microbial population as well as the saturation.

Bacterial transport is neglected in the developed model, but it should be modeled if significant biomass is forming on the top of the column, and significant biomass is detaching from the porous media. Modeling the transport of bacteria in the unsaturated zone should consider the attachment and detachment of bacteria to the solid surface. Inclusion of bacterial transport should improve the proposed model and allow it to better reflect reality.

Extensive research is required in the area of the growth kinetics of bacteria present in biofilters considering different condition such as aerobic or anaerobic. For this study, the Monod kinetics suggested for wastewater treatment or sludge treatment have been used, and therefore little is known of the Monod kinetics in typical filter media. As indicated in the results, the developed model is very sensitive to the Monod kinetic parameters, even within reasonable ranges as provided in the literature. An experimental

method should be developed for calibration of Monod kinetic input parameters with the proposed model.

The model assumes that it is only the growth of bacterial mass that fill the pore spaces and reduce the relative permeability. However, the build up of dead bacteria and solid residue should also be considered as factors which reduce the pore spaces.

The program was capable of refining the mesh in the areas where a sharp gradient existed to reduce the simulation time. However, simulation time is still problematic and is restricted to the temporal and spatial discretizations. To further improve the model in this case, it is suggested to change the type of finite element solver, Condur, from executive file to an internal process call.

Finally, this model could be extended to three dimensions to study the clogging mechanism and the phenomena of organic matter transport in unsaturated conditions more realistically.

REFERENCES

Alison, L.E. (1947). Effect of Microorganism on Permeability of Soil under Prolonged Submergence. Soil Science, 63,439-450.

Baveye, P., and A. Valocchi (1989). An Evaluation of Mathematical models of the Transport of Biologically Reacting Solutes in Saturated Soils and Aquifers. Water Resources Research, 25(6), 1413-1421.

Bazin, M. J., and J. I. Prosser (1976), Models of Microbial Interactions in the Soils. Critical Reviews in Microbiology, 4, 463-498.

Beach, D.N. and J.E. McCray (2003). Numerical Modeling of Unsaturated Flow in Wastewater Soil Absorption system. Ground Water Monitoring and Remediation, 23(2), 64-72.

Beal, C., T. Gardner, N.W. Menzies, D. Rassam and A. Veritz (2004). Prediction of Steady-state Flux Through Variably Saturated Zones within aSeptic Absorption Trench.3rd Australian New Zealand Soils Conference, 5-9 Dec. 2004.

Beal, C.D., E.A. Gardner and N.W. Menzies (2005). Process Performance and Pollution Potential: A Review of Septic Tank-Soil Absorption Systems. Australian Journal of Soil Research, 43(7), 781-802.

Bear, J. (1979). Hydraulics of Groundwater. McGraw-Hill Inc.

Brooks, R.H., and A.T. Corey (1964). Hydraulic Properties of Porous Medium. Hydrology Paper no. 3, Civil Engineering Department, Colorado State University, Fort Collins, Colo.

Bouma, J., J. C. Converse, and F. R. Magdoff (1974). Dosing and Resting to Improve Soil Absorption Beds. Transaction of ASAE, American Society of Agricultural Engineers, 17(2), 295-298.

Bouma, J. (1975). Unsaturated Flow during Soil Treatment of Septic Tank effluent. Journal of the Environmental Engineering Division, 101, 967-981.

Burdine, N.T. (1953). Relative Permeability Calculation from Pore Size Distribution Data. Transactions of the American Institute of Mining, Metallurgical, and Petroleum Engineers, 198, 7 1-78.

Clement, T.P., B. S. Hooker and R. S. Skeen, (1996). Macroscopic Models for Predicting Changes in Saturated Porous Media Properties Caused by Microbial Growth. Ground Water, 34(5), 934-942.

Converse, J. C. (1974). Distribution of Domestic Water Effluent in Soil Absorption Beds. Transaction of ASAE, American Society of Agricultural Engineers, 17(2), 299-309.

El-Farhan, H., K.M. Scow; L. W. de Jonge, D. E. Rolston, and P. Moldrup (1998). Coupling Transport and Biodegradation of Toluene and Trichloroethylene in Unsaturated Soils. Water Resources Research, 34(3), 437-445.

Freeze, R.A. and J. A. Cherry (1979). Groundwater, Prentice-Hall, Inc.

Frind, E.O. (1988). Solution of Advection-Dispersion Equation with Free Exit Boundary. Numerical Method in Partial Differential Equations, 4, 301-313.

Jones, J. H. and G. S. Taylor, (1965). Septic Tank Effluent Percolation Through Sands under Laboratory Conditions. Soil Science, 99(5), 301-309.

Kaplan, O. B. (1987). Septic Systems Handbook. Lewis Publishers.

Kennedy, P. (1998). Investigation of Flow through Peat Filters. M.Eng. Thesis, Carleton University

Kristiansen, Rolv (1981a). Sand-Filter Trenches for Purification of Septic Tank Effluent: II. The Fate of Nitrogen. Journal of Environmental Quality, 10(3), 358-361.

Kristiansen, Rolv (1981b). Sand-Filter Trenches for Purification of Septic Tank Effluent: III. The Microfloria. Journal of Environmental Quality, 10(3), 361-364.

Kurian, R., G. Nakhla, and A. Bassi (2006). Biodegradation Kinetics of High Strength Oily Pet Food Watewater in a Membrane-Coupled Bioreacter (MBR). Chemosphere, 65, 1204-1211.

Laak, R. (1976). Pollutant Load from Plumbing Fixtures and Pretreatment to Control Soil Clogging. Journal of Environmental Health, 39, 48-50.

Lenhard, R.J., J.C. Parker, and J.J. Kaluarachchi (1991). Comparing Simulated and Experimental Hysteretic Two-Phase Transient Fluid Flow Phenomena. Water Resources Research, 27(8), 2113-2124

Lenhard, R.J. and J.C. Parker (1987). A Model for Hysteretic Constitutive Relation Governing Multiphase Flow 2. Permeability-Saturation Relations. Water Resources Research, 23(12), 2197-2206.

Liu, L., Z. Wang, J. Yao, X. Sun, and W. Cai (2005). Investigation on the Formation and Kinetics of Glucose-fed Aerobic Granular Sludge. Enzyme and Microbial Technology, 36, 712-716.

McCalla, T.M. (1944). Influence of Microorganisms and Some Organic Substances on Soil Structure. US Department of Agriculture, (362).

McCalla, T.M. (1950). Studies on the Effect of Microorganism on Rate of Percolation of Water Through Soils. Soil Science Society of America Proc., 15, 182-186.

McGauhey, P.H., J.H.T. Winneberger (1964). Studies of the Failure of Septic Tank Percolation Systems. Water Pollution Control Federation, 36, 593-606.

Tchobanoglous, G., F. L. Burton, S. H. David and Metcalf and Eddy Inc. (2003). Wastewater Engineering : Treatment and Reuse, Boston : McGraw-Hill.

Ministry of Municipal Affairs and Housing Website. A Guide to Operating and Maintenance of Your Septic System. Housing Development and Buildings Branch,

Mitchell R., Z. Nevo (1964).Effect of Bacterial Polysaccharide Accumulation on Infiltration of Water through Sand. Applied Microbiology, 12(3): 219-223.

Molz, F.J.; M. A. Widdowson, and L. D. Benefield (1986). Simulation of Microbial Growth Dynamics Coupled to Nutrient and Oxygen Transport in Porous Media. Water Resources Research, 22(8), 1207-1216.

Monod, J. (1949). The Growth of Bacterial Cultures, Annual Review of Microbioogy, 3, 1949.

Mostafa, M. (2004). Conceptual Models for Biological Clogging of Unsaturated Soils. M.Sc. Thesis, Carleton University.

Mostafa, M. and P. J. Van Geel (2007). Conceptual Models and Simulations for Biological Clogging in Unsaturated Soils, Vadose Zone Journal 6,175–185.

Mualem, Y. (1976). A New Model for Predicting the Hydraulic Conductivity of Unsaturated Porous Media. Water Resources Research, 12(3), 5 13-521.

Okubo T. And J. Matsumoto (1979). Effect of infiltration rate on biological clogging and water quality changes during artificial recharge. Water Resource Research, 15(6),1536-1542.

Okubo T. And J. Matsumoto (1983). Biological Clogging of Sand and Changes of Organic Constituents during Artificial Recharge, Water Resource Research, 17(7), 813-821.

Otis, R.J. (1985). Soil Clogging Mechanism and Control. Proceeding of the Forth National Symposium on Individual and Small Community Sewage Systems. American Society of Agricultural Engineers, 238-251.

Pell, M., and F. Nyberg (1989 a). Infiltration of Wastewater in Newly Started Pilot Sand-Filter System: I. Reduction of Organic matter and Phosphorus. Journal of Environmental Quality, 18, 451-457.

Pell, M., and F. Nyberg (1989 b). Infiltration of Wastewater in Newly Started Pilot Sand-Filter System: II. Development and Distribution of the Bacterial population. Journal of Environmental Quality, 18, 457-462.

Platzer, C., and K. Mauch (1997). Soil Clogging in Vertical Flow Reed Beds-Mechanism, Parameters, Consequences and .... Solutions?. Water Science Technology, 35(5), 175-181.

Septic Smart! (1999). New Ideas for Household Septic Systems on Difficult Sites. Ontario Soil and Crop Improvement Association.

Shibchurn, A., Van Geel P. J., and Kennedy P. L. (2005). Impact of density on the hydraulic properties of peat and the time domain Reflectometry (TDR) moisture calibration curve, Canadian Geotechnical Journal 42, 279–286.

Siegrist, R. L., and W. C. Boyle (1987). Wastewater-Induced Soil Clogging Development. Journal of Environmental Engineers, 113(3), 550-565.

Siegrist, R. L. (1987). Soil Clogging during Subsurface Wastewater Infiltration as affected by effluent Composition and Loading Rate. Journal of Environmental Quality, 16(2), 181-187.

Taylor, S. W., Jaffé, P. R. (1990). Substrate and Biomass Transport in a Porous Medium. Water Resources Research, 26(9), 2181-2194.

Taylor, S. W., P. C. D. Milly, and P. R. Jaffé (1990). Biofilm Growth and the Related Changes in the Physical Properties of a Porous Medium. 2. Permeability. Water Resources Research, 26(9), 1261-2169.

Thomas, R. E. et al. (1966). Soil Chemical Changes and Infiltration Rate Reduction under Sewage Spreading. Soil Science Society of America Proceeding, 30, 641-646.

Thulliner, M., J. Zeyer and W. Kinzelbach (2002). Influence of Microbial Growth on Hydraulic Properties of Pore Networks. Transport in Porous Media, 49, 99–122.

Touma, J. and M. Vaclin, (1986). Experimental and Numerical Analysis of Two-Phase Infiltration in Partially Saturated Soil. Transport in Porous Media1 27-55.

U.S. Environmental Protection Agency (USEPA), (2002). Onsite Wastewater Treatment Systems Manual. EPA/625/R-00/008. U.S. Environmental Protection Agency, Office of Water Research and Development

http://www.epa.gov/nrmrl/pubs/625r00008/html/625R00008.htm

Van Genuchten, M.T. (1980). A Closed-Form Equation for Predicting the Hydraulic Conductivity of Unsaturated Soil. Soil Science Society of America Journal, 44, 892-898.

Vogelaar, J.C.T.; B. Klapwijk; H. Termmink, and J.B. Van Lier (2003). Kinetic Comparisons of Mesophilic and Thermophilic Aerobic Biomass. Journal of Microbiological Biotechnology, 30, 81-88.

Weintraub L., C.W. Chen, W. Tsai, J. Herr, R. A. Goldstein and R. Siegrist(2002). Modifications of WARMF to Assess the Efficacy of Onsite Wastewater Systems on

Public Health in proceedings from WEFTEC 2002, Chicago, IL, September 28-October 2, 2002.

Williamson, K. and P. L. McCarty (1976 a). A Model of Substrate Utilization by Bacterial Films. Water Pollution Control Federation, 48(1), 9-24.

Williamson, K. and P. L. McCarty (1976 b). Verification Studies of the Biofilm Model for Bacterial Substrate Utilization. Water Pollution Control Federation, 48(2), 281-296.

Zheng, C. and Bennett, G. B. (1995). Applied Contaminant Transport Modeling: Theory and Practice. Copyright Van Nostrand Reinhold.

APPENDICES

APPENDIX A- FLOW EQUATION DERIVATION BASED ON TOTAL HEAD

The equation of flow in unsaturated porous media is based on two unknowns, total head and water content.

$$\frac{\partial(\theta)}{\partial t} = \frac{\partial}{\partial x}(K_r K_{sat} \frac{\partial h}{\partial x}) + \frac{\partial}{\partial y}(K_r K_{sat} \frac{\partial h}{\partial y}) \quad \text{(A-1)}$$

In order to be able to solve this equation it should be converted into a form that has one independent variable. The conversion will be done by using the Van Genuchten $(\theta - P_c)$ relation:

$$\theta_e = \frac{\theta - \theta_r}{\varphi - \theta_r} = \left[1 + (\alpha \cdot P_C)^n\right]^{-m} \quad \text{(A-2)}$$

Solving for the derivative of the Van Genuchten relationship with respect to time and substituting the capillary pressure through the relationships $h = P_C + z$ and $P_C = -h_w$:

$$\frac{\partial \theta}{\partial t} = \frac{\partial \theta}{\partial h} \cdot \frac{\partial h}{\partial t} = C(h)\frac{\partial h}{\partial t} \quad \text{(A-3)}$$

where,

$$C(h) = m\ n\ \alpha\ (\varphi - \theta_r)\left[1 + [\alpha(z-h)]^n\right]^{-m-1}[\alpha(z-h)]^{n-1} \quad \text{(A-4)}$$

So the flow equation will be converted to:

$$C(h)\frac{\partial(h)}{\partial t} = \frac{\partial}{\partial x}(K_r K_{sat} \frac{\partial h}{\partial x}) + \frac{\partial}{\partial y}(K_r K_{sat} \frac{\partial h}{\partial y}) \quad \text{(A-5)}$$

n and α are Van Genuchten parameters and K_r is the relative permeability which is define in section 3.3 based on the saturation. By having the Van Genuchten relationship of saturation and total head the K_r can also be defined based on total head:

$$\text{Mualem: } K_r = \left(\left[1+(-\alpha(h-z))^n\right]^{-m}\right)^{1/2}\left(1-\left[1-\left[1+(-\alpha(h-z))^n\right]^{-1}\right]^m\right)^2 \quad \text{(A-6)}$$

$$\text{Burdine: } K_r = \left[1+(-\alpha(h-z))^n\right]^{-2m}\left(1-\left[1-\left[1+\left[-\alpha(h-z)\right]^n\right]^{-1}\right]^m\right) \quad \text{(A-7)}$$

APPENDIX B- GUIDE FOR DEVELOPED GRAPHIC USER INTERFACE

The developed model is coded in Visual Basic.Net 2003 with a user-friendly interface. It contains some commands on four tab pages consisting of the "Project Definition", "Geometry Data", "Soil and Microbial Properties", "Boundary and Initial Conditions", and "Run" tab pages.

B.1 PROJECT DEFINITION

The "Project Definition" tab page is the first tab page that contains the title of the project, the date of simulation, the dimensions of biofilter, the depth of distribution pipe, and the loading type (Figure B-1). In the "Loading Type" box, the user specifies the type of wastewater distribution on the filter (i.e. pulse or continuous loading). By clicking on each loading type, the related box for entering the data of that type of loading will be opened.

B.2 GEOMETRY DATA

In the second tab page, "Geometry Data", the user enters geometry of the nodes including their numbering and coordinates in the node table, and also enters the elements number and their connection in the elements table (Figure B-2). This can be done either manually or by clicking on the "Automatic mesh generation" button.

Clicking on the "Automatic mesh generation" button opens another form to define the specification of a desired mesh (Figure B-3). User can define different layers with different element sizes. The first layer is the bottom layer and starts from y=0. In the "Mesh Generator" form, X_inc and Y_inc are the number of elements in x and y

directions, respectively. Each layer is specified by defining the bottom and top boundary elevation (y1 and y2).

The "Draw mesh" button in the "Geometry Data" tab page (Fig. B-2) illustrates a schematic of element arrangement and shows mesh refinement location.

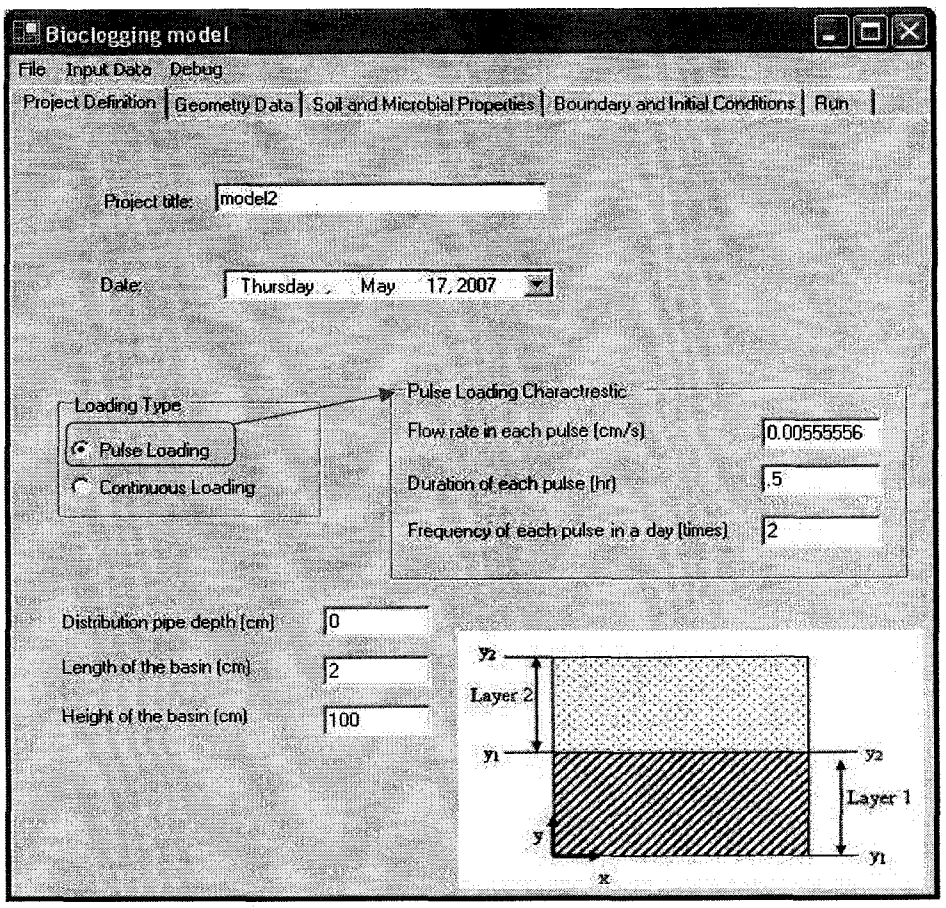

Figure B-1: "Project definition" tab page

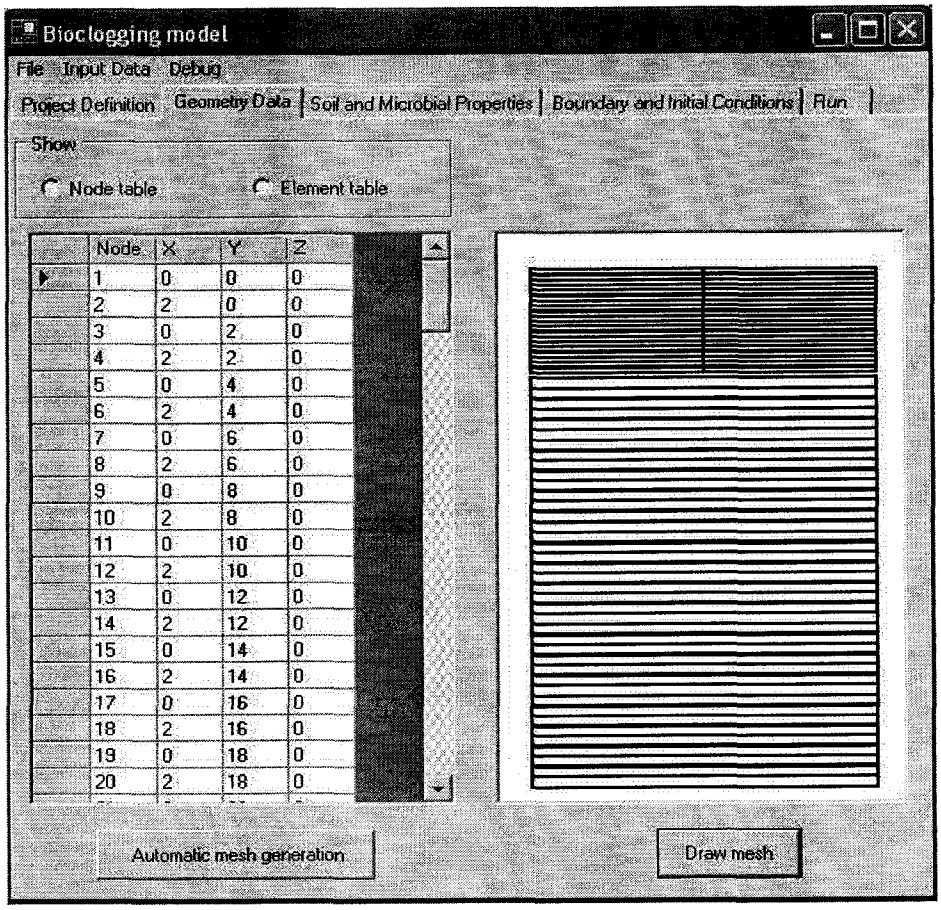

Figure B-2: "Geometry Data" tab page

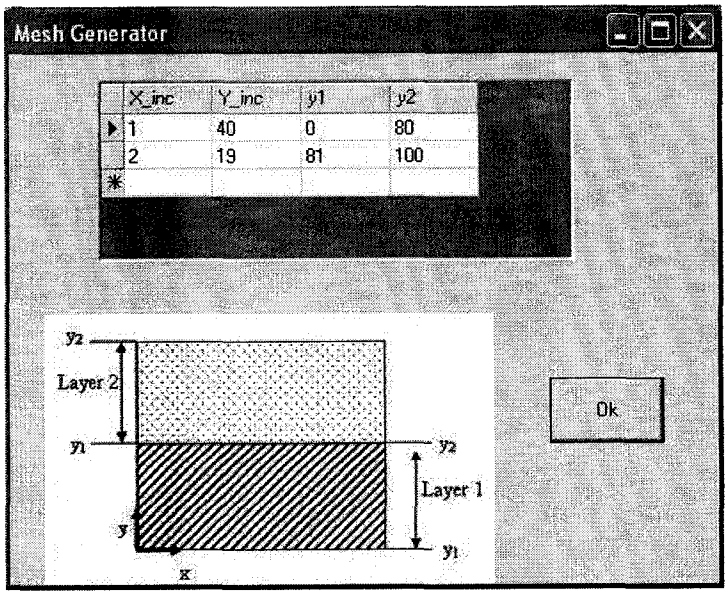

Figure B-3: Mesh Generator form

B.3 SOIL AND MICROBIAL PROPERTIES

The program has a feature to consider a domain with various soil properties in different elevations. The soil properties for each layer consists of the saturated hydraulic conductivity, porosity, irreducible saturation, and Van Genuchten parameters (n and α). They can be defined in the "Soil Properties" table (Figure B-4). Each layer is specified by its bottom and top elevation (y_1 and y_2) which are measured from the bottom of the basin.

Based on the desired substrate utilization method, the appropriate box for entering the input data for that method will be opened. For example, for the Monod substrate utilization method, the user will be asked to enter the half velocity constant, the maximum specific rate of substrate utilization, the yield coefficient, the endogenous decay coefficient and the bacterial density (Figure B-4).

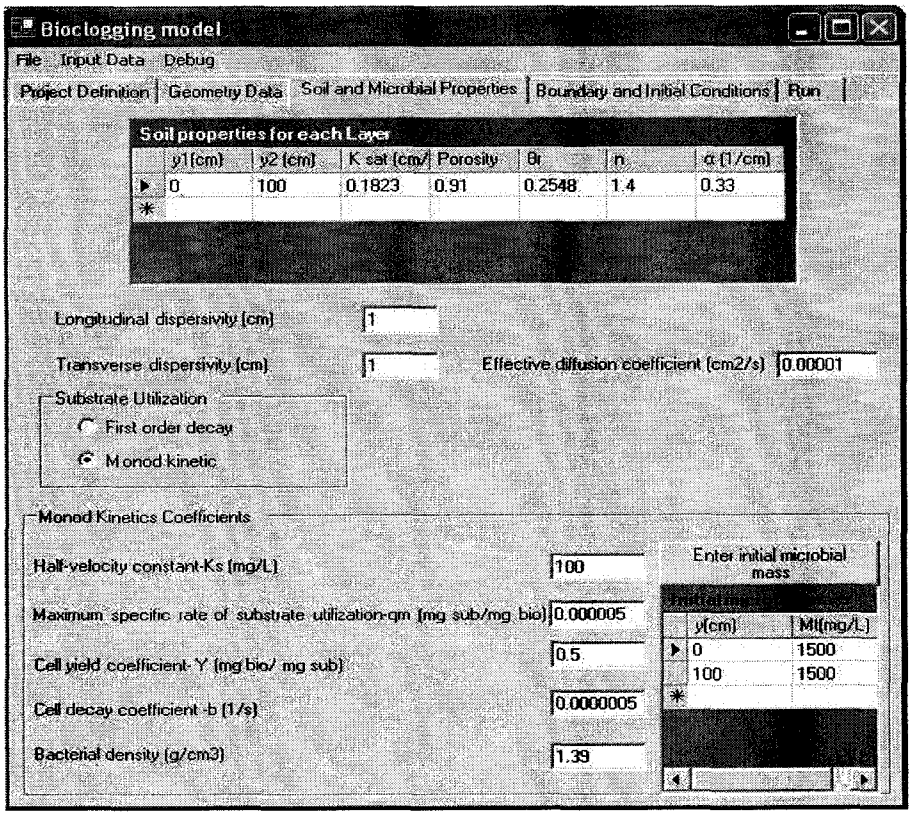

Figure B-4: Soil and Microbial Properties tab page

The initial microbial mass can be entered manually or by clicking the "Enter initial microbial mass" button and reading the initial data from a text file (Figure B-4). The text file should have the elevation and the initial microbial mass data for each elevation with a comma separator. The program has the ability to linearly interpolate the initial microbial mass data to obtain the initial mass for all levels between two specified elevations.

B.4 BOUNDARY AND INITIAL CONDITIONS

The initial conditions and the bottom and top boundary conditions for both flow and transport equation will be defined in "Boundary and Initial Conditions" tab page. The user can specify a prescribed top boundary condition for the flow equation by entering a constant head in the appropriate text box (Figure B-5). No top boundary condition will be assumed, if this text box is blank. Two types of prescribed bottom boundary condition for the flow equation can be assumed: variable prescribed head over the time or constant prescribed head during the entire simulation. By changing the type of bottom boundary condition for flow in the combo box (Figure B-5), the appropriate table (" Variable boundary condition" table) will be appeared to enter the prescribed head boundary condition in different stress periods or a text box will be appeared to enter the constant bottom head boundary condition.

The initial condition for flow is the total head in cm and the initial condition for transport equation is the concentration of organic matter in mg/L. The initial conditions can be entered manually in the appropriate tables. Clicking on the concentration initial condition or flow initial condition and clicking the "Enter initial condition" button will open an "Open File Dialogue" to let the user select a text file for entering the initial

conditions on the appropriate tables (Figure B-6). The text file starts with the number of data followed by the elevation and the initial condition data for each elevation with a comma separator. The program linearly interpolates the initial condition data to obtain the initial condition for the desired node between two nodes.

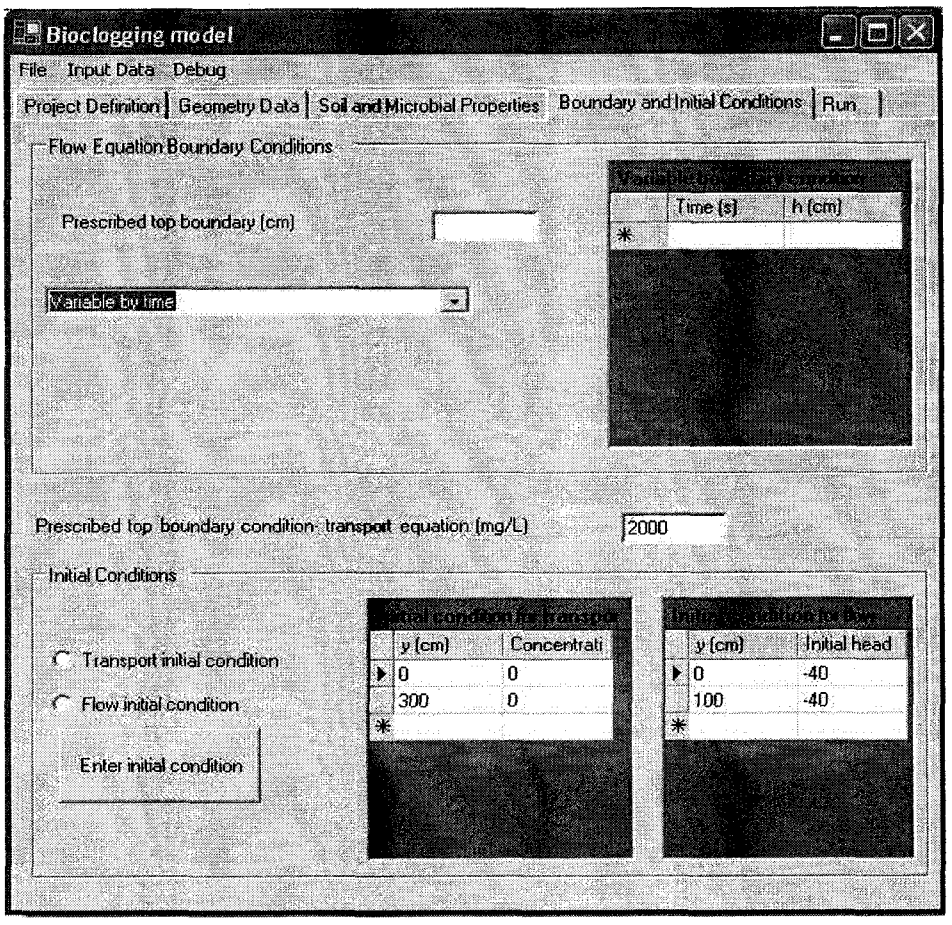

Figure B-5: Boundary and Initial Condition tab page

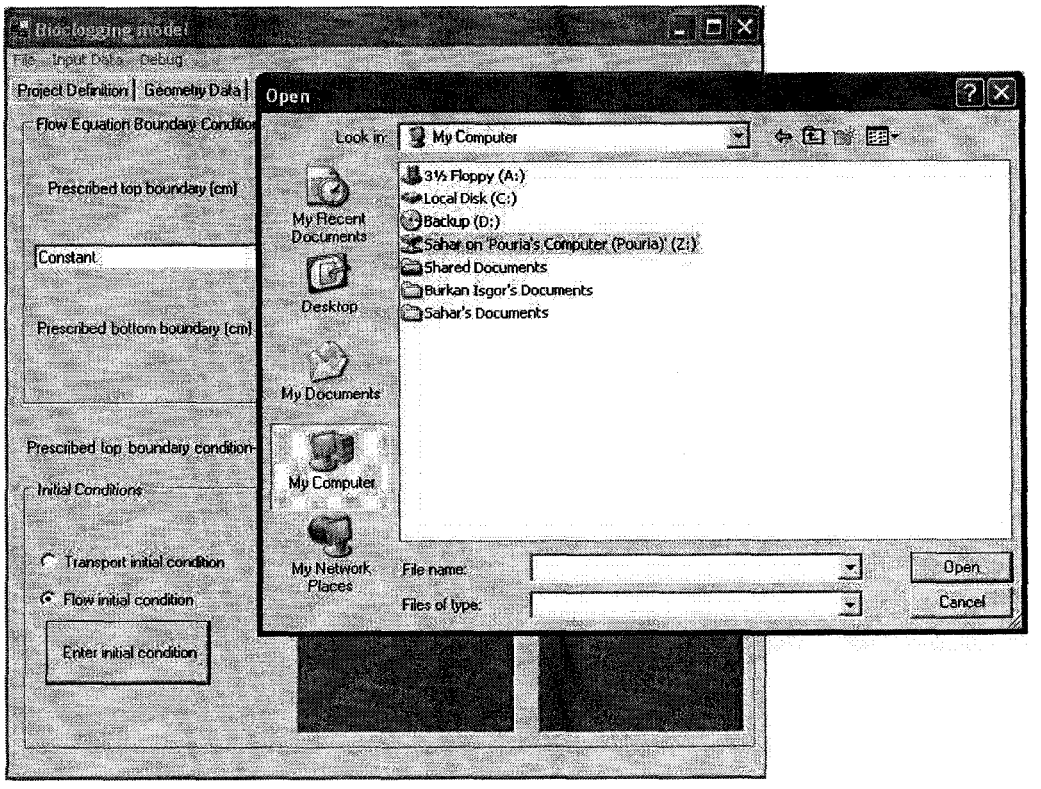

Figure B-6: Entering the initial condition

B.5 RUN

In the "Run" tab page, Figure B-7, the user will be asked to select the relative permeability estimation method (i.e. Mualem or Burdine) and the model number for estimating the relative permeability reduction (model #1, #2, or #3). Before clicking the "Run" button, the user should specify if the simulation is a one-dimensional or two-dimensional simulation.

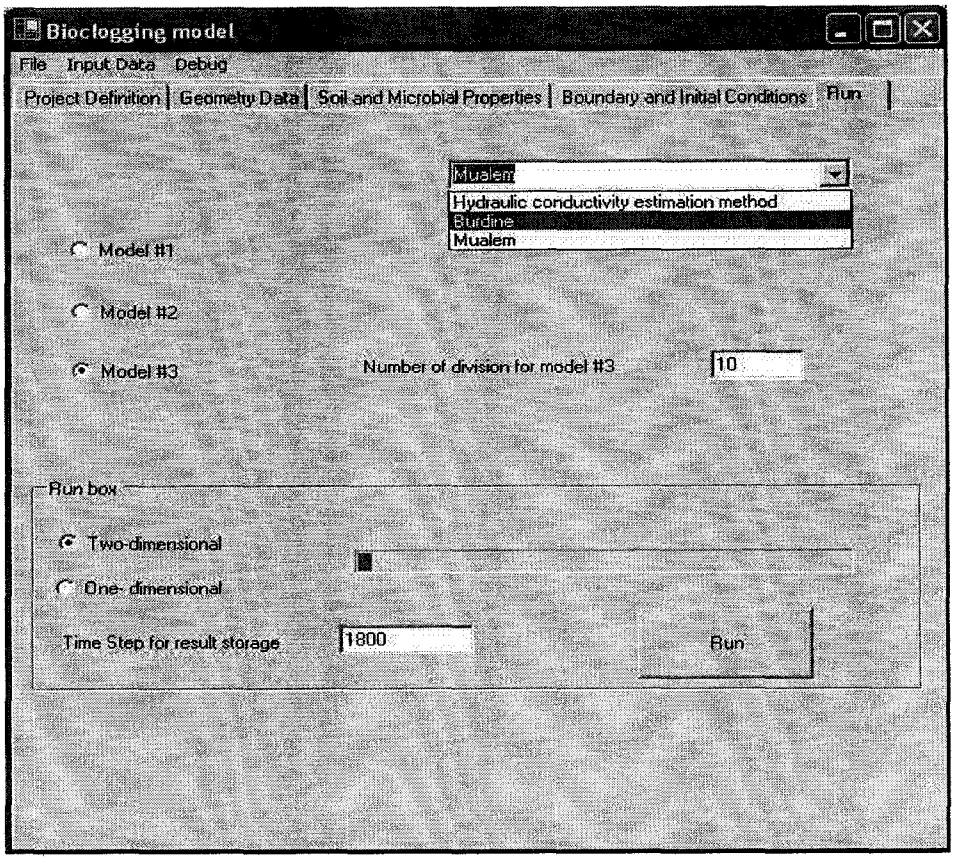

Figure B-7: "Run" tab page

The program is capable to connect to "Microsoft Excel Software" to store the result of simulations. The time step for storing the results should be specified. The program writes in 6 different spreadsheets of an "Excel" file; the results of water, total and microbial saturation as well as the results of hydraulic conductivity, microbial concentration and total head of each node at the time of data storage. The "Excel" file is saved in a directory where the input data file is located.

B.6 Menu bar

The input data which is entered in 4 tab pages can be saved by pressing the "Save" command on the "File" menu bar. The user can also open an existing input data file by

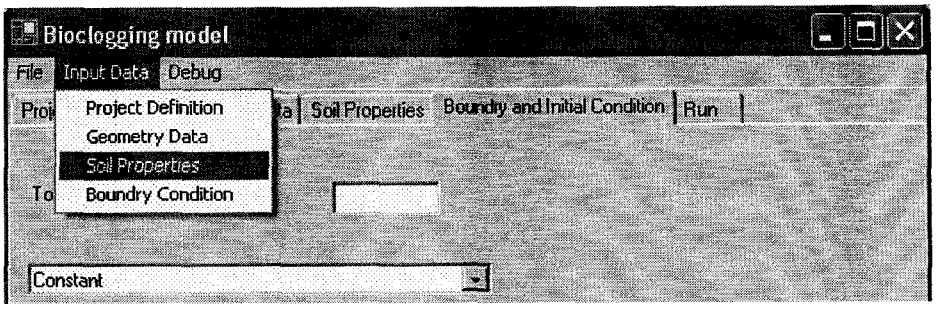

Figure B-8: Menu bar- File command

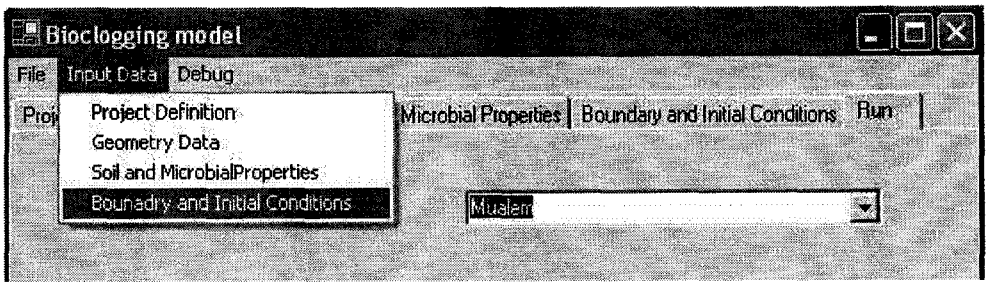

Figure B-9: Menu bar- Input Data command

pressing the "Open" command on the "File" menu bar. The program will be closed by pressing the "Exit" command on the "File" menu bar.

In the input data menu bar, four commands consisting of "Project Definition", "Geometry Data", "Soil Properties", and "Boundary Conditions" are accessible. Pressing each command in this menu bar leads the user to the appropriate tab page.